U.S. DEPARTMENT OF COMMERCE
National Technical Information Service

PB-253 300

NITRIC OXIDE AND COMPOSITION PROFILES AROUND BURNING DROPLETS OF ETHANOL AND ETHANOL-PYRIDINE MIXTURES

PRINCETON UNIVERSITY

PREPARED FOR
ENVIRONMENTAL PROTECTION AGENCY

1974

161053

Princeton University

PB 253 300

NITRIC OXIDE AND COMPOSITION PROFILES AROUND BURNING DROPLETS OF ETHANOL AND ETHANOL-PYRIDINE MIXTURES

Research Conducted Under Environmental Protection Agency Grant No. R-800844

Department of
Aerospace and
Mechanical Sciences

RECEIVED
'75 JAN 13 AM 11:04
EPA
GRANTS ADMIN. DIV.

REPRODUCED BY
NATIONAL TECHNICAL
INFORMATION SERVICE
U. S. DEPARTMENT OF COMMERCE
SPRINGFIELD, VA. 22161

NITRIC OXIDE AND COMPOSITION PROFILES AROUND BURNING DROPLETS OF ETHANOL AND ETHANOL-PYRIDINE MIXTURES

Research Conducted Under Environmental Protection Agency Grant No. R-800844

by

Dennis E. Ludwig

David T. Harrje

and

Frediano V. Bracco

AMS Report No. 1137

Department of Aerospace and Mechanical Sciences
PRINCETON UNIVERSITY
Princeton, New Jersey

1974

ABSTRACT

Composition profiles for the major species including nitric oxide along with temperature profiles are obtained for simulated ethanol fuel droplets burning at one atmosphere pressure and 300°K. Nitric oxide profiles are also obtained for simulated fuel droplets of ethanol seeded with various percentages of a compound containing nitrogen (pyridine).

The fuel droplet is simulated by a one millimeter porous carbon sphere supported by a fine stainless steel fuel line. Fuel is fed to the sphere using a motor driven syringe system. Gas samples are collected via a fine quartz microprobe introduced into the flame. The samples are immediately analyzed using a gas chromatograph and a nitric oxide chemiluminescent analyzer. Temperature measurements are made with standard quartz coated platinum/platinum-13% rhodium thermocouples.

Comparison of the data is then made with previous theoretical calculations. Composition profiles are in good agreement with the theory, however measured nitric oxide concentrations are somewhat higher than predicted.

TABLE OF CONTENTS

	Page
ACKNOWLEDGEMENTS	i
ABSTRACT	ii
TABLE OF CONTENTS	iii
NOMENCLATURE	v
LIST OF FIGURES	ix
CHAPTER I INTRODUCTION	1
1.1 Purpose for This Work	1
1.2 A Summary of Important Droplet Burning Research	3
1.3 The Fuel Nitrogen Problem and Research to Date	7
CHAPTER II DESIGN OF THE EXPERIMENT	13
2.1 Selection of the Steady State System	13
2.2 Selection of Droplet Size, Material, and Fuel	13
2.3 The Supported Sphere Technique	17
2.4 Gas Sampling Considerations	21
2.5 On-Line, Off-Line Analysis Considerations	26
2.6 The Gas Chromatograph	26
2.7 The Chemiluminescent NO Analyzer	29
2.8 Thermocouple Design and Temperature Measurement	32
2.8.1 Design	32
2.8.2 Temperature Correction Techniques	32
2.9 Experimental Arrangement and Procedure	36
CHAPTER III EXPERIMENTAL RESULTS AND DISCUSSION	38
3.1 Burning Rate Data	38
3.2 Temperature Data	38
3.3 Gas Composition Data	43
3.4 Nitric Oxide Data	48

Page

CHAPTER IV CONCLUSIONS AND RECOMMENDATIONS 51

4.1 Conclusions 51

4.2 Recommendations for Future Work 52

REFERENCES 54

FIGURES 58

APPENDIX A THEORETICAL ASPECTS OF DROPLET BURNING 90

APPENDIX B EXPERIMENTAL OBSERVATIONS AND SUGGESTIONS FOR IMPROVEMENT 102

APPENDIX C ENERGY BALANCE FOR THERMOCOUPLE ELEMENT 105

NOMENCLATURE

A = Quartz microprobe orifice area, cm^3

B = Transfer number, dimensionless

C = Discharge coefficient for microprobe choked flow

C_p = specific heat at constant pressure, cal/gm-^oK

$\bar{C}_p$ = average specific heat, cal/gm-^oK

D = diffusion coefficient, cm^2/s

G = species mass fraction gradient in radial direction, per mm

Gr = Grashof number $\equiv g D^3 \zeta^2 \Delta T / \mu^2 T$, for a perfect gas

h = heat transfer coefficient, cal/sec-cm^2-^oK

i = stoichiometric coefficient (Y_o/Y_F) stoich.

k = chemical reaction rate constant

L = heat of vaporization, cal/gm

$\dot{m}_f$ = fuel burning rate, gm/s

$\dot{m}_f^o$ = fuel burning rate in the absence of gravity, gm/s

$\dot{m}_{(net)_f}$ = fuel burning rate corrected for natural convection, gm/s

$\dot{m}_p$ = microprobe flow rate, gm/s

MW = molecular weight

Nu_D = Nusselt number $\equiv hD/\lambda$

p = pressure, dynes/cm^2 or atms.

p_{co} = calibration pressure without sample flow, mm Hg

p_{cs} = calibration pressure with sample flow, mm Hg

p_o = data pressure without sample flow, mm Hg

p_s = data pressure with sample flow, mm Hg

p_c = stagnation pressure used to calculate probe flow rate, dynes/cm^2

q_f = heat of reaction per unit mass of fuel, cal/gm

R = Universal Gas constant = 1.987 cal/mole$^\circ$K

Re_D = Reynolds number $\equiv \rho UD/\mu = 2\rho U r_2/\mu$

R_p = Thermocouple wire diameter, cm

R_q = Thermocouple wire diameter with silica coating, cm

r = radial coordinate from droplet center, cm

r_2 = droplet radius, cm

T = temperature, $^\circ$K

T_∞ = temperature of gas far from droplet, $^\circ$K

T_ℓ = temperature of droplet surface $\approx$ fuel boiling point, $^\circ K$

T_c = stagnation temperature used to calculate probe flow rate, $^\circ K$

T_f = maximum flame temperauure, $^\circ K$

T_g = flame gas temperature, $^\circ K$

U_∞ = maximum flame convection current velocity, cm/s

V_s = syringe volume, cm^3

y = mass fraction, gm/gm

y_o = mass fraction of oxidizer, gm/gm

y_F = mass fraction of fuel, gm/gm

$y_{o,\infty}$ = mass fraction of oxidizer far from droplet, gm/gm

$\dot{Q}$ = volumetric flow rate of liquid fuel, volume/time

α = thermal diffusivity $\equiv \lambda/\rho C_p$

ν = kinematic viscosity, cm^2/s

μ = dynamic viscosity, gm/s-cm

λ = thermal conductivity, $cal/s\text{-}cm^\circ K$

λ_p = thermal conductivity of thermocouple wire, $cal/s\text{-}cm^\circ K$

λ_q = thermal conductivity of quartz, $cal/s\text{-}cm^\circ K$

γ = ratio of specific heats

ϵ = emmissivity of quartz coated thermocouple

σ = Stefan- Boltzmann constant, cal/s-cm^2°K^4

ρ = density, gm/cm^3

LIST OF FIGURES

Figure 1. Schematic of the Basic Spray Combustion Problem ____ 58

Figure 2. Photograph of Droplet and Quartz Probe with Blow-ups Showing Construction Details ____ 59

Figure 3. Modified Chromatograph System ____ 60

Figure 4. Chemiluminescent Analyzer ____ 61

Figure 5. Top View of Thermocouple and Probing Technique ____ 62

Figure 6. Thermocouple Element ____ 63

Figure 7. Photograph of Experimental Arrangement ____ 64

Figure 8. Gas Analysis System ____ 65

Figure 9. Thermocouple Temperature Analysis System ____ 66

Figure 10. Suggestion for NO Analyzer Improvement ____ 67

Figure 11. Droplet Burning Rates Versus Diameter ____ 68

Figure 12. Theoretical Steady, Spherical Diffusion Flame: Ethanol in Air ____ 69

Figure 13. Temperature Profiles for a .648mm Radius Ethanol Droplet ____ 70

Figure 14. Temperature Profiles for a .648mm Radius Ethanol Droplet ____ 71

Figure 15. Uncorrected Temperature Distribution Along Thermocouple Wire. Junction at Position $r/r_\ell = 1.0$. ____ 72

Figure 16. Uncorrected Temperature Distribution Along Thermocouple Wire. Junction at Position $r/r_\ell = 3.3$. ____ 73

Figure 17. Composition Profiles, Run No. 1, $r_\ell = .66$mm ____ 74

Figure 18. Composition Profiles, Run No. 2, $r_\ell = .66$mm ____ 75

Figure 19. Composition Profiles, Run No. 3, $r_\ell = .66$mm ____ 76

Figure 20. Composition Profiles, mass percent, Run No. 3 ____ 77

Figure 21. Rate of Disappearance of Ethanol with Position in Flame ____ 78

Figure 22. Rate of Appearance of CO_2 with Position in Flame ____ 79

Figure 23. Nitric Oxide Profiles, $r_\ell = .66$mm, Pure Ethanol ____ 80

Figure 24. Nitric Oxide Profiles, $r_\ell = .648$mm, .096% Pyridine ____ 81

Figure 25. Nitric Oxide Profiles, $r_\ell = .648$mm, .1999% Pyridine ____ 82

Figure 26. Nitric Oxide Profiles, $r_\ell = .66$mm, .3853% Pyridine ____ 83

Figure 27. Nitric Oxide Profiles, $r_\ell = .66$mm, .591% Pyridine ____ 84

Figure 28. Nitric Oxide Profiles, $r_\ell = .66$mm, .78% Pyridine ____ 85

Figure 29. Nitric Oxide Profiles, $r_\ell = .66$mm, .9878% Pyridine ____ 86

Figure 30. Nitric Oxide Profiles, r_ℓ=.648mm, 1.976% Pyridine _____ 87
Figure 31. Nitric Oxide Profiles, r_ℓ=.648mm, 3.98% Pyridine _____ 88
Figure 32. Conversion of Fuel N to NO _____ 89
Figure 33. Conversion of Fuel N to NO _____ 90

CHAPTER I

INTRODUCTION

1.1 Purpose for This Work

The burning of liquid hydrocarbon fuel sprays is an important source of energy for the production of electricity, shaft work in turbines and diesel engines, and for heating buildings. Recently, however, renewed attention has been drawn to the design of these systems since they are contributing significantly to the deterioration of air quality.

One major pollutant emitted by these systems is nitric oxide. Until recently, the formation of nitric oxide was believed to occur only from reactions between atmospheric oxygen and nitrogen in the high temperature region where combustion takes place. Evidence now indicates, however, that organic nitrogen compounds found in typical fuel oils can be very significant additional sources of nitric oxide. Very few investigations have been carried out on this problem, but the information available suggests that there is a definite relationship between the amount of nitrogen in the fuel and the nitric oxide produced under specific operating conditions.[1] There does not, however, appear to be a strong relationship between the molecular form of fuel bound nitrogen and the amount of NO produced.[2]

To date, research reported in the literature on the fuel bound nitrogen problem has been carried out on large combustion furnaces with little attention being paid to the molecular kinetic mechanisms by which nitric oxide is formed. The purpose of this work is in part to open the door for the indentification of the primary kinetic mechanisms which are responsible for conversion of fuel bound nitrogen to nitrogen oxide (or oxides).

The above stated problem is, however, only a small (but equally important) aspect of a set of interrelated and more fundamental phenomena which have yet to be fully solved. This is the problem of spray combustion. Simply stated, spray combustion involves injecting an atomized liquid fuel into a flowing oxidizer stream. The droplets enter a region of pre-heating in which some vaporization occurs. Following this the mixture of droplets, vapor and oxidizer enter the hot region in which chemical reaction is taking place and the droplets burn. The description of spray combustion involves understanding the basic processes of a) individual droplet burning, b) interaction between individual droplets in the spray, c) formation and statistical distributions of the spray itself and d) the fluid mechanics of mixing and recirculation. The interrelationship of these processes is indicated in Figure 1.[3]

The importance of understanding the burning of single droplets and their relationship to spray combustion is obvious, however, this aspect is not fully understood at present. Therefore, this work was undertaken with the following two-fold purpose:

1) To gain a fuller understanding of the general problem of droplet burning. This has been accomplished by determining composition profiles of the species surrounding the droplet and by making temperature measurements. By careful selection of the droplet size and fuel, gravitational effects can be minimized so that a comparison can then be made with the flame structure predicted theoretically.

2) To determine what relationships exist between the concentration of fuel bound nitrogen and the concentration of nitric oxide

produced. This has been accomplished primarily by determining NO profiles for a given fuel nitrogen concentration.

Before the work undertaken here can be put into perspective, a brief summary of the important aspects of droplet burning should be presented.

1.2 A Summary of Important Droplet Burning Research

There has been much research on the burning of fuel droplets. A recent review by Williams[4] references over 200 separate papers published on the subject. Clearly, only papers with pertinent information can be referenced here.

The basic foundation for droplet combustion research was laid by Godsave[5] and Spalding.[6] Both contributed significantly to the understanding of the physical processes taking place. Godsave was able to show that the square of the droplet diameter decreases linearly with time. Spalding contributed significantly to the theoretical understanding and isolated the functional relationships for droplets burning under natural and forced convection.

Spalding and Godsave solved the basic theoretical problem based on the following assumptions:

a) the liquid is a single component

b) spherical symmetry

c) combustion occurs under quasi-steady state, i.e., the velocity of the fuel vapor flowing away from the surface is very much greater than the rate of change of the droplet radius

d) the temperature of the droplet surface is approximately equal to the fuel boiling point

e) radiation and thermal diffusion effects are negligible

f) constant pressure throughout the system

g) chemical kinetics are infinitely rapid. This means that the reaction flame zone is of infinitesimal thickness.

Based on the above assumptions, the following standard solution for the fuel burning rate is

$$\dot{m}_f = 4\pi r_\ell \bar{\rho} \bar{D} \ln (1+B)$$

where

$$B = \frac{1}{L}\left[\bar{C}_p (T_\infty - T_\ell) + \frac{q Y_{O,\infty}}{\nu}\right]$$

If it is assumed that the rate at which energy transported by conduction is equal to the rate at which energy transported by diffusion (i.e., the Lewis number = 1), then

$$\dot{m}_f = 4\pi r_\ell \frac{\bar{\lambda}}{\bar{C}_p} \ln (1+B)$$

Wise and Agoston[7] expanded on the theory to present the following results:

$$T_f = T_\ell + \frac{q-L}{\bar{C}_p}\left[\frac{1}{1+\frac{1}{Y_{O,\infty}}}\right] + \left[\frac{T_\infty - T_\ell}{1+Y_{O,\infty}/\nu}\right]$$

$$r_{flame}/r_s = \ln(1+B)/\ln\left(1+\frac{Y_{O,\infty}}{i}\right)$$

$$Y_{F,s} = 1 - \frac{1+(Y_{O,\infty}/i)}{1+B}$$

The mass burning rate equation is the only relation which appears to hold well under real conditions. The above theory breaks down because three basic assumptions are not usually met under laboratory and combustion conditions:

1) Gravity or flowing oxidizer increase rates of mass and energy transfer and distort the flame front from spherical symmetry.
2) Chemical kinetics are finite. This changes the position of the flame front and tends to reduce the maximum flame temperature.
3) The quasi-steady assumption is not supported by experimental evidence.[8] The ratio of the flame diameter to the droplet diameter appears to increase linearly with time. This is contrary to the quasi-steady prediction of a constant value.

Very little theoretical work has been done on the above real effects. Usually, analogies are drawn between boundary layer theory with heat transfer for flat plates and spheres and the burning of droplets under natural and forced convection. The semi-empirical results are usually presented in the form[4]

$$\dot{m}_f = \dot{m}_f^\circ\,(1+f(Gr, Sc, Le)) \qquad \text{for natural convection}$$

and

$$\dot{m}_f = \dot{m}_f^\circ\,(1+f(Re, Pr, Sc)) \qquad \text{for forced convection.}$$

The amount of work reported in the literature using finite rate kinetics is also limited. Due to a general lack of sufficient kinetic rate data, finite rate studies usually assume an overall reaction rate expression of the form[10]

$$\text{Rate} = A[\text{Fuel}][\text{Oxidizer}]\, e^{-E/RT}$$

where A and E are the usual Arrhenius reaction rate parameters. Lorell, Wise, and Carr[10] used this type of expression to show how variation of the activation energy, E , affects the composition and temperature profiles and the flame thickness. They indicate that the flame zone width may become so thick that steady-state combustion cannot continue. This was concluded from the fact that no steady-state solution of the equations can be obtained for activation energies above a certain value. Apparently, a flattening of the temperature profile causes a reduction of the heat transfer to the liquid. A critical point is reached in which the rate of vaporization cannot keep pace with the rate of chemical reaction.

A recent theoretical study of droplets burning under gravity free conditions was carried out by Bracco.[11] The flame structure and nitric oxide formation were studied for droplets ranging in size from 10μ - 200μ and ambient pressures ranging from 1 - 36 atmospheres. Based on his studies Bracco reached the following conclusions:

1) Burning fuel droplets could generate significant amounts of nitric oxide, especially at high ambient temperatures.
2) The effects of species diffusion must be included in the calculation for the formation of nitric oxide within the flame.

3) The ratio of the rate of production of nitric oxide to the rate of combustion of fuel increases with increasing drop radius.

4) The amount of nitric oxide produced per mass of fuel burned decreases as the spray becomes finer.

Bracco's paper has been the basis for comparison of experimental results obtained from this work and will be discussed in more detail later. A summary of the theoretical aspects of his work is discussed in Appendix A.

1.3 The Fuel Nitrogen Problem and Research to Date

Studies conducted by the Environmental Protection Agency[1] indicated that amines and nitrates added to fuels substantially increased NO_x emissions corresponding to about 50% conversion of the nitrogen in the fuel. The increase has also been reported in large oil-fired boilers. One 175 MW front wall fired boiler showed an increase in NO production from 320 ppm base to 580 ppm when the fuel contained 1% nitrogen.

The problem of fuel nitrogen conversion to NO was given serious consideration when it was realized that fuels can contain significant quantities of nitrogen compounds. The average nitrogen concentration in the United States crude oils in 1956 was 0.148%, Table 1 and 2 give a breakdown for nitrogen concentration for typical California crudes.

Table 1

Distribution of Nitrogen by Fuel Fraction

Oil Fraction	Fraction of Crude	Range of N%	Average Nitrogen
Crude	100	NA	0.65
Asphaltines	7	2.15-2.50	2.30
Heavy Oil (4-6)	40	0.60-2.15	1.40
Gasolines and Distillates (1-3)	53	0.00-0.60	0.07

Table 2

Major Nitrogen Compounds in Crude Oil Fractions

Compound Class	Distillate Oil, 400-700°F		Heavy Oil, 700-850°F	
	wt%	%N	wt%	%N
Indoles	0.07	0.0084	0.59	0.07
Carbazoles	0.28	0.024	3.38	0.29
Pyridines	0.35	0.063	0.65	0.11
Quinolines	0.21	0.023	1.71	0.19

Burning No. 2 fuel oil seeded with various nitrogen compounds in a high pressure atomizing distillate oil-fired on-off cycle lab furnace, Martin and Berkau[13] arrived at the following conclusions:

a) Pollutant formation during the cycle appears to be related to furnace wall temperature. Radient heat transfer from the flame decreases as the wall temperature increases. This increases the effective flame temperature resulting in lower smoke and hydrocarbon emissions but

higher NO_x emissions.

b) The cycle averaged nitric oxide produced from pure fuel remains almost constant as the stoichiometric ratio is varied, however, the conversion of fuel nitrogen to NO increases rapidly as the stoichiometric ratio is increased from 1.0. Note that Martin and Berkau define the "stoichiometric ratio" as the mass of air supplied to the combustion processes divided by the theoretical mass of air required for complete combustion.

c) For a given stoichiometric ratio > 1, as the nitrogen concentration in the fuel increases, the fraction of the fuel nitrogen converted to NO to the amount of N in the fuel decreases.

d) The fraction of N in the fuel which is converted to NO increases as the stoichiometric ratio is increased and decreases as the amount of nitrogen in the fuel increases.

e) Conversion of fuel nitrogen to NO appears to be independent of fuel type.

f) The nitrogen in the fuel is converted to NO by first forming active intermediates (such as NH_2, NH_3, CN, HCN, C_2N_2) which then react with oxygen to form NO. Since conversion is not 100% complete, recombination reactions forming N_2 probably take place in fuel-rich zones.

g) The conversion of fuel N to NO is much less temperature sensitive than thermal NO. This is becasue fuel N can be converted chemically to NO at temperatures which are too low to thermally dissociate N .

Martin and Berkau also conclude that thermal formation and fuel nitrogen conversion are independent and additive mechanisms for NO_x formation. However, this is not at all clear from their work.

They also proposed a possible mechanism for conversion of fuel nitrogen to NO:

$$2RNH \rightarrow 2R \cdot + 2NH \rightarrow 2N \cdot + O_2 \rightarrow 2NO \text{ or } N_2$$

where R refers to a specie radical.

The relative amounts of N_2 or NO formed would be determined primarily by the availability of oxygen. They speculate two possible paths for conversion:

1) The nitrogen compound breaks up (by either pyrolysis or partial oxidation) into intermediates which then react with oxygen to form NO_x.
2) The nitrogen compound may release nitrogen atoms which then add to thermally formed nitrogen atoms to give a super-equilibrium N concentration. Conventional kinetics (i.e., the Zeldovich mechanism) would then determine NO_x formation.

Incomplete conversion of fuel N to NO_x is accounted for by noting that in fuel-rich zones oxygen concentrations are small suggesting that recombination reactions dominate:

$$N + N + M \rightarrow N_2 + M$$

$$NH + NH \rightarrow N_2 + H_2$$

They point out that in droplet burning, fuel-rich zones exist between the droplet surface and the flame zone.

Turner, Andrews, and Siegmund[2] did considerable fuel nitrogen studies using a modified 50 HP Cleaver Brooks boiler to permit fuel gas recirculation. They tested twenty nitrogen containing additives (1^o Amines, 2^o Amines, 3^o Amines and heterocyclic compounds) and were able to arrive at the same basic conclusions as Martin and Berkau. Turner, Andrews, and Siegmund also studied the process of recirculation and were also able to arrive at the following additional conclusions:

a) Recirculation of cool fluc gas up to about 30% decreased NO_x emissions by almost a constant 100 ppm irrespective of fuel N concentration.

b) Recirculation is effective in reducing only thermal NO.

c) The fractional reduction of thermal NO using recirculation is independent of the absolute level of thermal NO_x emission at any recycle rate.

d) When burned under fuel-rich conditions, nitrogen containing fuels produced almost no NO_x.

They also assumed that thermal fixation of NO and fuel nitrogen conversion are independent mechanisms, and analysis of their data strongly suggests that any coupling between the two types is not strong.

Fenimore[12] studied fuel nitrogen combustion using premixed ethylene flames seeded with various nitrogen compounds. He concluded that the nitric oxide yield depended only on the concentration of nitrogen in the fuel, the flame temperature and the mixture strength (quantity of air/stoichiometric amount of air). The yield was independent of the molecular form of the nitrogen compound.

He assumed that all of the nitrogen in the fuel forms an intermediate which can react only through the following mechanisms:

$$I + R \xrightarrow{k_2} \cdots \rightarrow NO + \cdots$$

$$I + NO \xrightarrow{k_3} \cdots \rightarrow N_2 + \cdots$$

He then postulated that R is a nitrogen free species and concluded that the best candidate is the OH radical. He also postulated that I was the same specie irrespective of the fuel type and concluded that I is probably NH_2, NH, or N atoms. That is, the nitric oxide is both created and destroyed by the same nitrogen containing intermediate.

Fenimore was able to fit all of his data on a universal curve using a normalizing factor, X, which is the maximum NO concentration when formation of NO becomes independent of the fuel N concentration. He also argues that X is proportional to the OH radical concentration in the reaction zone and is able to account qualitatively for the variation in NO formation with X by comparing the NO formed with the fact that the concentration of the OH radical is expected to be higher for cool flames than hot flames and to be higher in fuel-rich mixtures than in fuel-lean ones.

The only known theoretical study on the formation of nitric oxide around burning fuel droplets containing nitrogen compounds is the work done by Bracco.[13] He first calculated the flame structure assuming finite rate kinetics. The nitric oxide formation was calculated using the Zeldovich mechanism taking into account the diffusion of species. The effect of fuel bound nitrogen was taken into account by assuming that nitrogen is released from the fuel as N at the rate and at the location at which the fuel burns. This source of N was then added to the Zeldovich mechanism. Thus no assumption was made that conversion is 100%. He found that for an ethanol fuel drop seeded with 1% nitrogen burning at 1 atm pressure and at an ambient temperature of 300°K, the production of NO increases from 10 ppm base to 360 ppm. However, at a pressure of 35 atmospheres and 1200°K ambient, the fuel nitrogen had no effect since a sufficient quantity of nitrogen atoms was produced thermally.

The above study is very useful in determining the relative importance of fuel nitrogen under various conditions and should prove useful for qualitatively explaining the observed emissions from actual combustion systems. It is becoming increasingly clear, however, that fuel nitrogen is converted to NO via the intermediates such as HN, NH_2, CN, etc. and not primarily by releasing N atoms. The above assumption had to be made due to a lack of kinetic data.

CHAPTER II

DESIGN OF EXPERIMENT AND EQUIPMENT

2.1 Selection of the Steady State System

In order to satisfy the twofold purpose previously discussed, gas composition and temperature profiles must be obtained. There are three basic experimental techniques for studying burning fuel droplets:[9,14]

1) Captive drop method in which a small drop of fuel is suspended on a fine silica support fiber via surface tension. The burning is non-steady state since the diameter of the drop is constantly decreasing. The primary parameter obtained is the burning rate coefficient or the rate of decrease of droplet diameter, 2) Free droplet method in which small droplets fall through a furnace. Ignition delay times and burning rate coefficients are obtained from this method. This is also a non steady-state experiment, and 3) Supporting sphere technique in which the simulated droplet diameter is held constant during combustion. Fuel is continuously supplied to the surface of a sphere of inert material, usually a ceramic or porous metal. This technique gives a steady-state flame and is useful for studying aerodynamic effects, flame structure and burning rate coefficients. This technique also permits the effect of different sphere diameters to be studied.

From these considerations, it is apparent that the supported sphere technique will satisfy the stated purposes.

2.2 Selection of Droplet Size, Material and Fuel

Since one of our objectives is to compare the experimentally determined composition and temperature profile with a theoretical model which neglects gravitational effects, the first requirement is that we reduce the effects

of gravity as much as possible. By doing so, we also simulate to a high degree the very small droplets found in practical sprays.

The effect of gravity is to create buoyancy forces which induce convection currents and distort the flame front from that of a sphere. As a result, for a given droplet radius, the mass burning rate is increased over that of the gravity free case. Although the convection currents cannot be eliminated, it is possible to select the fuel and droplet size so that these effects tend to be negligible.

For droplets burning in a gravity free atmosphere, the mass burning rate is given both theoretically[6] and experimentally by

$$\dot{m}_f = 4\pi r_\ell \frac{\bar{\lambda}}{\bar{c}_p} \ln(1+B)$$

(assuming Le = 1)

$$\frac{\dot{m}_f}{2\pi r_\ell} \frac{\bar{c}_p}{\bar{\lambda}} = 2\ln(1+B)$$

For burning fuel droplets with the range of transfer numbers, B, between 2.5 and 3.0, Spalding gives the following semi-empirical expression[6] for the burning rate when convection effects dominate the burning:

$$\frac{\bar{c}_p}{\bar{\lambda}} \frac{\dot{m}_f}{2\pi r_\ell} = .45\, B^{3/4} \left(\frac{g r_\ell^3}{\alpha^2}\right)^{1/4}$$

where g is the acceleration of gravity and α is the thermal diffusivity.

This expression is based on the relationship between the burning rate and transfer number obtained from boundary layer theory for free convection from a vertical flat plate. Spalding draws an analogy with burning droplets since the heat transfer by natural convection from flat plates, cylinders,

and spheres all have the same functional relationship. The above relationship was found to be in good agreement with experiment.

By equating these two equations, we should be able to solve the critical diameter, below which gravitational effects are small and which gravitational effects are dominant. Solving, we get

$$\text{Diameter} = \left\{ \frac{\alpha^2}{g} \left[\frac{\ln(1+B)}{.225\, B^{3/4}} \right]^4 \right\}^{1/3}$$

From simple kinetic theory, it can be shown that the thermal diffusivity, α, and the kinematic viscosity, ν, are equal. Thus

$$\text{Diameter} = \left[\frac{\nu^2}{g} \right]^{1/3} \frac{[\ln(1+B)]^{4/3}}{.137 B}$$

We see that as the transfer number goes down, the droplet diameter goes up. Since large droplets are easier to work with, we would choose a fuel such as ethanol, which has a transfer number of about three. As Spalding suggests, we evaluate the parameters at ambient conditions. If we let $\nu = .154$ cm^2/sec, $g = 9.8 \times 10^2$ cm^2/sec^2 we obtain $D \approx 1$ mm.

We can check this value by considering a different relationship presented by Williams.[4] He references the following semi-empirical formula which corrects for the effects of natural convection:

$$\dot{m}_{(nat)_f} = \dot{m}_f^\circ \left\{ 1 + \frac{.2}{B^{.44}} Gr^{.3} \right\}$$

where

$$Gr \equiv \frac{g\rho^2(2r_f)^3}{\mu^2}\ \frac{\Delta T}{T_{avg}}$$

The parameters are evaluated at the average temperature, T_{avg}, which is chosen as one-half the sum of the maximum flame and ambient temperatures.

Thus the gravitational effects are negligible if the second term in brackets is much less than the first term. Thus,

$$\frac{.2}{B^{.44}}\, Gr^{.3} << 1$$

or if $$\text{Diameter} << \left[\frac{T_{avg}}{\Delta T}\frac{\mu^2}{g\rho^2}\right]^{1/3}\left\{\frac{B^{.44}}{.2}\right\}^{1.11}$$

Theoretical analysis indicates that the maximum flame temperature is about 2000°K. If the ambient temperature is 300°K, then $\Delta T = 1700°K$ and $T_{avg} \simeq 1150°K$. Assuming properties for air, then

$\mu \approx 450 \times 10^{-6}$ gm/sec-cm

$\rho \approx 3.06 \times 10^{-4}$ gm/cc

$g \approx 9.8 \times 10^{2}$ cm/sec^2

This gives $D \ll 11.5$ mm

and $Gr \gtrsim 10.2$

A one millimeter droplet is then the proper choice. It is amenable to construction and is in the upper size range of droplets actually found in sprays. This last equation also reveals the parameters which determine the magnitude of the gravitational effects. For a given droplet size, gravity effects can be reduced by 1) using fuels with a lower adiabatic flame temperature, 2) lowering the pressure (decreasing the density) of the oxidizing atmosphere, and 3) using fuels with smaller transfer numbers since $\ln(1+B)/B^{.44}$ increases with increasing B.

2.3 The Supported Sphere Technique

The technique employed in this study involves delivering a constant flow of fuel to a small porous sphere supported on a fine feed line. An important consideration is the method by which fuel is fed to the sphere. Three techniques were attempted: 1) a gravity feed system in which a pressure drop across the porous sphere was produced by raising the fuel reservoir the required height above the sphere, 2) a pressure feed system in which the fuel reservoir was placed under regulated gas pressure, and 3) a motor driven syringe system in which a synchronous motor is mechanically linked to push a syringe plunger at a constant rate. Due to practical considerations, it was difficult to attain the proper height in the first method. The second method was bulky and required sensitive regulation. Beyond these considerations, the third method was felt to be the only reliable technique for producing a truly constant flow rate since the first two rely on a potentially variable pressure drop across the porous sphere. The

motor driven syringe also permits fuel flow rates to be easily measured.

The syringe system involves gearing a synchronous motor to a precision threaded rod. The threaded rod advances the linkage which pushes the plunger of the syringe at a constant rate. The speed of the synchronous motor was finely controlled by the power supply which consisted of a frequency generator coupled to a 100 watt audio amplifier. In this way the proper combination of frequency and voltage could be applied to the motor.

The proper syringe volume was determined by considering the anticipated sampling and analysis time for each data point, the number of data points required, and the calculated fuel burning rate. As discussed in Section 2.6 the analysis time (20 min.) dominates the sampling time (5 min.) and the required number of data points is about 10. The fuel burning rate is calculated from the theoretical gravity free burning rate equation and the transfer number, B, is based on the heat released by the overall stoichiometric reaction

$$C_2H_5OH + 3O_2 \rightarrow 3H_2O + 2CO_2$$

From Dickerson[15] the following heats of formation at 298°K were then:

$CO_2(g)$: $\Delta H^\circ_{298} = -94.0518$ kcal/mole

$H_2O(g)$: $\Delta H^\circ_{298} = -57.798$

$C_2H_5OH(g)$: $\Delta H^\circ_{298} = -56.24$

O_2: $\Delta H^\circ_{298} = 0$

The heat of reaction per unit mass of fuel is then

$$q = [3(-57.798) + 2(-94.0518) - (-56.24)]/46.07$$

$$q = 6.625 \text{ kcal/gm}$$

The stoichiometric coefficient $i = 2.085$.

Other parameters which are needed to calculate B are

$L = 204.3$ cal/gm for ethanol

$\bar{C}_p = .279$ cal/gm°K for air at 1150°k

$T_\infty \simeq 300°K$

$T_\ell = 351.3°K$, for ethanol

$Y_{o,\infty} = .234$ = mass fraction of oxygen far from the droplet, std. atmosphere

Putting these into the equation for B, we obtain

$$B = \frac{1}{L}\left[\bar{C}_p(T_{os} - T_\ell) + \frac{q\, Y_{o,\infty}}{i}\right]$$

$$B \approx 3.57$$

Parameters which are needed to calculate $\dot{m}$ are

$r_\ell = .66$ mm

$\bar{\lambda} = 2.0 \times 10^{-4}$ cal/sec-cm°K for air at 1150°K

Putting these values into the equation for $\dot{m}$ we obtain

$$\dot{m}_f = 4\pi r_s \frac{\bar{\lambda}}{c_p} \ln(1+B)$$

$$\dot{m}_f \approx 9.4 \times 10^{-4} \text{ gm/s}$$

The density of ethanol is .789 gm/cc, therefore

$$\dot{Q}_f \approx 11.9 \times 10^{-4} \text{ cc/s}$$

Therefore the syringe volume required is about

$$V_s = \dot{Q}_f \times (\text{Number of data points}) \times (\text{analysis time})$$

$$V_s \approx (11.9 \times 10^{-4})(10)(30)(60) \text{ cc} = 21.4 \text{ cc}$$

We would therefore assume a 30 cc syringe would be sufficient. A 30 cc syringe using a teflon plunger was obtained from Precision Sampling Company.

From the syringe, the fuel flows through a teflon line to the .304 mm O.D. stainless steel hypodermic tubing on which the porous sphere is supported.

The only successful material from which the spheres were made was a porous carbon material which had been used on a previous project. Due to its porosity, the smallest diameter which could be fabricated was about 1.2 mm. Other materials (such as ball point spheres, solid graphite, low porosity ceramics, activated carbon chunks) were tried but were discarded because of lack of machinability

or poor flames. The spheres were turned down from stock using a Dremel tool and emery paper. A hole for the hypodermic tubing was drilled in the stock using a drill of the proper size. With practice a very symmetrical sphere could be fabricated. The sphere was attached to the hypodermic tubing using high temperature cement. The sphere (see Fig. 2a,b) was supported from below by the feed line. This orientation is reported in the literature[23,24] and eliminates the need for a water cooling jacket had the reverse orientation been chosen (i.e., droplet being fed from above).

2.4 Gas Sampling Considerations

The technique of probing flames with quartz microprobes is documented and widely used.[17,18,19,20,21] The purposes in using these small probes are

a) To obtain composition samples with minimal influence upon the flame structure.

b) To mimimize catalytic effects by the use of quartz.

c) To rapidly reduce and quench the reaction rate so that reasonably accurate values of the composition at the probe position can be obtained.

Several important points must be kept in mind, however, when using this technique.

1) The presence of the probe allows for some removal of radicals on its surface. Further, since the probe is usually at a slightly lower temperature than the surrouding gas ,heat will be transferred to the probe, lowering the temperature and reaction rate of the nearby gas.

2) The concentration gradients are changed slightly due to the aerodynamics of sample drawing.

3) Such radicals as O, N, OH, CH_3, HCO, etc. are not quenched since they continue to rapidly react even at room temperature. Hence this technique cannot be used to study radical or extremely reactive specie concentrations.

4) Pyrolysis can occur in very slender probes.

5) The gas might be subjected to catalytic effects within the probe. These are of two types. The first is a quenching effect in which collision with the relatively cold walls immediately stops all reaction. In the second type, the wall serves to initiate reaction by catalytic mechanisms.

These five aspects have been extensively studied and the general conclusion is that these effects are small. Specifically, if the diffusional velocities and flow velocities in the flame are small compared with the sonic velocity at the probe orifice, then the sampled gas represents that of the flame.[17] Also, experience with quartz-coated thermocouples has substantiated the belief that catalytic effects are very small.

In Section 2.6 the conclusion is reached that the pressure in the quartz probe should be kept at about 2 cm Hg. At this pressure the probe is definitely choked, however the reaction quenching efficiency should be considered. This can be readily checked by considering a typical, rapid reaction mechanism such as the following:

$$CH_2O + OH \xrightarrow{k} H_2O + HCO$$

$$k = 3 \times 10^{14} e^{-4000/RT} \quad \text{moles/cc-s}$$

The rate of disappearance of CH_2O is given by

$$\frac{d(CH_2O)}{dt} = -k(CH_2O)(OH)$$

We can simply check the rates of reaction at two different conditions, one at 76 cm Hg and 2000°K, the other at 2 cm Hg and 500°K.

The rate of reaction is affected by 1) the drop in species concentrations and 2) the drop in temperature.

$$\frac{\left.\frac{d(CH_2O)}{dt}\right|_{\substack{2000°K \\ 76\,cm\,Hg}}}{\left.\frac{d(CH_2O)}{dt}\right|_{\substack{500°K \\ 2\,cm\,Hg}}} = \frac{e^{\frac{-4600}{1.987(2000)}}}{e^{\frac{-4800}{1.987(500)}}} \left(\frac{76}{2000}\,\frac{500}{2}\right)^2$$

$$\approx 1840$$

This analysis then indicates that the reaction rate drops by about a factor of 2000. Less reactive reactions should drop by even greater factors. We conclude that the reactions are sufficiently quenched.

Another important consideration in the selection of a quartz probe involves the probe orifice diameter and resolution. The general conclusion[17] is that the spacial resolution of a microprobe is between 10-20 orifice diameters.

It is desirable to select a probe which samples and affects a region in which the concentration of a species (in particular, the species whose concentration gradient is the steepest) does not change by more than a required percentage. Consider, for example, the mass fraction gradient of ethanol as predicted theoretically[11] (see Fig.12). For a one millimeter droplet, the radial gradient is approximately

$$G = \frac{\Delta Y_F}{\Delta r} = \frac{.75 - .14}{(2.5-1)\,r_2} \approx .4/mm$$

If it is desired to sample a region in which Y_F changes by less than 10 percent of its range, then we require

$$\Delta Y_F \leq .1\,(Y_{F_{max}}) = .1\,(.75)$$

In general we can say

(Gradient) x (probe resolution) = (ΔY_F region sampled).

Thus we require the probe resolution to be better than $.075/.4 \approx .2$ mm. This means the probe orifice must be less than or equal to 20 μ. This is a perfectly feasible size to construct. However previous experience indicates that the flame structure is 5 to 10 times more compact than the theory predicts. Thus the concentration gradient will be 5 to 10 times steeper than predicted. Based on a gradient of 2.0/mm, we find that the required probe orifice must be 3.7 μ. Probes this small are not used and have not been reported in the literature for three reasons:

1) They are very difficult to construct and maintain free from plugging.

2) Sampling times become prohibitively long.

3) More importantly, simple kinetic theory[22] indicates that the mean free path for a molecule in the less dense parts of the flame is on the order of 6 μ. This is smaller than the 20 μ probe but about the same magnitude as the 4 μ probe. It is important that the mean free path be much smaller than the probe orifice in order to prevent selective sampling of the lighter components. It appears that the 20 μ probe is about the smallest which can be tolerated under this consideration.

The remaining item which must be checked is a comparison of the probe mass flow rate and the droplet burning rate. The flow rate is calculated from the standard equation for flow through a sonic orifice.

$$\dot{m}_p = C A P_c \left[\frac{\gamma (MW)}{R T_c} \left(\frac{2}{\gamma+1} \right)^{\frac{\gamma+1}{\gamma-1}} \right]^{1/2}$$

If we let the discharge coefficient[21] $C = .5$, $T = 500^{\circ}K$, $MW = 29$, $A = \pi \frac{D^2}{4}$, $D = 20$ μ, and $\gamma = 1.4$, it is found that $\dot{m}_p = 2.9 \times 10^{-5}$ gm/s.

The droplet burning rate was previously found to be about 9×10^{-4} gm/s. Thus

$$\frac{\dot{m}_p}{\dot{m}_f} \approx 3 \times 10^{-2}$$

We would therefore not expect the flame structure to be severely altered, even when probing near the droplet surface.

2.5 On-Line, Off-Line Analysis Considerations

The two basic methods for collecting and analyzing gas samples are 1) the on-line method in which the gas is sampled and then immediately analyzed and 2) the off-line method which simply takes samples and stores them in containers for analysis at a later date.

The final decision to use an on-line system was based on the following considerations:

1) An accurate and uncontaminated sample can be collected.
2) The sample is in a form that can readily be analyzed. That is, the sample does not have to be diluted to atmospheric pressure nor does it have to be pressurized with a substance such as mercury. (It should be noted that NO reacts with mercury).
3) The system is relatively simple and economical.
4) Sample collection times are short (3-5 minutes based on a 20 μ probe).
5) Analysis times are reasonable (about 25 minutes as discussed in the next section).

At one time, the off-line method was considered because severe control problems with the syringe feed system were encountered and because initial tests indicated unacceptable chromatograph analysis times. It was concluded to be much simpler and more economical to solve these problems than to change to an off-line system since it was neither clear how samples would be put into a form which could be easily analyzed nor if such a system could be made economical and vacuum tight.

2.6 The Gas Chromatograph

Since the purpose of this work was to obtain the basic flame structure,

a gas chromatograph was the logical choice since it is simple and economical. It cannot analyze free radicals, unstable species, and cannot accurately analyze molecules which tend to polymerize on surfaces (such as aldehydes).

It was previously mentioned that quenching is efficient if the sample line is maintained at a pressure of 2 cm Hg or less. This pressure is based on the fact that a 25 cc sample loop is about the maximum which should be used since chromatograph resolution decreases as sample size increases. Noting that standard chromatograph sampling parameters[23] are .5 cc to 1cc at one atmosphere of pressure, we conclude that our sampling pressure for a 25cc loop is

$$p \geq \frac{76(.5)}{25} \approx 1.5 \text{ cm Hg}$$

The sensitivity of the chromatograph detector was determined by considering the anticipated concentrations of the pyrolysis species for ethanol. The most complex and stable molecule would probably be C_2H_6, and is expected to be in low concentrations but not trace amounts. A thermal conductivity detector was concluded to be the best choice.[23] It can detect down to about 100 ppm; it responds to all gases; and it is simple and inexpensive.

A Carle Instruments model 8004 thermal conductivity gas chromatograph was obtained. The original unit used two columns, a 1/8 in. O.D., 10 ft. length of Porapak Q, and a 1/8 in. O.D., 6 ft. length of Molecular Sieve 5A. The two are connected in series with a valve which can be used to bypass the molecular sieve while still passing carrier through the Porapak Q. Attempts to duplicate the operation and separation of the gases as advertised were

not successful. The main problems encountered were these: at a column temperature sufficiently low to separate gases in the molecular sieve, the retention time and quality of the ethanol and C_2H_6 peaks were unacceptable; at a column temperature sufficiently high to give a good ethanol peak, the molecular sieve would not separate and switching the valve had to occur in the middle of the CO_2 peak. Thus the CO_2 analysis was lost.

Modifications were made which corrected the above problems (see Fig. 3). They involved removing the molecular sieve from the oven and adding a 6 ft. Porapak T column. Analysis then proceeded as follows (refer to Fig. 3):

1) A sample is injected while all columns are in series (see Fig. 3, position (a)). The gases O_2, N_2, CO, CO_2, CH_4 are allowed to pass through the Porapak Q column.
2) Valve No. 1 is switched (see position in (b)) thereby bypassing Porapak T and the molecular sieve. Gases C_2H_2, C_2H_4, and H_2O are allowed to pass through Porapak Q to the detector.
3) Valve No. 1 is switched (to position in (a)) placing all columns in series and allowing O_2 and N_2 to elute (i.e., pass to the detector).
4) Valve No. 1 is switched (to position in (b)) allowing a hydrocarbon (probably CH_2O) to elute. Meanwhile, bypass the molecular sieve by switching valve No. 2 to the position indicated in position (c).
5) Switch valve No. 1 to elute CO_2 from Porapak T (see position (c)).
6) After CO_2 elutes, put all columns in series (position a) by switching valve No. 2. Allow CO to elute.

7) Switch valve No. 1 to position (b) and allow ethanol to elute.

8) Switch valve No. 1 back to position (a) to allow CH_4 to elute.

The analysis is then complete.

The process is somewhat complex and timing of the switching is important, however, this technique will yield an analysis time of about 19 minutes as compared to 30 minutes if a simpler (but still workable) technique is employed. The Porapak T and Molecular Sieve columns are kept at room temperature while the Porapak Q is kept between 85 and 90°C. The carrier flow is Helium at 60 cc/min. One nice feature about this system is that no temperature programming is required.

Data from the chromatograph was recorded on a Bristol Dynamaster chart recorder. The chromatograph and chart recorder were calibrated using gases of known concentration. Peak areas were estimated using the standard technique of mutliplying the peak height times the peak width at one-half the height. Reasonably accurate data was obtained since all peaks were baseline separated except for C_2H_4 which tended to elute during one of the stabilization transients which occurred after valve switching. When this happended, the switching transient curve was extrapolated through the peak and this curve used as the peak baseline.

2.7 The Chemiluminescent NO Analyzer

Since a chemiluminescent analyzer requires a flow of sample gas and a flow of ozone into a reaction chamber, it seems logical to use the flame probe sampling flow directly. This is the method employed. However, commercial nitric oxide analyzers have not been designed to accept samples at such low pressures as are encountered in our sample lines. It was apparent, therefore,

that a specialized NO analyzer had to be designed which would be compatable with our system.

In order to obtain the proper design parameters, Aero Chem Research Corporation was consulted. After describing our specialized needs, they suggested the following parameters:

1) A cylindrical reactor volume of 137 cm^3 with the diameter equal to the photomultiplier tube diameter.
2) Sample flow rate of .02 cc/sec at STP.
3) Ozone flow rate of .5 cc/sec ($\geq$ 1% O_3) at STP.
4) An EMI 9558A-S20 extended red sensitive photomultiplier tube cooled to less than -20°C. A similar but more sensitive and specially selected EMI 9658A tube was used.
5) Reactor chamber pressure held at .5 ton.
6) A red filter which cuts off light less than 7500 Å wavelength. Analysis of NO_2^* spectra indicated the best choice is Corning filter CS-64 cutting off light < 6000 Å.

Under the above conditions, concentrations as low as .1 ppm NO can be detected. The final system used in this experiment is shown in Figure 4.

One problem has plagued this design, however. One of the requirements for accurate nitric oxide analysis is stable and constant sample flow rate. In this particular experiment, the sample flow rate can change by a factor of 2 to 3. This results because the temperature of the gases surrounding the droplet varies as a function of the microprobe position. As the position of the probes changes, the effective stagnation temperature in the equation for the probe flow rate also changes. The following technique was used to correct for this problem.

It was observed that the pumping speed of the vacuum pump remained essentially constant in the range of desired reaction chamber pressure (.3 - 1 torr). If this is true, then the intensity of light emitted in the reaction chamber would be proportional to the partial pressure of the sample,[24] assuming the partial pressure of ozone-oxygen and mole fraction of NO in the sample are constant.

Now, data from the chemiluminescent analyzer is taken in the form of current. Before and after each set of data is taken, the NO analyzer is calibrated at room temperature and pressure using a calibration gas with known nitric oxide concentration. Had the sample flow rate remained constant while probing the flame, the nitric oxide concentration would have been calculated from the following relation:

$$NO_{ppm} = (\text{calibration ppm}) \times \frac{\text{data current, } A_s}{\text{calibration current, } A_c}$$

However, since the flow rate varies with position in the flame, the data amperage reading is pressure corrected to the pressure at which the calibration is made:

$$A_{pcs} = A_s \frac{P_{cs} - P_{c0}}{P_s - P_0}$$

The equation for nitric oxide concentration in the flame then becomes

$$NO_{ppm} = (\text{calibration ppm}) \frac{A_{pcs}}{A_c}$$

2.8 Thermocouple Design and Temperature Measurement

2.8.1 Design

Temperature measurements in the flame were made using standard thermocouple techniques and are well documented.[25,26,21,27] Briefly, the thermocouples are constructed by welding the ends of fine wires composed of different materials. This is done by positioning the wires using micromanipulators and then by melting the two ends together with an ox-acetylene microtorch to form a bead whose diameter is no more than 1 1/2 times the original wire diameter.

The thermoccuples were constructed from platinum-platinum/13% rhodium. The choice was made primarily because these metals withstand the flame temperatures without significant oxidation or deterioration and because the voltage response is higher than other combinations.

Since temperature measurements were made in regions where reactions were occurring the thermocouples were coated with quartz to minimize catalytic effects. The coating is done by placing the thermocouple in an 1800^{o}K region of a propane-air Fischer burner. If the propane is bubbled through hexamethyldisiloxane, the flame will contain quartz vapor which will then deposit to form a clear layer on the wires.

The actual thermocouple design is shown in Figure 5. The design choice was based on minimizing aerodynamic disturbances from the legs while permitting a geometry amenable to temperature correction techniques described later. Practical considerations limited the thermocouple wires to .0015 in; smaller diameters would be preferable.

2.8.2 Temperature Correction Techniques

At high temperature and in regions where chemical reactions are taking place, the thermocouple will usually be at a temperature which is different

than that of the gas. The difference arises for the following reasons:

1) Radiative heat transfer from the probe. For optically thick flames, this is usually small but for clear flames such as the ethanol flame, the error could be 100°K.
2) Heat transfer between the gas and the probe which tends to lower the temperature of the gas near the probe. This effect along with junction size determines the probe's resolution.
3) Conduction axially along the probe.
4) Catalytic heating of the probe. Experience reported in the literature[27] indicates this effect can be essentially eliminated by coating the probe with a layer of silica.

The commonly used temperature correction is simply a balance between heat conducted from the gas to the probe and the heat lost from the probe by radiation:[25]

$$h \Delta T_{rad} = \epsilon \sigma T^4$$

Radiative transfer to the probe, catalytic effects, and conduction along the probe are all neglected.

Conductive effects axially along the probe can be neglected if the probe can be oriented along surfaces of constant temperature. In the burning droplet problem, however, the thermocouple is situated in regions where the temperature gradients are steep. No probe considered could minimize both aerodynamic and conductive effects. The choice was to minimize aerodynamic disturbances to the flame and try to estimate the axial probe conductive effects.

In order to do this we must first write the equation for an element of thermocouple wire coated with quartz. Figure 6 shows such an element. Assuming the temperature of the wire is uniform on the surface formed by a plane perpendicular to the Z axis and no axial conduction through the quartz coating, the differential equation for the element is (see Appendix C)

$$R_p^2 \lambda_p \frac{d^2T}{dz^2} = 2K(T-T_g) + \epsilon\sigma 2R_g(T^4-T_a^4)$$

where

$$K = 1 \div \left[\frac{1}{R_g h} + \frac{\ln(R_g/R_p)}{\lambda_g}\right]$$

This equation is applicable along the entire thermocouple wire, however, only the temperature of the junction is known. An estimation of the conductive correction term then amounts to obtaining an estimation of d^2T/dZ^2 at the junction. This was done in the manner described below based on the following assumptions:

a) each data point represents the temperature of the thermocouple junction, and is positioned along the same radius vector from the droplet's center. That is, the distance, r (not to be confused with the r in Figure 6), from the droplet's center to the junction represents the magnitude of a vector whose direction is a constant for all data points. In practice, the positioning of the thermocouple junction could be done well within the resolution of the probe (5-10 probe diameters).

b) The thermocouple wire is perpendicular to the radius vector from the droplet's center.

c) The temperature distribution along the thermocouple wire is symmetrical about the junction.

It has also been assumed that for each position, r, the local temperature of the wire in the region of the junction is given by a transformation of the raw data (taken along the vector radius from the droplet's center) to the Z direction. It should be recognized that this is an ad hoc assumption, and has been made for estimation purposes only. The following analysis employs this assumption to obtain

a form for d^2T/dZ^2 which is readily adapted to the experimental data.

If Z represents the position along the wire with the junction at Z = 0, and if $R = \sqrt{r^2 + Z^2}$ represents the distance from the droplet's center to position Z, then the following estimation is obtained for d^2T/dZ^2 :

$$\left(\frac{\partial T}{\partial Z}\right)_r = \frac{\partial T}{\partial R}\,\frac{\partial R}{\partial Z}\Big)_r$$

$$\left(\frac{\partial^2 T}{\partial Z^2}\right)_r = \frac{\partial^2 T}{\partial R^2}\,\frac{\partial R}{\partial Z}\Big)_r + \frac{\partial T}{\partial R}\,\frac{\partial^2 R}{\partial Z^2}\Big)_r$$

which, at the junction (Z = 0) becomes

$$\frac{d^2T}{dZ^2} \equiv \left(\frac{\partial^2 T}{\partial Z^2}\right)_r\Bigg|_{Z=0} = \left(\frac{\partial T}{\partial R}\,\frac{1}{r}\right)_{Z=0} = \left(\frac{\partial T}{\partial r}\,\frac{1}{r}\right)_{Z=0}$$

since

$$\frac{\partial T}{\partial R} = \frac{\partial T}{\partial r} \quad \text{at } Z = 0$$

The derivative $\partial T/\partial r$ is then approximated from the experimental data.

Two other methods should be mentioned which could have been used for estimating $\dfrac{d^2T}{dZ^2}$:

a) experimental approach - temperature data along the thermocouple wire is obtained by moving the junction axially along the wire. If this could be done accurately, a reasonably accurate value for the derivative could be obtained. To be complete, this data would be required for each radial position of the junction. Experimental difficulties and time constraints prohibited the use of this method.

b) theoretical approach - the differential equation for the thermocouple could be integrated along the entire wire. One technique would require the solution of a boundary value problem using a guess for the temperature profile. It was not clear whether such an undertaking would yield results more accurate than the technique finally used. Time constraints also prohibited any investigation of this method.

The other parameter which must be estimated is the heat transfer coefficient, h. Based on simple energy considerations, the convection currents around a burning fuel droplet are about 80 cm/sec. Using average values for the wire diameter, density, and viscosity, the Reynolds number for the flow over the probe is about .5. The heat transfer for low Reynolds number flow over single tubes was calculated from an equation presented by Hsu:[28]

$$N_{U_D} = \frac{h 2r_t}{\lambda_f} = .43 + .48 \left(\frac{2\rho U_\infty}{\nu_f}\right)^{1/2} \quad \text{for } Re_D < 500$$

where the subscript f indicates evaluation is to be made at the film temperature.

As a check, calculations were made assuming heat transfer by free convection from the thermocouple. It was found that heat transfer by forced convection dominates.

A computer program was used to calculate the temperature correction. The equations as presented above were used except that the gas thermal conductivity, viscosity and convection current velocities were assumed to be linearly related to the temperature recorded by the probe.

It should be pointed out that the temperature corrections presented here can only be approximations. Conductive effects axially along the probe are significant but difficult to accurately estimate. This difficulty is partly related to the fact that the heat transfer coefficient is also very difficult to estimate. The probe is situated in a region where every element of the wire is subjected to different convection currents and changing

values of the transport properties. Results of this technique are discussed in Chapter III.

2.9 Experimental Arrangement and Procedure

In the previous sections an attempt was made to describe each basic component in the experimental system. This section will indicate the overall design of the experimental setup.

The technique for probing the flame is shown in Figures 2, 5 and 7. The porous sphere is suspended in the center of a plexiglas chamber (10 x 10 x 25 cm) via the fuel feed line. The top and bottom of the chamber are covered with several layers of 100 mesh stainless steel gauze to eliminate aerodynamic disturbances from the outside. The bottom of the chamber is suspended above the working area about 2 cm and is surrounded by a plexiglas fence to further reduce aerodynamic disturbances. The quartz microprobe and the thermocouples are introduced into the chamber via a slit on the side opposite to the side through which the fuel feed line is introduced. Once the probes and droplet are positioned, the slits are taped to completely isolate the combustion system.

Both the quartz microprobe and the thermocouple are accurately supported and positioned on all three spacial axes by a micromanipulator. Precise positioning of the microprobe tip or thermocouple junction is done visually with the aid of a variable magnification microscope. Radical positioning of the probes can be accomplished with an accuracy of ± .025 mm, which is well under the resolution of either the microprobe or the thermocouple. Note also that the microscope permits close monitoring of the droplet burning characterisitics.

The entire gas analysis system is shown in Figure 8. The gas chromatograph and chemiluminescent analyzer are isolated via the switching valve which permits the sample to flow either to the chromatograph or to the NO analyzer. Pressure in the chromatograph sample loop is selected and maintained by the Todd vacuum pressure regulator. Pressure in the chemiluminescent analyzer reaction chamber is determined by the ozone flow rate and the sample flow rate.

The complete temperature analysis system is indicated in Figure 9. It was decided to use an ice bath reference junction in order to minimize analysis times and to eliminate possible errors when using a room temperature reference junction. The thermocouple output was recorded on a Bristol Dynamaster chart recorder. This permitted visual observation of the fluxuation to determine when steady state had been achieved.

Tests were made to determine if the chart recorder impedence was much larger than the thermocouple and its lead wire. This was the case. Calibration of the chart recorder was also double checked with both a digital volt meter and another calibration unit.

CHAPTER III

EXPERIMENTAL RESULTS AND DISCUSSION

3.1 Burning Rate Data

In order to verify that the chosen droplet size was indeed small enough to significantly reduce gravity effects, variation in the mass burning rate with droplet diameter was studied (see Figure 11). The theory for gravity free burning droplets predicts a constant value for $\dot{m}/r_\ell$. The mass burning rate with gravity rises rapidly above a droplet diameter of about 3 mm. It appears that gravitational effects are small for droplet diameters below 3 mm. The value for the burning rate measured by Agoston, Wise, and Rosser[29] for a 6.35 mm diameter sphere burning under natural convection is 5.1×10^{-3} gm/s. The value obtained in this work is 5.2×10^{-3} gm/s. For smaller droplet diameters, the burning rate measured in this work are about 20% higher than those reported by Wise, Lorell, and Wood.[16] These variations result probably because as the droplet diameter is reduced, the effect of the supporting feed line increases and it becomes more difficult to obtain a spherical liquid surface.

3.2 Temperature Data

Theoretical calculations which have been used as a basis for comparison are plotted in Figure 12. Experimental temperature profiles are plotted in Figures 13 and 14. The first question which must be resolved regards the temperature at the drop surface (which is wetted with ethanol). Using the measured value of $Y_{i,\ell}$, the Clausius-Clapeyron equation

$$Y_{F,\ell} = \frac{MW_F}{MW} e^{-\frac{L}{R}\left(\frac{1}{T_\ell} - \frac{1}{T_b}\right)}$$

with

$$Y_{F,\ell} = .735$$
$$T_b = 355\ ^\circ K$$
$$\overline{MW} = 31.66$$
$$MW_F = 46.07$$
$$R = 1.987/31.66\ \text{cal/gm-}^\circ K$$
$$L = 204\ \text{cal/gm}$$

gives $T_\ell \approx 331\ ^\circ K$

Theoretically, $T_\ell = 325\ ^\circ K$ for $Y_{F,\ell} = .75$ and equal molecular weights. These two are in good agreement, however the value is not as measured with the thermocouple even though the junction was touching the liquid surface. Figures 13 and 14 suggest that the major source of error in this region of the flame is conduction of heat to the junction through the probe wire. The profile obtained in Figure 14 results from the use of the conductive correction technique described in Section 2.8.2. The dashed line is required in the region near the drop surface because this technique proved inadequate since the data points are too far apart for the required accuracy with the steep gradients in this region. A better estimate of the conductive effects can be made from Figure 15, which is a plot of the uncorrected temperature profile along the thermocouple wire, the bead being at z = 0. A better estimate of the second derivative of temperature at the bead can be made from the simple formula

$$\frac{d}{dz}\left(\frac{dT}{dz}\right)_{z=0} = \frac{\left.\frac{dT}{dz}\right|_{z=0} - \left.\frac{dT}{dz}\right|_{z=z_1}}{z_0 - z_1}$$

But at z = 0, $\frac{dT}{dz} \cong 0$ hence, approximately,

$$\left.\frac{d^2T}{dz^2}\right|_{z=z_0} \approx \frac{1}{z_1 - z_0} \left.\frac{dT}{dz}\right|_{z=z_1}$$

This better estimate of $\frac{d^2T}{dz^2}$ is then used in the following equation, neglecting radiation (see Section 2.8.2)

$$T_{flame} \approx T - \frac{R_p^2 \lambda_p}{2K} \frac{1}{\Delta z} \frac{dT}{dz}$$

where

$R_p \approx 1.9 \times 10^{-3}$ cm

$\lambda_p \approx 1.79 \times 10^{-1}$ cal/sec-cm°K

$T \approx 675$ °K

$\left.\frac{dT}{dz}\right|_{z=.01cm} \approx 560$ °K/cm

$\Delta z \approx .01$ cm

Near the surface, the heat transfer coefficient, h , was found to be .021 cal/s-cm^2°K giving

$$K = R_p h = 4.79 \times 10^{-5} \text{ cal/sec °K}$$

These values give a better temperature estimate at the droplet surface of approximately 300°K. Since the curve of Figure 15 is an estimation of the temperature profile within the thermocouple wire based on observed temperatures, the conduction correction is based on local temperature gradients.

However, even this first approximation of the local gradient indicates the significance of conduction in this region. Above $r/r_\ell = 1.5$, it appears that the correction technique described in Section 2.8.2 gives a reasonable estimation of the conductive errors.

Another question regards the determination of the maximum flame temperature. As Figure 16 indicates, the gradient along the wire in this region of the flame is very flat. In a similar manner as previously described, the conductive error was estimated. In this region, the heat transfer coefficient was found to be about .03 cal/s-cm^2°K and the slope at $z = .02$ cm is approximately -150. This gives a conductive correction of 35°K. The radiative correction is found to be 80°K. These corrections yield a maximum flame temperature of 1829°K —170°K lower than predicted theoretically. In order to try to understand this difference, the sensitivity of the correction technique to the parameters which were estimated and subject to error was investigated. The estimated convection current velocity of 80 cm/s was doubled and halved. The effect on the flame temperature was only ±6°K. The overall heat transfer coefficient, h , which was calculated to vary depending on the position in the flame was also varied. Doubling this coefficient dropped the flame temperature by 40°K, while having it increased the flame temperature by about 85°K. Although halving the coefficient does increase the estimated flame temperature, no heat transfer references consulted would suggest the use of such a low value. One other possibility is that the radiative correction term is in error. Kaskan[25] has determined the emissivity of clear quartz coated platinum probes to be about .22 at the flame temperatures. In the hot portion of our flames, no carbon was observed to condense on the probe surface (implying an increase

in ϵ), however, the quartz coating did very slowly evaporate. The emissivity of platinum in the flame temperature range is about .2, therefore significant error appears unlikely in the estimation of the emissivity (i.e., the maximum flame temperature plotted in Figure 14 is probably correct within about 50°K).

The final possibility is that the theoretical prediction may be in error. The parameter which most affects the calculated flame temperature is the coefficient of specific heat. If the equation presented in Section 1.2 is used for calculating the maximum flame temperature and if the value for $\overline{C_p}$ as given by Lorell, Wise, and Carr[10] is used, the maximum flame temperature is found to be 2100°K. If that value for the specific heat is increased ten percent, the calculated flame temperature drops to 1935°K - a difference of 165°K. Since the value for specific heats rise rapidly at those temperatures, and since thermal dissociation of the species will increase the effective specific heat, it is possible that in the flame zone, temperatures may be lower than predicted.

It should also be pointed out that these apparent discrepancies between expected and measured temperatures have also been reported in the literature. Aldred, Patel, and Williams[30] studied the burning of spheres of liquid n-Heptane (boiling point of 371°K) and reported droplet "surface" temperatures of 750°K. Their maximum flame temperatures were 300°-400°K lower than their calculated value. They did not correct for conductive effects, nor did they discuss this aspect.

One of the more obvious discrepancies between theoretical prediction and experimental determination is the location of maximum temperature. Theoretically, this point is located at $r/r_\ell \approx 10$, however experimentally

it is found to be located at $r/r_\ell \approx 3.6$. (The ratio of the two values being 2.8). The cause and significance of this difference is discussed in the next section.

3.3 Gas Chromatograph Data

The basic flame structure is presented in Figures 17, 18, and 19 in terms of mole percent versus a non-dimensional distance from the drop center. The droplet was burned in a normal atmosphere under conditions of natural convection at one atmospheric pressure, and an ambient temperature between 300°K and 310°K. It is seen that the reproducibility of the major species profiles is very good. The minor species are generally in agreement except that in Runs No. 1 and 3, the data suggest a dip in the concentrations of CO, C_2H_6, and $C_2H_4+C_2H_2$ near $r/r_\ell = 1.3$. Run No. 3 was selected as the basis for comparison with theory since this run exhibited minimum scatter in the data, and because this run agreed qualitatively with Run No. 1. Although water was not directly analyzed, it was deduced as the principal specie not accounted for by the analyzed species. It should be kept in mind, however, that the profile for water in Figure 19 does contain small percentages (probably not more than a total of 3-4%) of compounds not analyzed (such as aldehydes). For calculation purposes, however, this profile was assumed to be H_2O.

Since the theoretical results are presented in terms of mass fraction, the data of Figure 19 were converted to mass fraction (percent) via the equation

$$Y_i = X_i \left(\frac{MW_i}{\sum X_i MW_i} \right)$$

where X_i is the mole fraction of species i. These data are plotted in

Figure 20. Several immediate observations can be made:

1) Even for these small droplet sizes, the flame is still compressed. The profiles are compressed by about a factor of 3 compared with the theoretical prediction. This could be a Bernoulli effect resulting from convection currents although simplifications in estimating the transport coefficients may also play a small role.

2) Calculated and experimental values for the mass fractions at the droplet surface are in excellent agreement (see Table 3).

Table 3

	Theoretical	Experimental
$Y_F (C_2H_5OH)$	0.75	0.735
$Y_P (CO_2+H_2O)$	0.075	0.09
$Y_{H_2} (N_2)$	0.14	0.18

3) Although oxygen is theoretically predicted to penetrate the flame zone, it is not predicted to be in measurable quantities at the droplet surface. The experimental data indicate oxygen pentration to the surface.

As is well known, a complex molecule such as ethanol generally pyrolyzes (thermally decomposes) to simpler compounds before it reaches the region where primary combustion is taking place (the region where heat is being rapidly released chemically). In the region where pyrolysis is taking place (somewhere between the droplet surface and the position where the ethanol concentration is zero), the net heat release is negative, i.e., more energy is consumed in the pyrolysis reactions than is released by

reaction. In order to gain a better understanding of the region where pyrolysis is occuring, the experimental data was used to calculate the rate of disappearance of ethanol at several positions. This was done with the help of the conservation of species equation (see Appendix A):

$$\frac{d}{dr}\left[r^2\left(\rho Y_i v_i + \rho Y_i v\right)\right] = \omega_i$$

By employing Fick's Law,

$$Y_i v_i = -D \frac{d}{dr} Y_i$$

global continuity, $\dot{M} = 4\pi r^2 \rho v$

and assuming $\overline{\rho D}$ = constant

we obtain

$$\omega_i = \frac{\partial Y_i}{\partial r}\left[\frac{\dot{M}_F}{4\pi r^2} - \frac{2\overline{\rho D}}{r}\right] - \overline{\rho D}\ \frac{\partial^2 Y_i}{\partial r^2}$$

The value for $\dot{M}$ is 9.25×10^{-4} gm/s for r_ℓ = .66 mm. An average value for $\overline{\rho D}$ was obtained from the following equation[13] evaluated at the droplet surface and at the position where the ethanol concentration is zero.

$$\rho D \approx D^\circ \frac{p^\circ T^{\nu-1}}{T^{\circ\nu}} \frac{\overline{MW}}{R}$$

where

$$p^\circ = 1.013 \times 10^6 \text{ dynes/cm}^2$$
$$T^\circ = 273.2\ ^\circ\text{K}$$
$$\nu \approx 1.6$$

and $$D^{\circ} \approx .15 \text{ cm}^2/\text{s}$$

From this we obtain $$\overline{\rho D} \approx 3.845 \times 10^{-4} \text{ gm/cm-s}$$

Since the species profiles are not known as explicit functions, standard finite difference methods using equally spaced data were employed to calculate the derivatives of Y_i. The data points were obtained from the best curves fitted through the experimental data. Letting the subscripts 0, 1, 2 indicate the order of the data, the following formulas were used to calculate the derivatives of Y_i :

$$\left.\frac{\partial Y_i}{\partial r}\right|_{r_1} \approx \frac{Y_{i_2} - Y_{i_0}}{r_2 - r_0}$$

and

$$\left.\frac{\partial^2 Y_i}{\partial r^2}\right|_{r_1} \approx \frac{Y_{i_0} - 2Y_{i_1} + Y_{i_2}}{(\Delta r)^2}$$

where $\Delta r = r_2 - r_1 = r_1 - r_0$

The results from these calculations are shown in Figure 21. Maximum rate of ethanol decomposition appears to occur around a position of $r/r_\ell \approx 1.3$. In this region, the temperature is between 600°K and 800°K. Little information is available on ethanol decomposition, but it appears that Freeman[32] has conducted one of the more complete studies. He investigated ethanol decomposition at 798°K and concluded that it decomposes via two mechanisms:

$$C_2H_5OH \rightarrow CH_3CHO + H_2$$

$$C_2H_5OH \rightarrow C_2H_4 + H_2O$$

He also concluded that the overall decomposition is first order when the initiating step is first order and deduced the following mechanism to explain his results

$$C_2H_5OH \rightarrow C_2H_4 + H_2O \quad (1)$$

$$C_2H_5OH \rightarrow CH_3CHO + H_2 \quad (2)$$

$$C_2H_5OH \rightarrow CH_3 + CH_2OH \quad (3)$$

$$CH_3 + C_2H_5OH \rightarrow CH_4 + CH_3CHOH \quad (4)$$

$$CH_3 + C_2H_5OH \rightarrow CH_4 + CH_2CH_2OH \quad (5)$$

$$CH_3CHOH \rightarrow CH_3CHO + H \quad (6)$$

$$CH_2CH_2OH \rightarrow C_2H_4 + OH \quad (7)$$

$$H(OH) + C_2H_5OH \rightarrow H_2(H_2O) + CH_3CHOH \quad (8)$$

$$H(OH) + C_2H_5OH \rightarrow H_2(H_2O) + C_2H_2CH_2OH \quad (9)$$

$$CH_2OH \rightarrow HCHO + H \quad (10)$$

$$CH_2OH + C_2H_5OH \rightarrow CH_2OH + CH_3CHOH(CH_2CH_2OH) \quad (11)$$

$$H(OH,CH_3) + CH_2CH_2OH \rightarrow end \quad (12)$$

$$H(OH,CH_3) + CH_3CHOH \rightarrow end \quad (13)$$

He concluded that reactions (4) and (8) are five times as frequent as (5) and (9). We see that this mechanism predicts the observed CH_4, C_2H_4, and H_2O.

The rate of formation of CO_2 was next calculated. The same technique was used except that an average $\overline{\rho D}$ was recalculated using the values at the surface and at the position of maximum temperature. The results of these calculations are plotted in Figure 22. There are apparently two regions of almost equal importance in which CO_2 is formed. One is in the flame zone and the other occurs around $r/r_2 \approx 1.3$. Apparently, in addition to the thermal decomposition of ethanol, partial oxidation is also occuring in the same region. Since CH_3 and OH radicals plus oxygen would exist in this region, the following reactions are probably important:

$$CH_3CH_2OH \rightarrow CH_3CHOH + HO_2$$
$$CH_3CHOH + O_2 \rightarrow CH_3CHO + O_2$$
$$CH_3 + O_2 \rightarrow HCHO + CO$$
$$OH + HCHO \rightarrow H_2O + CO + H$$
$$OH + C_2H_4 \rightarrow HCHO + CH_2$$
$$CO + OH \rightarrow CO_2 + H$$
$$CO + HO_2 \rightarrow CO_2 + OH$$

3.4 Nitric Oxide Data

Nitric oxide profiles for pure ethanol and for ethanol seeded with various percentages are shown in Figures 23-31. Theoretically, the maximum NO concentration calculated for pure ethanol is about 20 ppm. Experimentally, we

measured about 48 ppm. Since the rate constants for the kinetic mechanism used to calculate NO formation are fairly well established (see Appendix A), the difference between the two numbers is probably accounted for in three ways: 1) Inaccuracies inherent in the present equipment design and data reduction methods, 2) Invalid assumptions regarding equilibrium oxygen concentrations and steady state N used to predict NO (see Appendix A), 3) Approximation of the transport and/or thermodynamic properties in the flame structure calculation.

Under given droplet burning conditions, only one theoretical calculation has been done for NO formation from fuel nitrogen. For a fuel nitrogen content of 1%, it was found that the maximum NO concentration increased to 360 ppm. Experimentally, we measured maximum NO concentrations near 800 ppm. The differences again are probably due to the same considerations previously discussed, however, there is one other consideration. In arriving at 360 ppm, it was assumed that the nitrogen compound released N atoms which create a new steady state N concentration. These assumptions were necessary for lack of any better kinetic data. As described in Section 1.3, recent research indicates, however, that nitrogen is not released as atoms but reacts via active intermediates and radicals. Still, the calculations performed by Bracco are useful for predicting trends.

The results from this work do confirm the suggestion that diffusion flames can be a very strong source of NO from nitrogen containing fuels. Published data for NO formation in diffusion flames is scarce, but recent work by Williams[11] on a 5.85 mm radius cylinder burning under our conditions indicates NO concentrations in the forward stagnation region of the flame zone to be 3 ppm for pure ethanol and the same order of magnitude for

for ethanol containing .1% wt. pyridine. Between the liquid surface and the flame zone he measured concentrations an order of magnitude higher for ethanol-pyridine than for pure ethanol. His conclusion is that most of the NO is destroyed in the flame zone. His measurements are an order of magnitude lower than ours and no conclusion regarding destruction of NO can be made based on the data of our work. Even though Williams' studies were on cylinders, there appears to be a fundamental discrepancy between his observed trends and the trends reported in this work. Figure 32 is a plot of peak NO ppm versus molar percent pyridine in ethanol. The range is from 190 ppm for .1% fuel N to about 1200 ppm for 4% fuel N. It is difficult to make definitive statements from the plots of Figures 32 and 33 which are based only on peak NO measured. They do strongly suggest however (with some physical justification) that as the amount of N in the fuel increases, its effectiveness in enhancing the production of NO decreases. This would appear to result in a larger fraction of the nitorgen forming N_2 and possibly other nitrogen compounds due to an insufficient oxygen concentration in the regions where NO is formed.

CHAPTER V

CONCLUSIONS AND RECOMMENDATIONS

4.1 Conclusions

The following are the primary conclusions regarding the equipment and experimental technique:

a) Using ethanol as a fuel, a one to two millimeter diameter droplet is a good choice for reducing gravitational effects to a minimum while still permitting flame structure studies.

b) The gas chromatograph and the general sampling technique reduces data scatter to a minimum and thus reproduces the flame structure very well.

c) The NO analyzer reproduces NO profiles with an accuracy better than 10% in most cases.

d) The thermocouple technique is useful for obtaining temperature profiles. The use of the smallest possible thermocouple wire (.0005 in or less) cannot be over emphasized if the desire is to minimize conductive effects. This was a major obstacle in obtaining trustworthy data.

The following primary conclusions were drawn after data reduction:

a) The conductive effects along the thermocouple wire can reasonably be taken into account by a simple estimation technique.

b) The maximum flame temperature measured is lower than the predicted temperature by about 200°K. Error in the measured temperature is probably by no more than 50°-70°K.

c) Gas composition and the droplet surface temperature are in excellent agreement with theory.

d) Oxygen penetration to the droplet surface is significant.

e) Although the flame structure is compressed when compared with theory, the effect is not as severe as reported in the literature, primarily because of the small droplet sizes used here.

f) Pyrolysis and partial oxidation of ethanol occur very near the droplet surface.

g) Production of nitric oxide is greater than predicted theoretically, both for pure ethanol, and for ethanol containing pyridine.

h) Diffusion flames are significant sources of NO when the fuel contains nitrogen.

4.2 Recommendation for Future Work

The study of chemical kinetic processes using a diffusion flame as the technique is extremely difficult. Whenever possible, a flow reactor technique as employed in Professor Glassman's laboratory should be used for such studies. Since the conversion of fuel nitrogen to nitric oxide is felt to be primarily a chemical rather than a thermal conversion, a flow reactor study would appear appropriate because the extremely high temperatures required to dissociate the nitrogen molecule are not required.

Since fuel nitrogen compounds are very complex molecules, it is doubtful that specific chemical kinetic reactions and rates can be obtained using current knowledge. However, overall rate constants for the disappearance of the nitrogen compound and the appearance of nitric oxide could be obtained. This information could then be applied to a theoretical study of droplet burning.

The study of the structure of droplet diffusion flames could yield some very useful information. The following suggestions may answer several

important questions:

a) In furnace studies, the conversion of fuel nitrogen to nitric oxide appears to be independent of the molecular structure of the nitrogen compound. Thus, ethanol could be seeded with many different nitrogen compounds to confirm whether the same result applies to individual droplet burning.

b) Previous studies assumed or concluded that thermal and fuel nitrogen conversion to nitric oxide were independent and uncoupled processes. It would seem that confidence in this result could be improved (or shattered) by obtaining nitric oxide profiles for seeded ethanol drops burning in an atmosphere in which the nitrogen has been replaced by argon or neon. These would then be compared with the same droplets burning in a normal atmosphere. If the results differ by the same constant, then the current conclusions would be strengthened.

c) Effect on the general flame structure could be studied by 1) varying the ambient temperature, 2) varying the composition of the atmosphere both in relative amounts and in constituency, 3) variation of the ambient pressure, and 4) variation in droplet size.

d) It is well known that pyridine will dissolve many of the organic compounds which generally constitute coal. Therefore, it may be possible to study certain aspects of coal combustion via a liquid droplet route.

REFERENCES

1. Martin, G. B. and Berkau, E. E., "An Investigation of the Conversion of Various Fuel Nitrogen Compounds to Nitrogen Oxides in Oil Combustion", Air Pollution and Its Control, Vol. 68, 1972, AIChE Symposium Series, pp. 45-54.

2. Turner, D. W., Andrews, R. L., and Siegmund, C. W., "Influence of Combustion Modification and Fuel Nitrogen Content on Nitrogen Oxide Emissions from Fuel Oil Combustion", Air Pollution and Its Control, Vol. 68, 1972, AIChE Symposium Series, pp. 55-65.

3. Tipper, C. F. H., "Notes on Spray Combustion", Oxidation and Combustion Reviews, Vol. 3, 1968, pp. 3-5.

4. Williams, A., "Combustion of Droplets of Liquid Fuels: A Review", Combustion and Flame, Vol. 21, 1973, pp. 1-31.

5. Godsave, G. A. E., "Studies of the Combustion of Drops in a Fuel Spray - the Burning of Single Dropes of Fuel", Fourth Symposium (International) on Combustion, The Standing Committee on Combustion Symposia, MIT, September 1-5, 1952, pp. 818-829.

6. Spalding, D. B., "The Combustion of Liquid Fuels", Fourth Symposium (International) on Combustion, The Standing Committee on Combustion Symposia, MIT, September 1-5, 1952, pp. 847-864.

7. Wise, H. and Agoston, G. A., "Burning of a Liquid Droplet", Literature of the Combustion of Petroleum, Advances in Chemistry Series, No. 2, 1958, The American Chemical Society, pp. 116-119.

8. Krier, H. and Wronkiewicz, J. A., "Combustion of Single Drops of Fuel", Combustion and Flame, Vol. 18, 1972, p. 159.

9. Williams, A., "The Mechanism of Combustion of Droplets and Sprays of Liquid Fuels", Oxidation and Combustion Reviews, Vol. 3, 1968, pp. 12-13.

10. Lorell, J., Wise, H., and Carr, R., "Steady-State Burning of a Liquid Droplet, II. Bipropellant Flame", Journal of Chemical Physics, Vol. 25, 1956, pp. 325-331.

11. Dracco, F. V., "Nitric Oxide Formation in Droplet Diffusion Flames", Presented at the Fourteenth Symposium (International) on Combustion, The Combustion Institute, Pittsburgh, Pennsylvania, 1973, pp. 831-842.

12. Fenimore, C. P., "Formation of Nitric Oxide from Fuel Nitrogen in Ethylene Flames", Combustion and Flame, Vol. 19, 1972, pp. 289-296.

13. Bracco, F. V., "Investigation of the Mechanism and Chemistry of Fuel Nitrogen Conversion to Nitric Oxides in Flames", Proposal for an Environmental Protection Agency Grant No. R-800844, June 1972 - March 1973.

14. Williams, F. A., Combustion Theory, (Reading, Massachusetts: Addison Wesley Company, 1965).

15. Dickerson, R. E., Molecular Thermodynamics, (New York: W. A. Benjamin, Inc., 1969) p. 427.

16. Wise, H., Lorell, J., and Wood, B., "The Effects of Chemical and Physical Parameters on the Burning Rate of a Liquid Droplet", Fifth Symposium (International) on Combustion, The Standing Committee on Combustion Symposia, University of Pittsburgh, August 30-September 3, 1954, pp. 132-141.

17. Fristrom, R. M., Prescott, R., and Greenfelder, C., "Flame Zone Studies III - Techniques for the Determination of Composition Profiles of Flame Fronts", Combustion and Flame, Vol. 1, 1957, pp. 102-113.

18. Smith, S. R. and Gordon, A. S., "Recombination Reactions in Hydrocarbon Diffusion Flames: The Paraffin Candle Flame", Journal of Chemical Physics, Vol. 22, 1954, p. 1150.

19. Westenberg, A. A., Raezer, S. D. and Fristrom, R. M., "Interpretation of the Sample Taken by a Probe in a Laminar Concentration Gradient", Combustion and Flame, Vol. 1, No. 4, December 1957, pp. 467-478.

20. Prescott, R., Hudson, R., Forner, S., and Avery, W., "Composition Profiles in Pre-Mixed Laminar Flames", Journal of Chemical Physics, Vol. 22, 1954, p. 145.

21. Fristrom, R. M. and Westenburg, A. M., Flame Structure, (New York: McGraw-Hill Book Company, Inc., 1965) pp. 180-196.

22. Vincenti, W. G. and Kruger, C. H., Introduction to Physical Gas Dynamics, (New York: John Wiley and Sons, Inc., 1967) p. 25.

23. McNair, H. M. and Bonelli, E. J., Basic Gas Chromatography, (Berkeley, California: Consolidated Printers, 1968).

24. Sigsby, J. E., Black, F. M., Bellar, T. A., and Klostersmar, D. L., "Chemiluminescent Method for Analysis of Nitrogen Compounds in Mobile Source (NO, NO_2, and NH_3)", Journal of the Air Pollution Control Association, Vol. 7, January 1973, p. 51.

25. Kaskan, W. E., "The Dependence of Flame Temperature on Mass Burning Velocity", Sixth Symposium (International) on Combustion, The Standing Committee on Combustion, University of Pittsburgh, August 30-September 3, 1954, pp. 134-143.

26. Bascombe, K. N., "Hydrogen Atom Concentrations in Hydrogen O_2/N_2 Flames", Tenth Symposium (International) on Combustion, The Combustion Institute, Pittsburgh, Pennsylvania, 1965, pp. 55-64.

27. Freidman, R., "Measurement of the Temperature Profile in a Laminar Flame", Fourth Symposium (International) on Combustion, The Standing Committee on Combustion Symposia, MIT, September 1-5, 1952, p. 259.

28. Hsu, S. T., Engineering Heat Transfer, (Princeton, New Jersey: D. Van Nostrand Company, Inc., 1963) p. 332.

29. Agoston, G. A., Wise, H., and Rosser, W. A., "Dynamic Factors Affecting the Combustion of Liquid Spheres", Sixth Symposium (International) on Combustion, The Standing Committee on Combustion Symposia, University of Pittsburgh, August 30 - September 3, 1954, pp. 708-717.

30. Aldred, J. W., Patel, J. C., and Williams, A., "The Mechanism of Combustion of Droplets and Spheres of Liquid n - Heptane", Combustion and Flame, Vol. 17, 1971, pp. 139-148.

31. Bowman, C., "Kinetics of Nitric Oxide Formation in Combustion Processes", Forteenth Symposium (International) on Combustion, The Combustion Institute, Pittsburgh, Pennsylvania, 1967, pp. 729-737.

32. Freeman, G. R., "The Thermal Decomposition of Diethyl Ether V. The Production of Ethanol from Diethyl Ether and the Pyrolysis of Ethanol", Proceedings of the Royal Society, Series A, Mathematical and Physical Sciences, Vol. 245, May 6, 1958, pp. 75-83.

33. Chapman, A., Heat Transfer, (Toronto, Canada: The MacMillan Company, 1969).

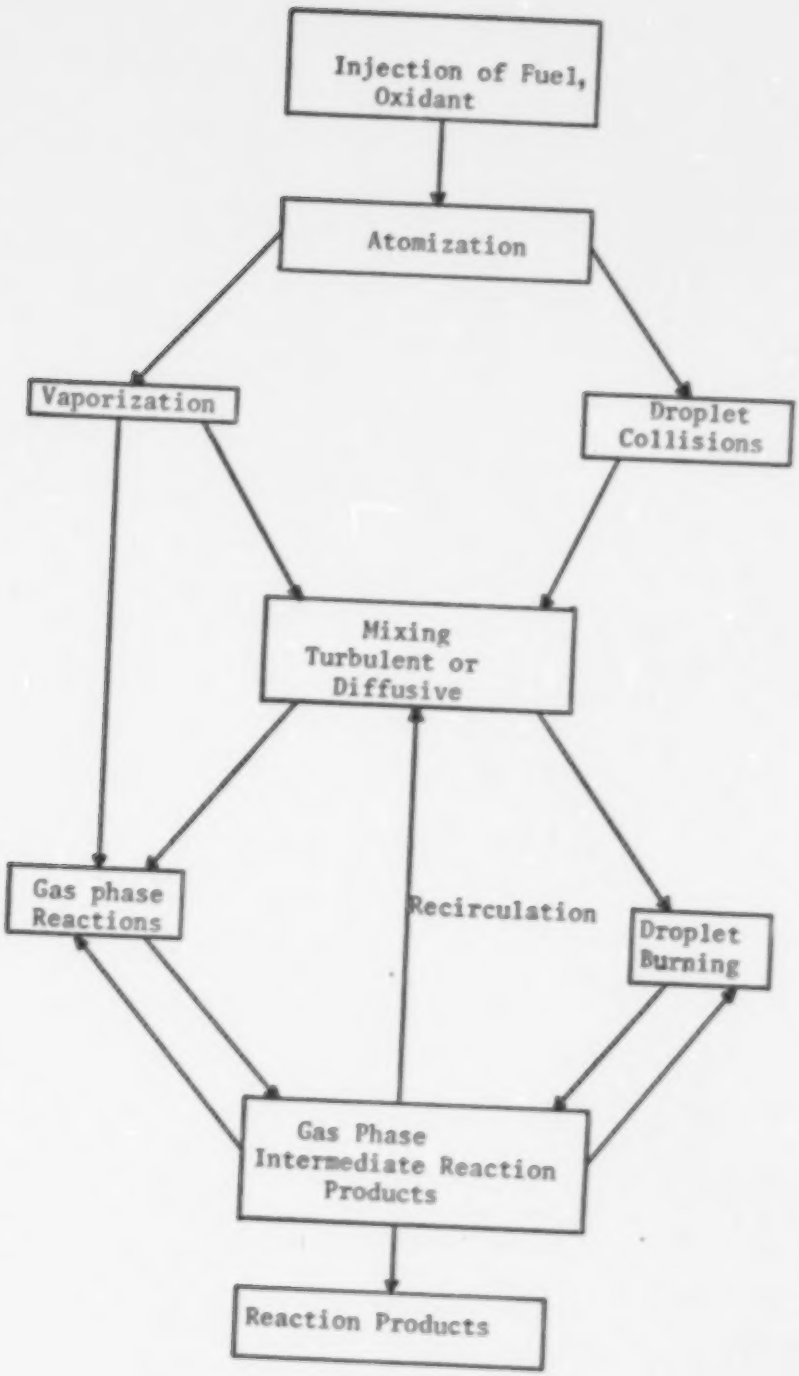

FIGURE 1: SCHEMATIC OF THE BASIC SPRAY COMBUSTION PROBLEM

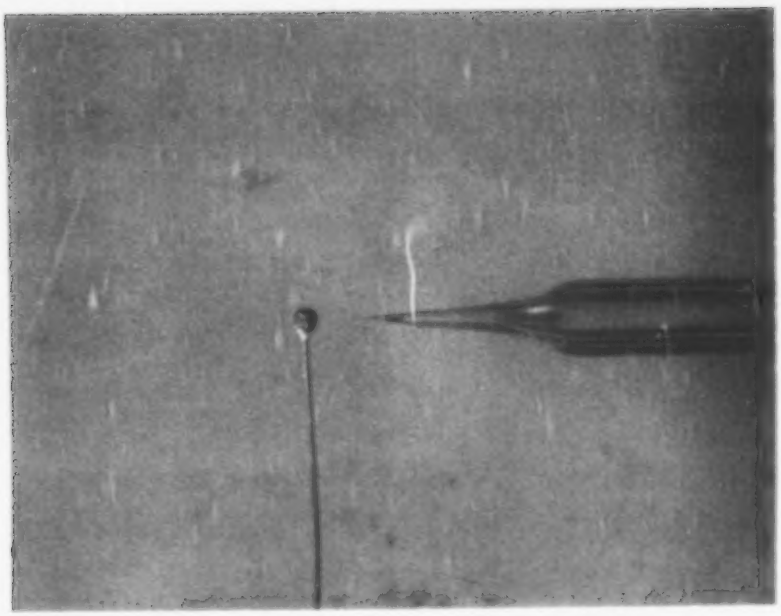

(a)

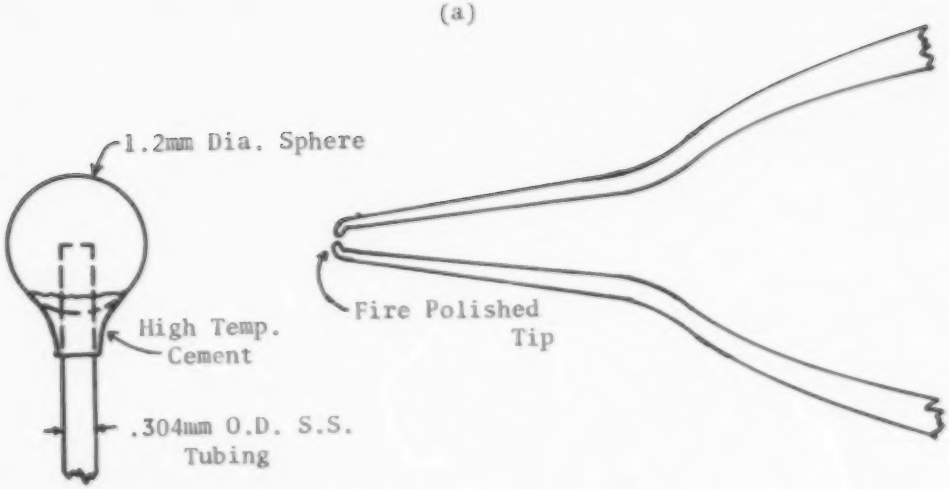

(b) (c)

· FIGURE 2 : PHOTO OF DROPLET AND QUARTZ PROBE WITH SKETCHES SHOWING CONSTRUCTION DETAILS

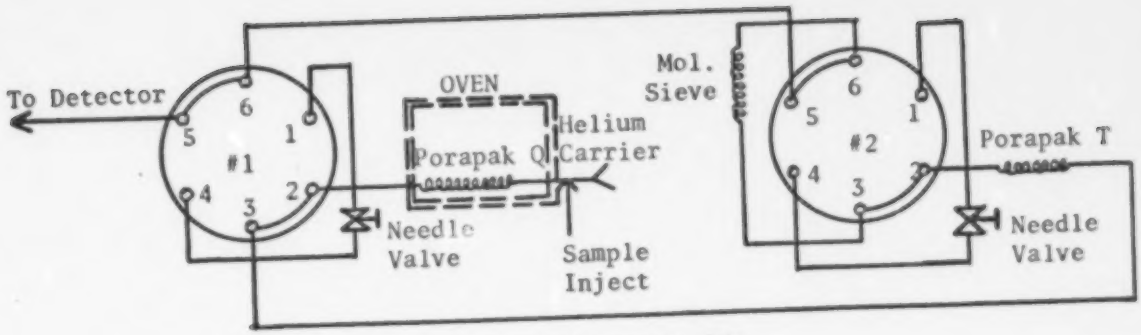

POSITION (a)

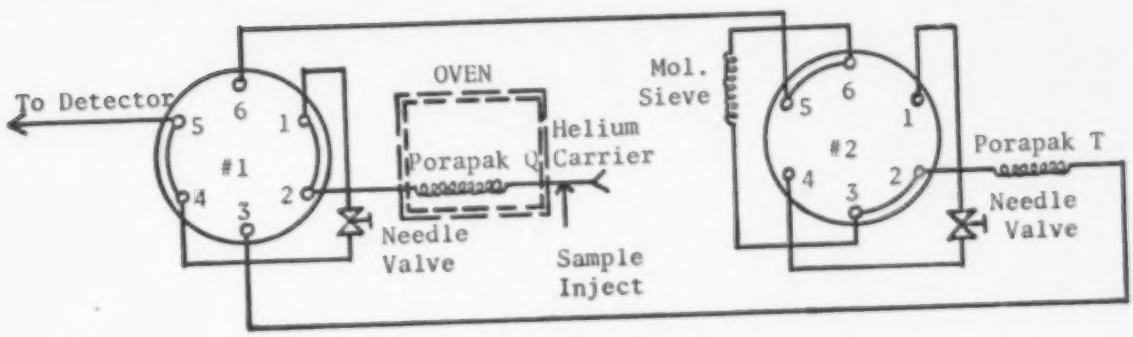

POSITION (b)

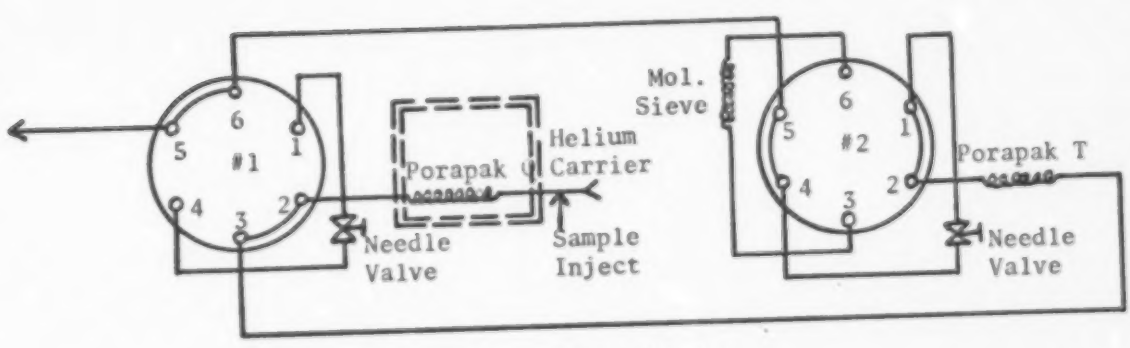

POSITION (c)

NOTE: Valve Reference Numbers Oriented By Viewing From Tube End.

FIGURE 3 : MODIFIED CHROMATOGRAPH SYSTEM

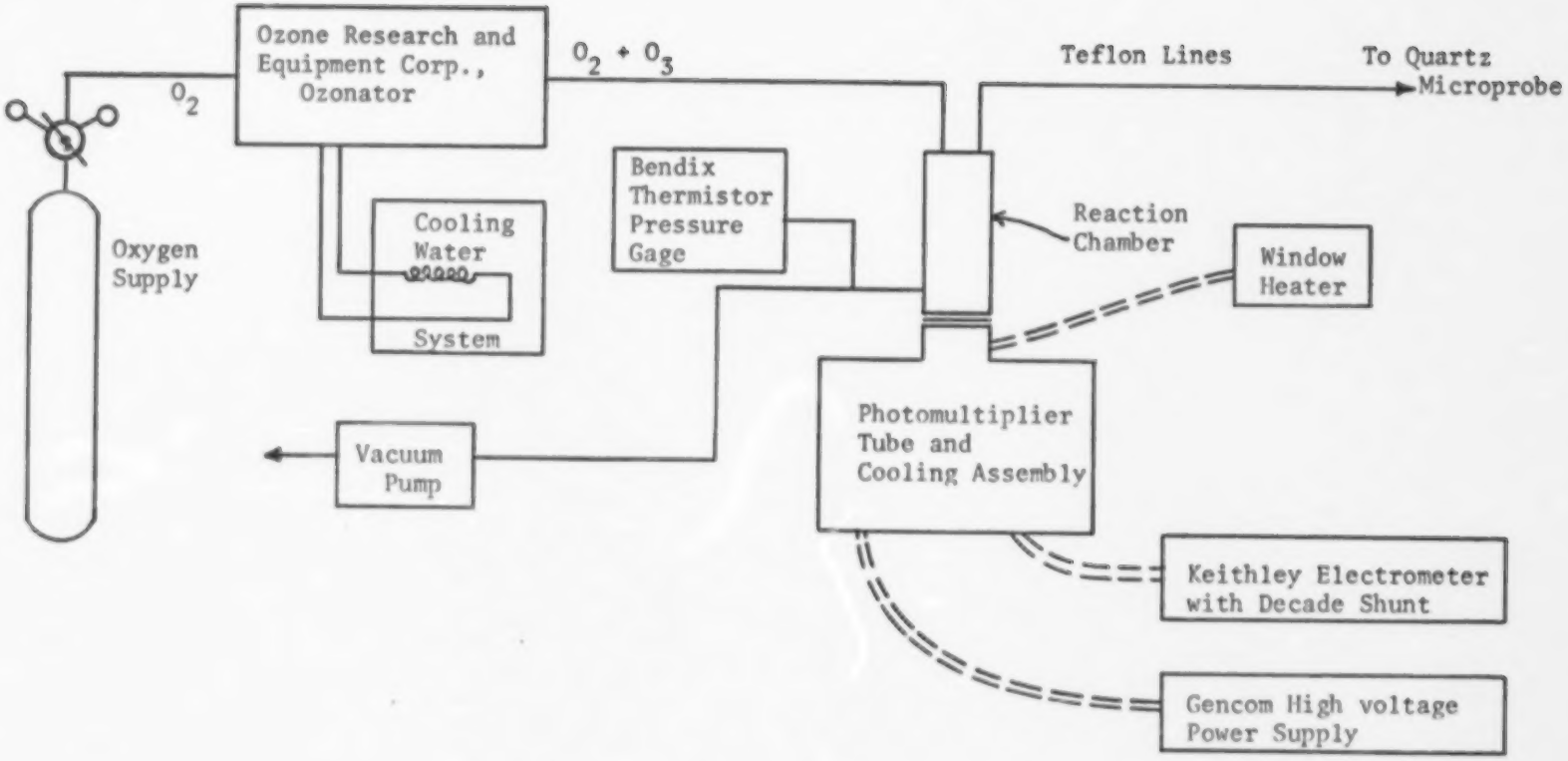

FIGURE 4 : CHEMILUMINESCENT NO ANALYZER

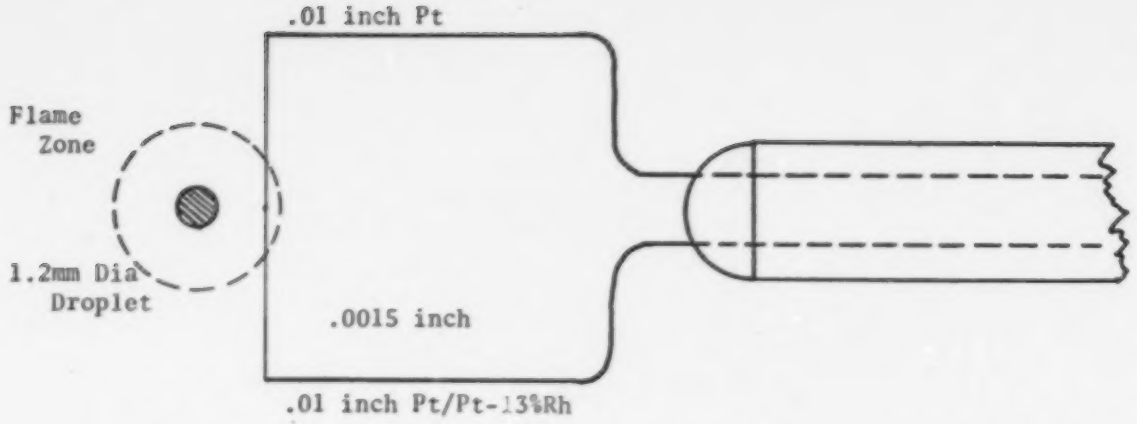

FIGURE 5 : TOP VIEW OF THERMOCOUPLE AND PROBING TECHNIQUE

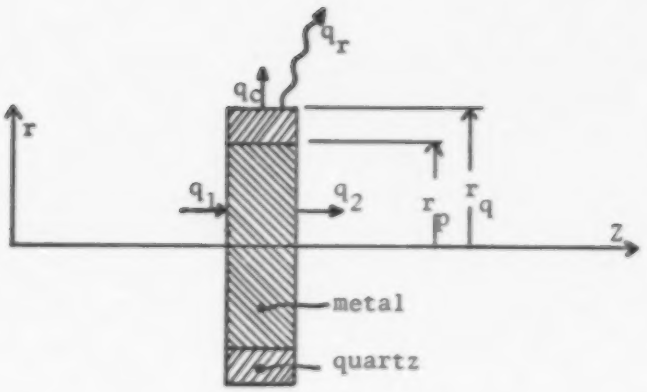

FIGURE 6 : THERMOCOUPLE ELEMENT

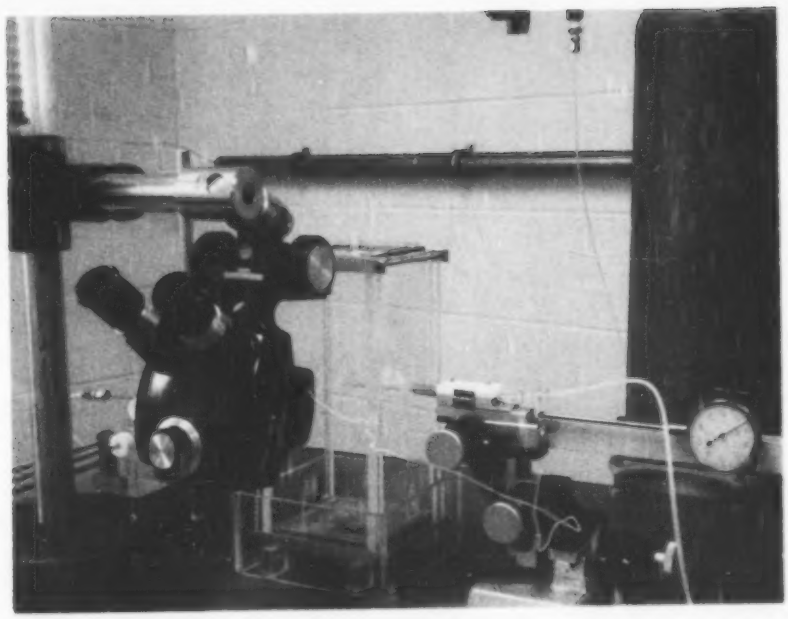

FIGURE 7 : PHOTOGRAPH SHOWING EXPERIMENTAL ARRANGEMENT

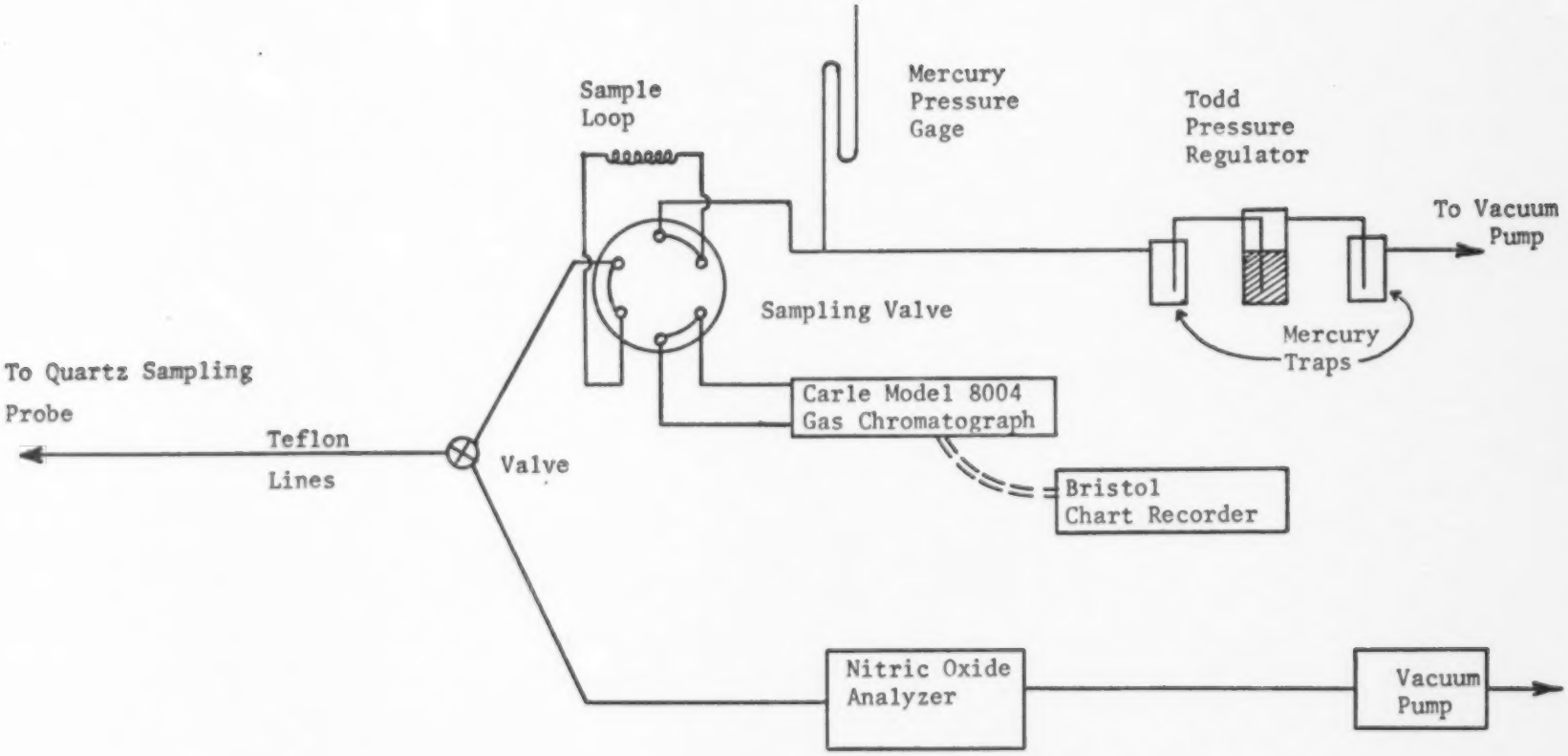

FIGURE 8: GAS ANALYSIS SYSTEM

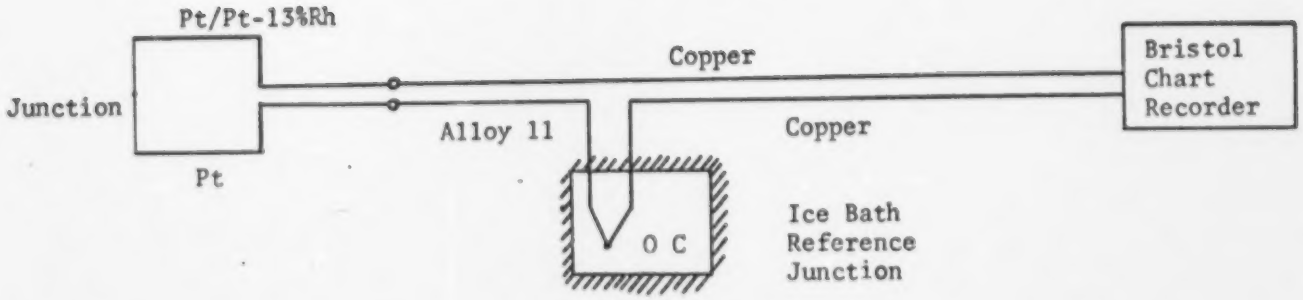

FIGURE 9 : THERMOCOUPLE TEMPERATURE ANALYSIS SYSTEM

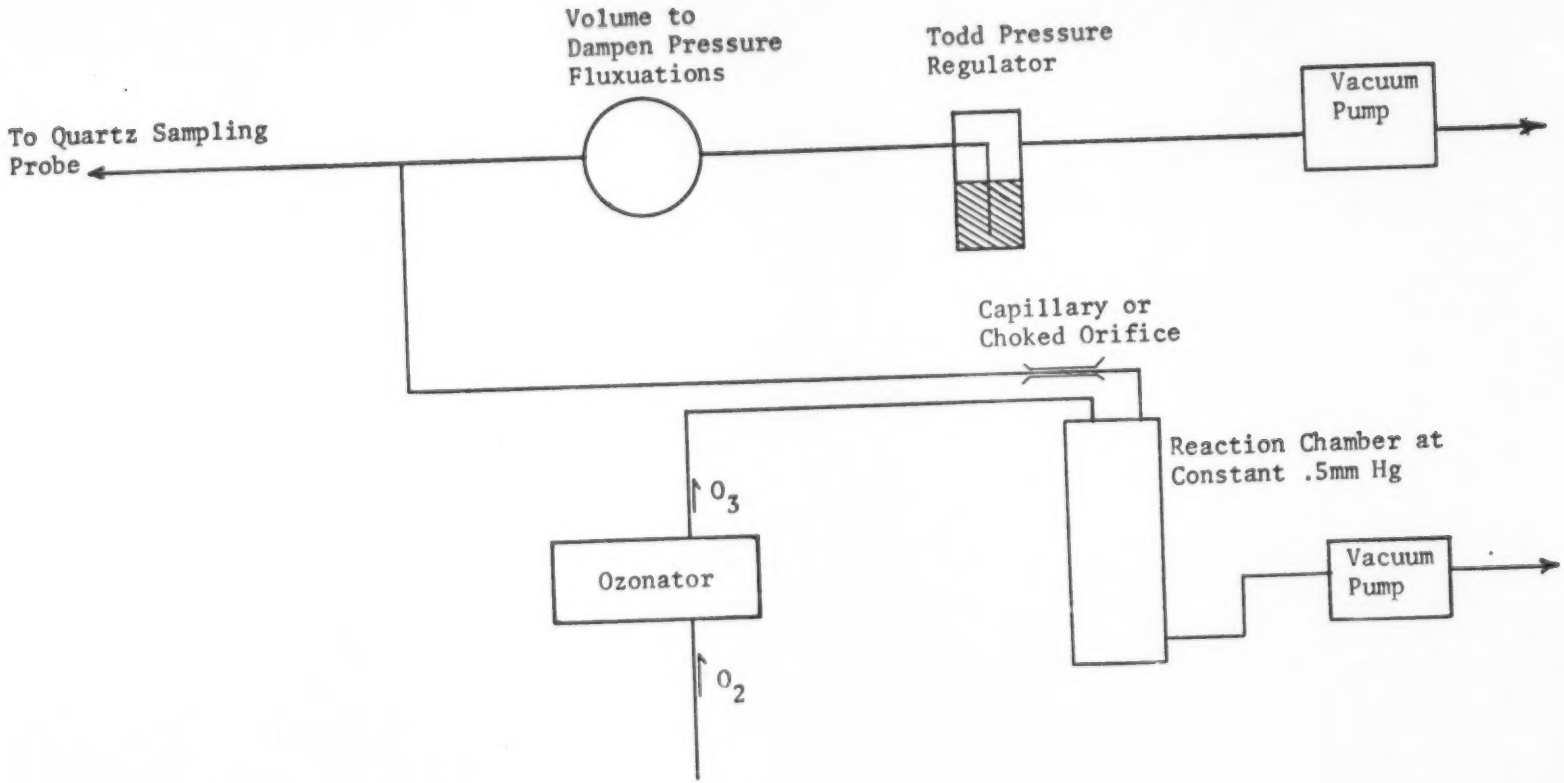

FIGURE 10 : SUGGESTION FOR NO ANALYZER IMPROVEMENT

(see Appendix B)

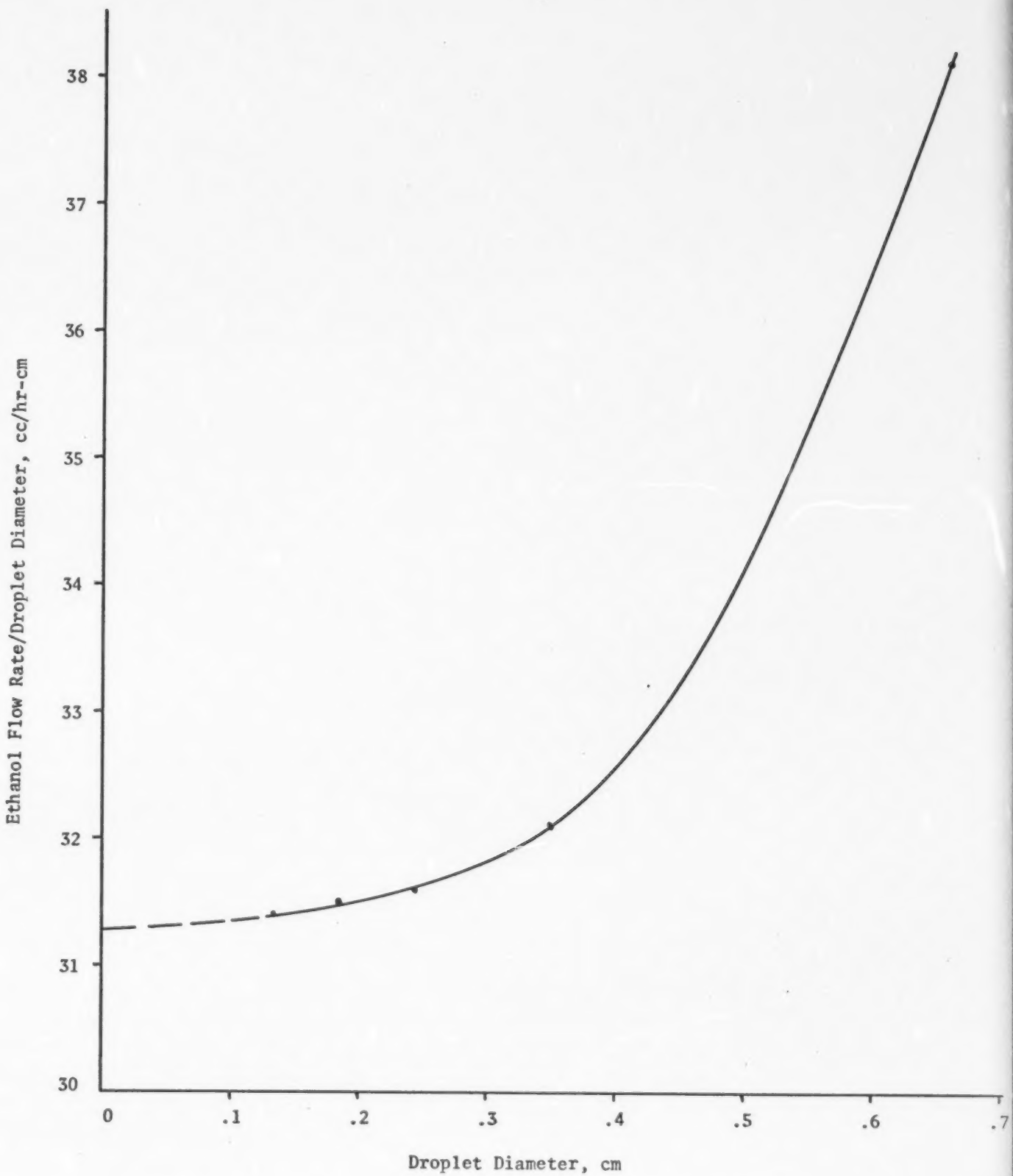

FIGURE 11: DROPLET BURNING RATES VERSUS DIAMETER

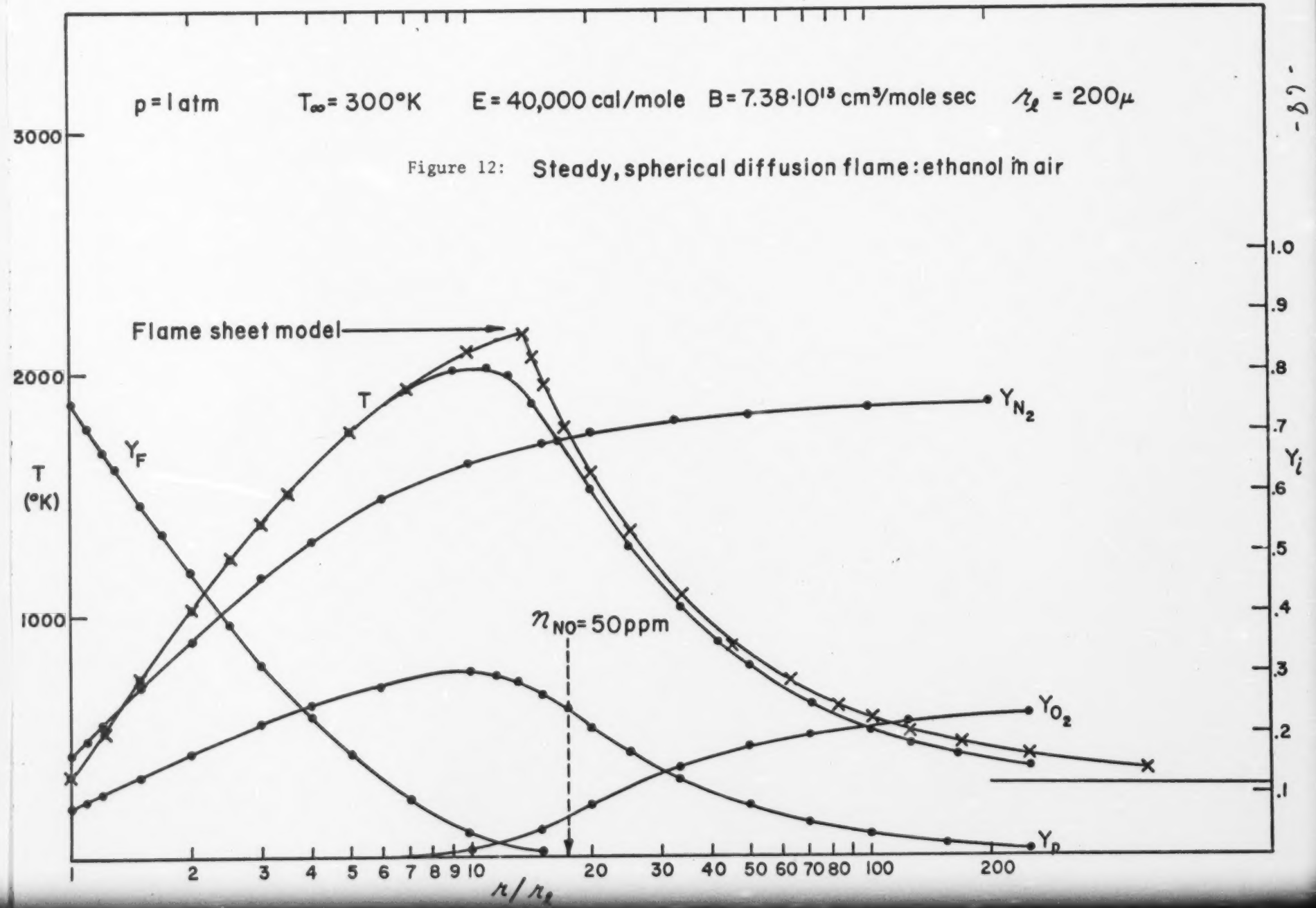

Figure 12: Steady, spherical diffusion flame: ethanol in air

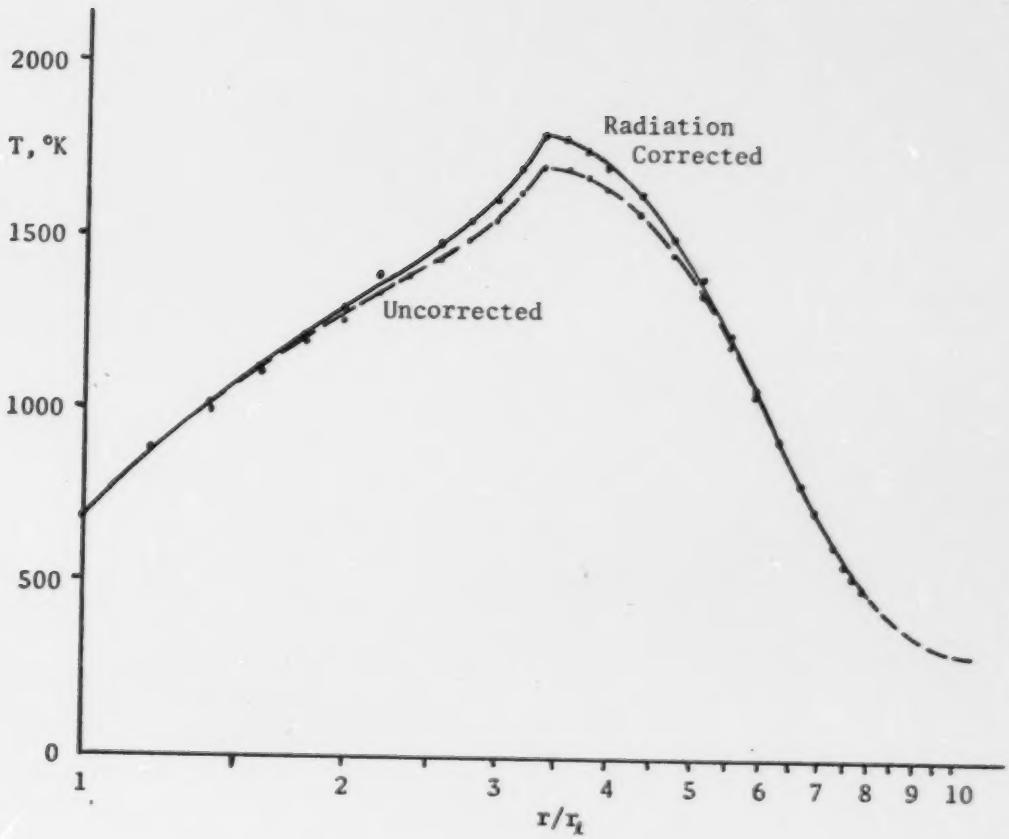

FIGURE 13: TEMPERATURE PROFILES FOR A .648mm RADIUS ETHANOL DROPLET

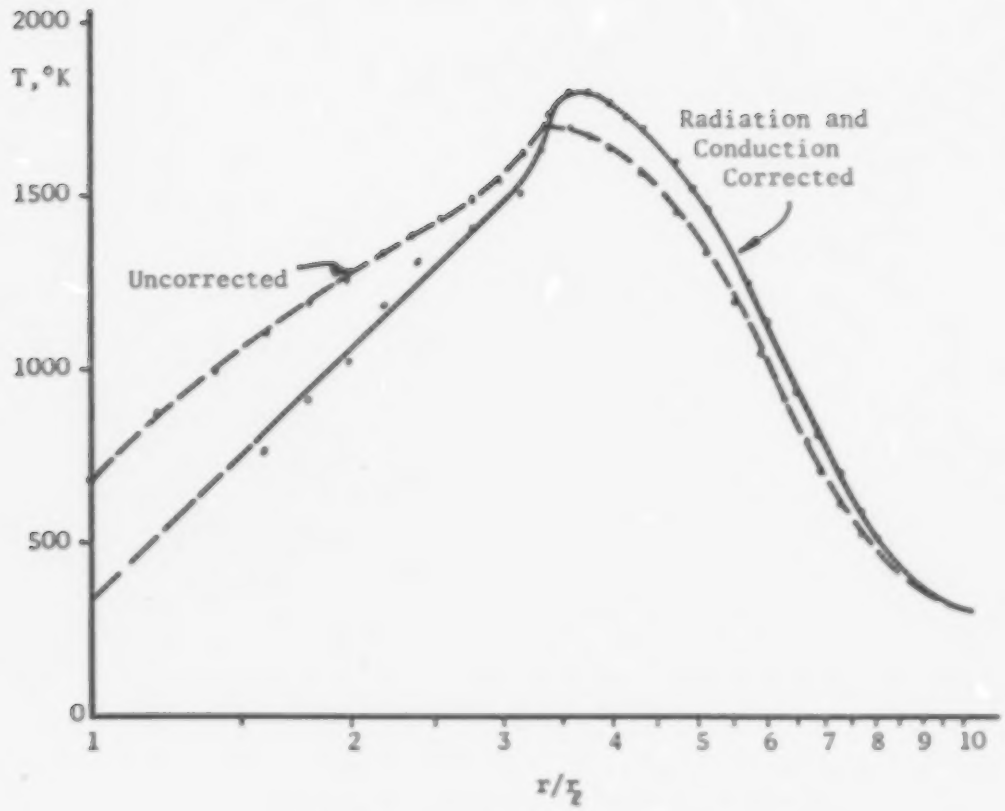

FIGURE 14: TEMPERATURE PROFILES FOR A .648mm RADIUS ETHANOL DROPLET

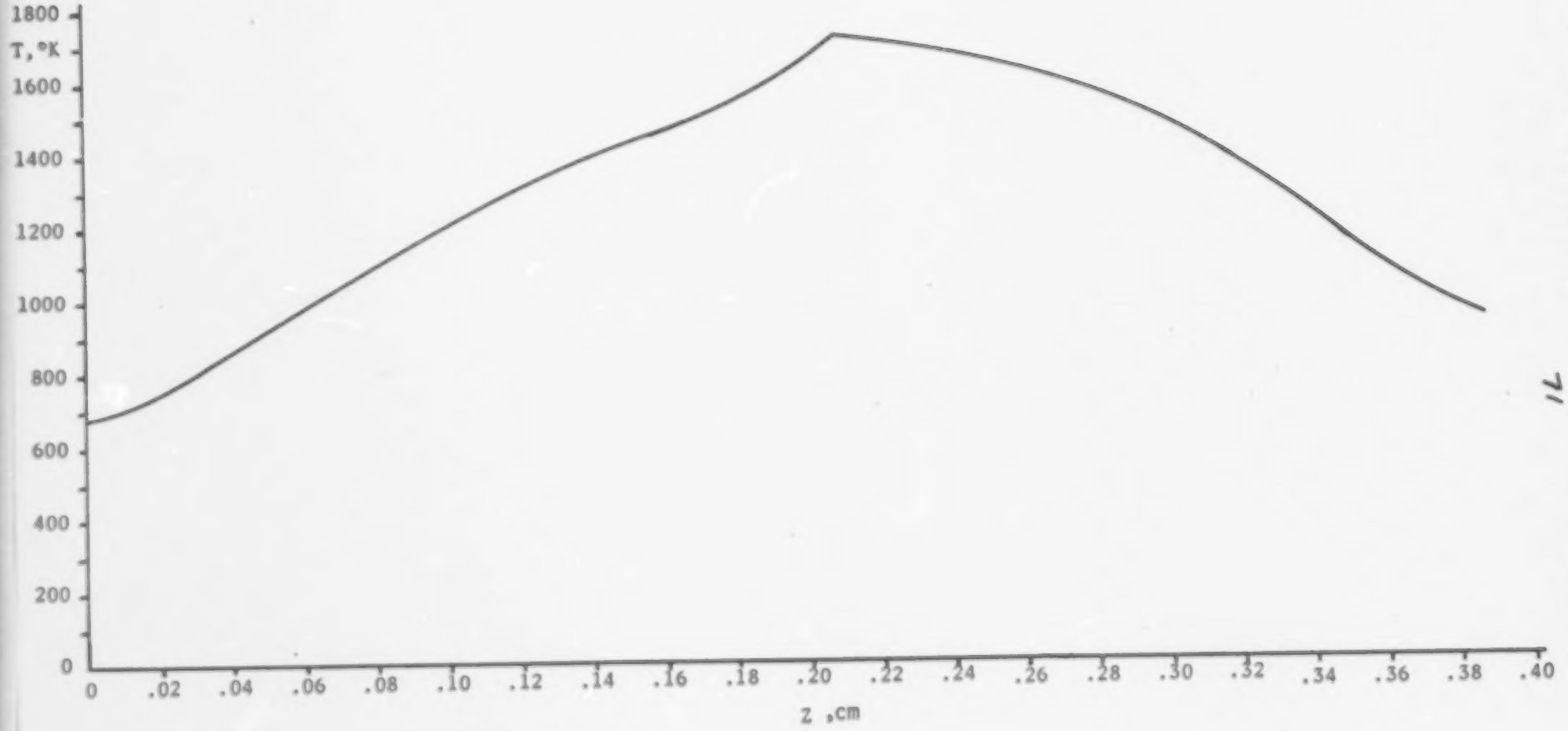

FIGURE 15: UNCORRECTED TEMPERATURE DISTRIBUTION ALONG THERMOCOUPLE WIRE. JUNCTION POSITION AT r/r_j =1.0. Z=0 DENOTES JUNCTION.

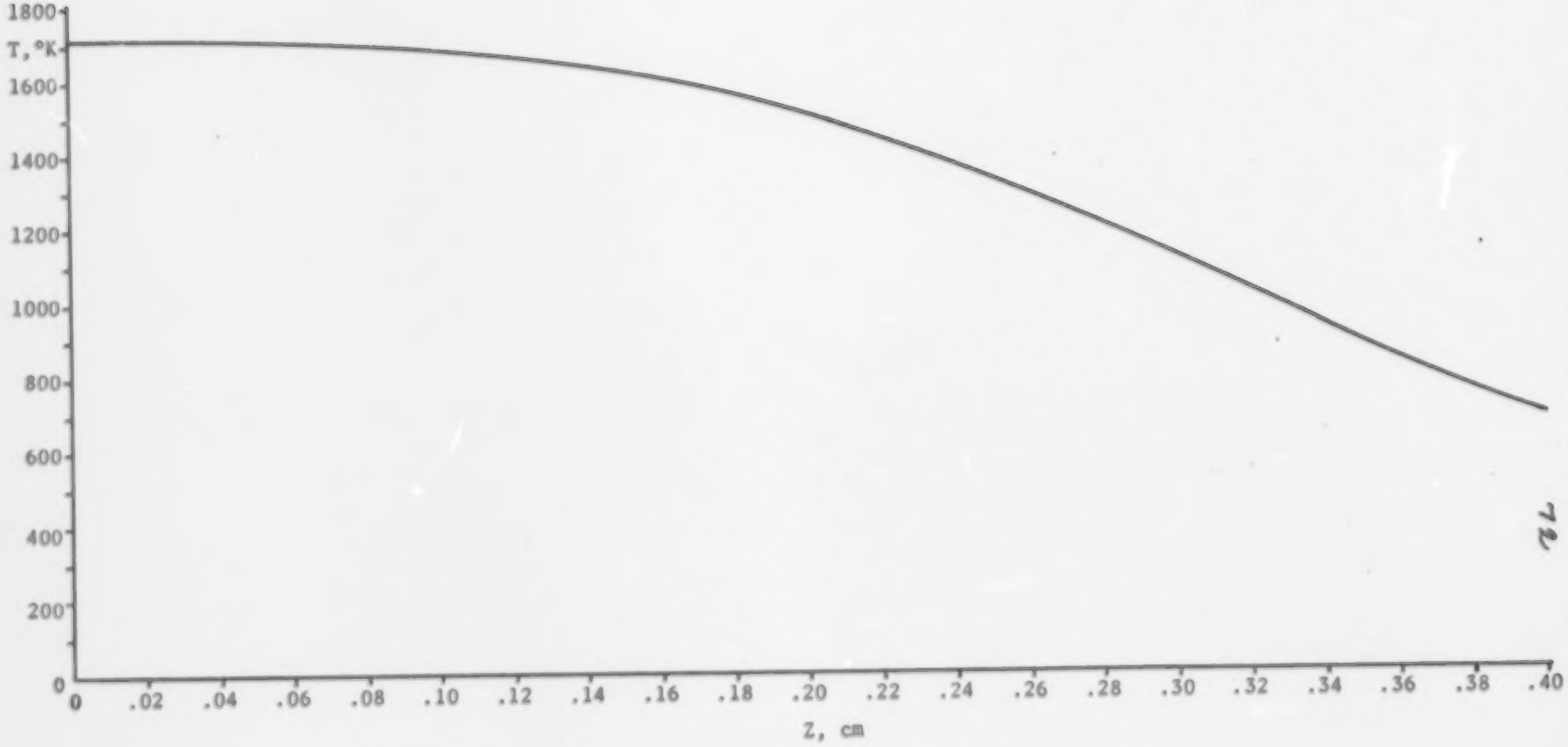

FIGURE 16: UNCORRECTED TEMPERATURE DISTIBUTION ALONG THERMOCOUPLE WIRE. JUNCTION POSITION AT r/r_t =3.3. Z=0 DENOTES JUNCTION.

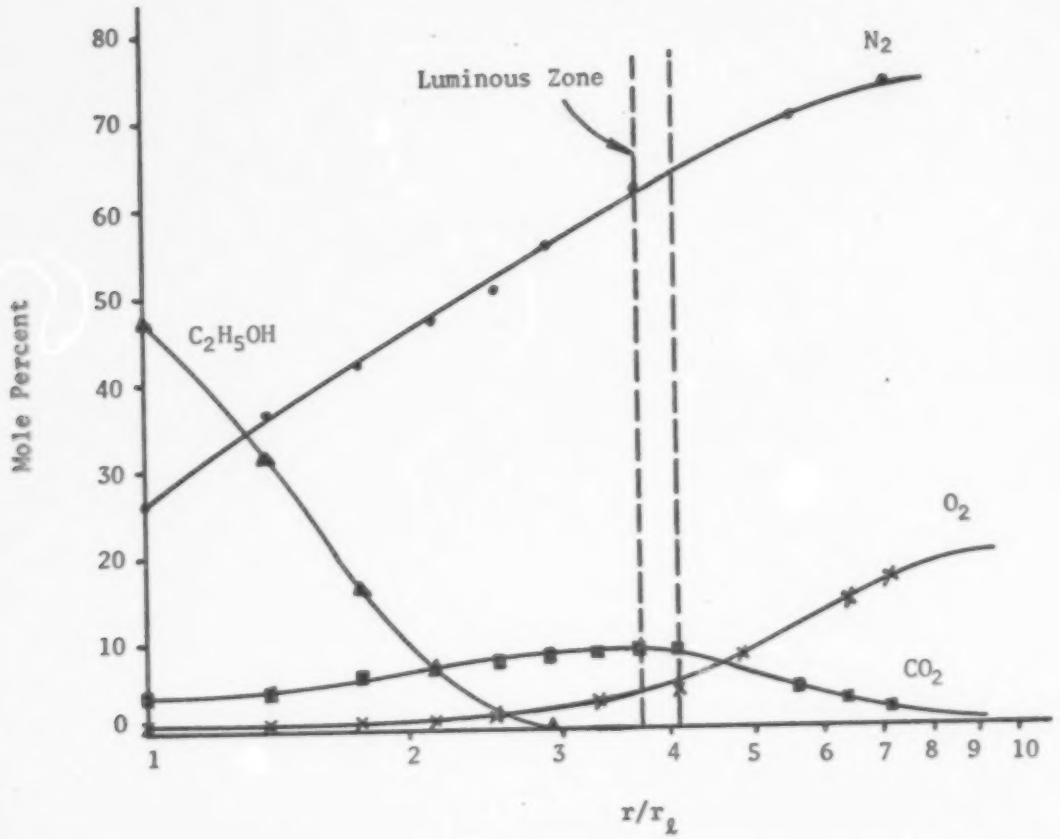

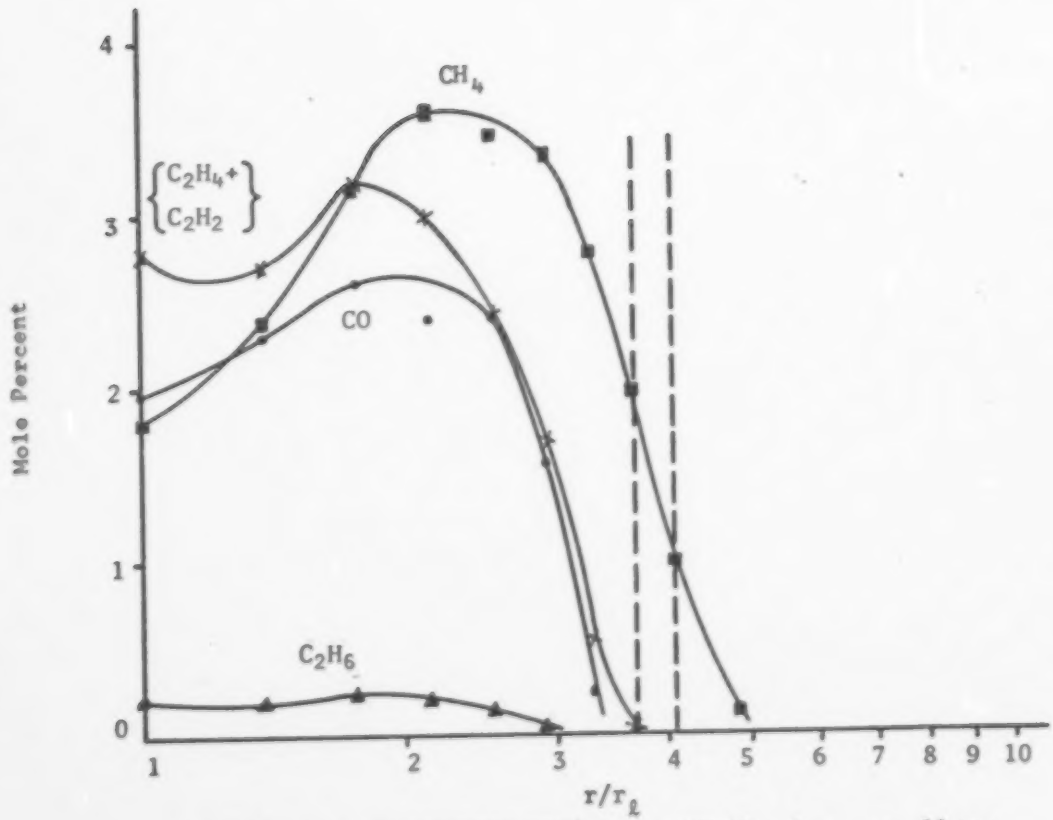

FIGURE 17: COMPOSITION PROFILES, RUN NO. 1, r_ℓ = .66 mm

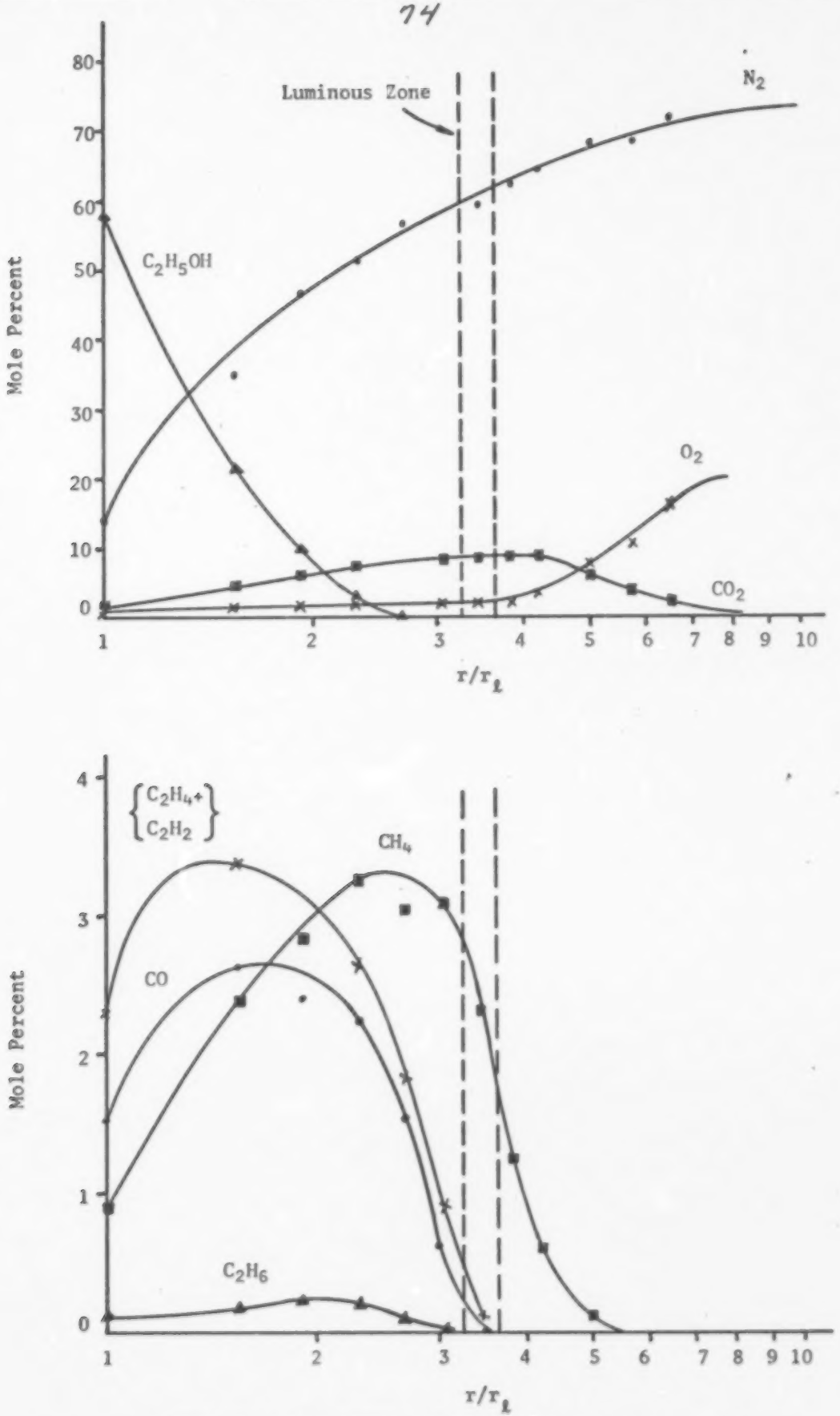

FIGURE 18: COMPOSITION PROFILES, RUN NO. 2, r_ℓ = .66 mm

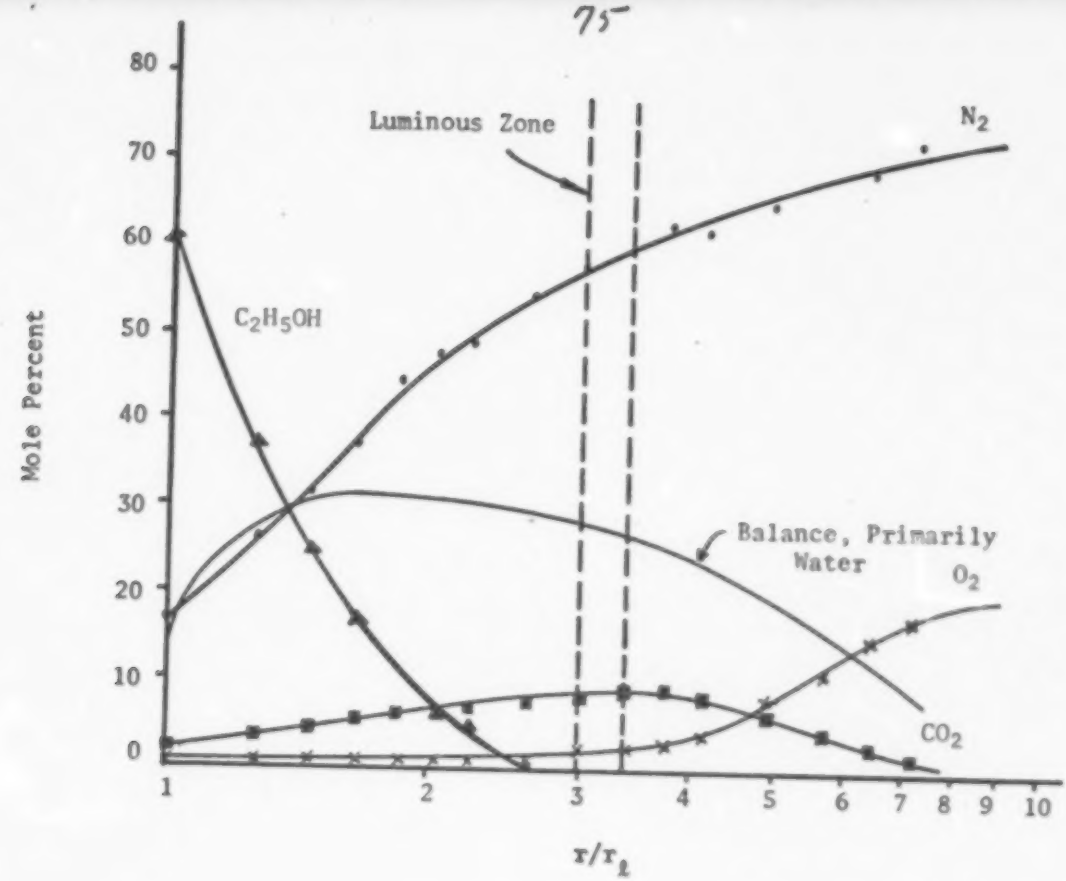

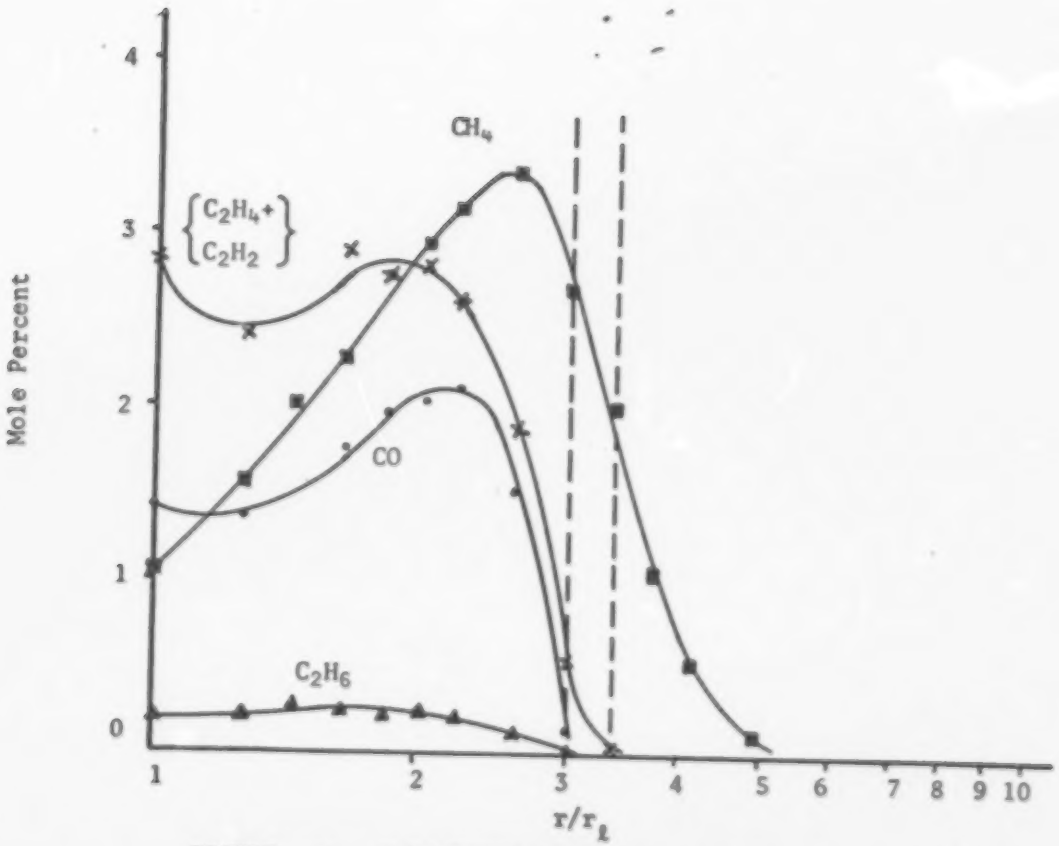

FIGURE 19: COMPOSITION PROFILES, RUN NO. 3, r_ℓ = .66 mm

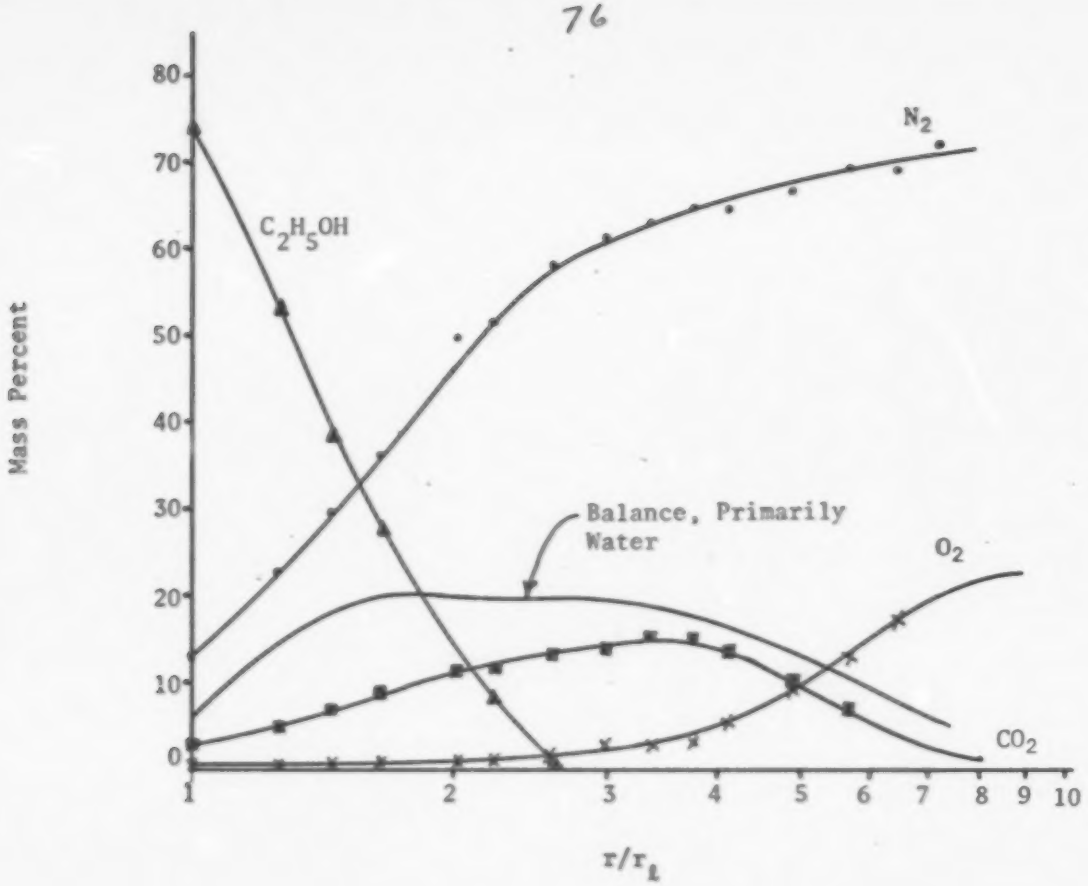

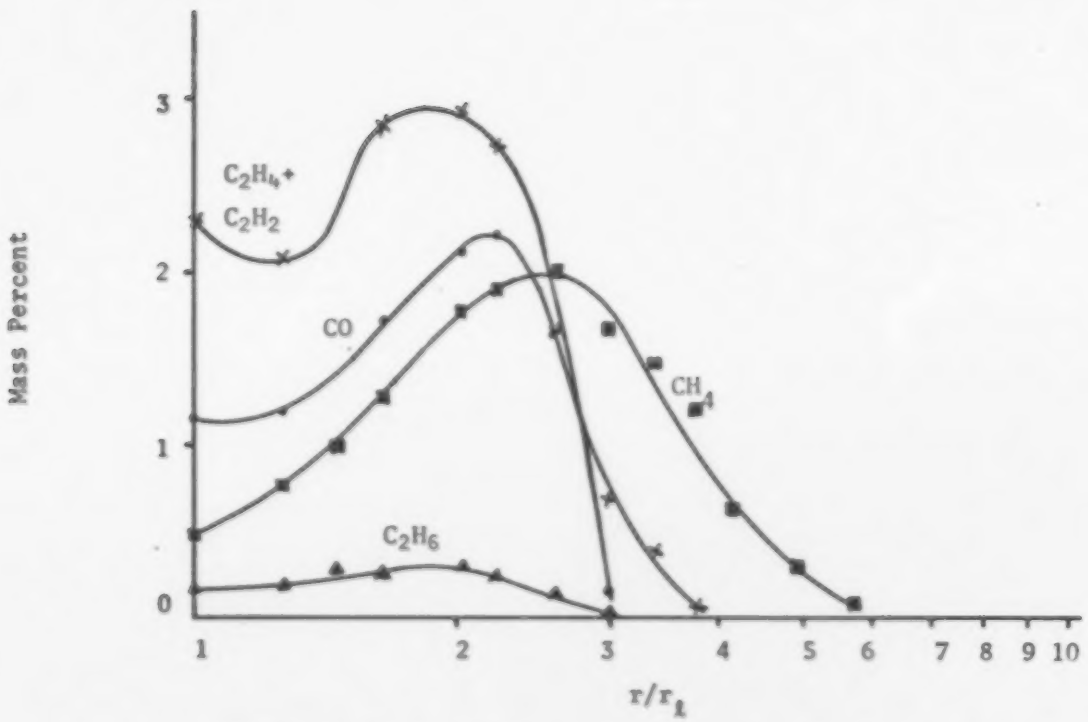

FIGURE 20: COMPOSITION PROFILES, RUN NO. 3, r_ℓ = .66 mm

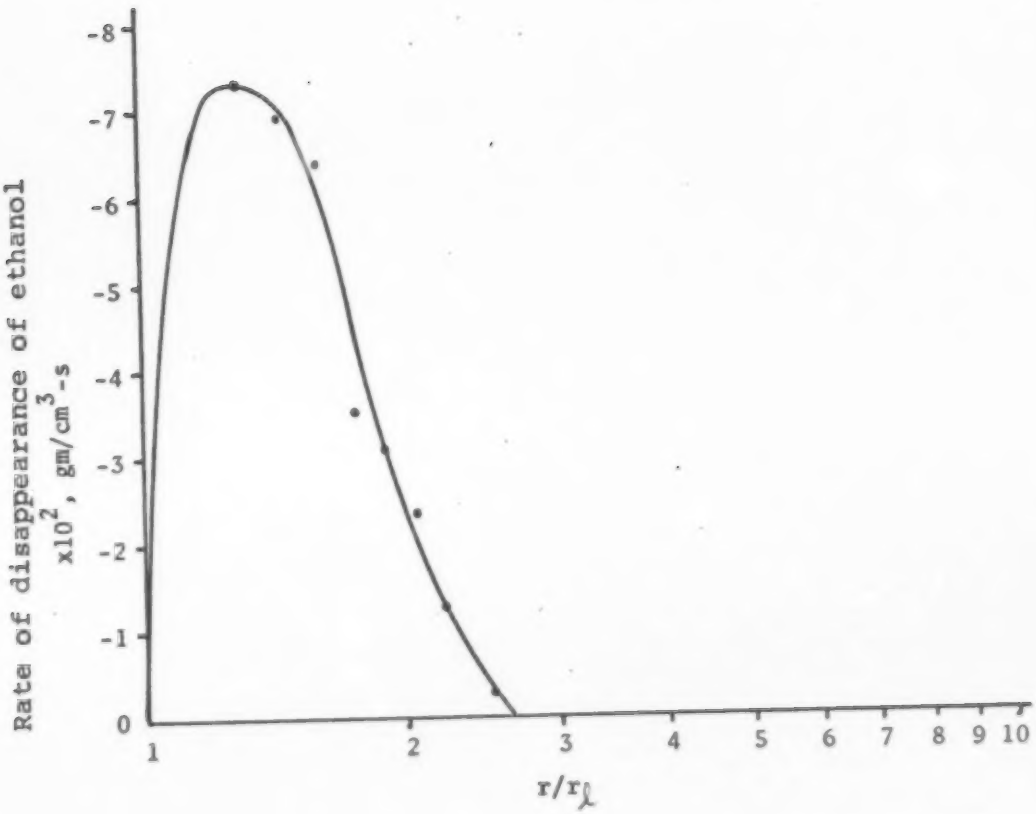

FIGURE 21: RATE OF DISAPPEARANCE OF ETHANOL WITH POSITION IN FLAME, BASED ON RUN NO. 3.

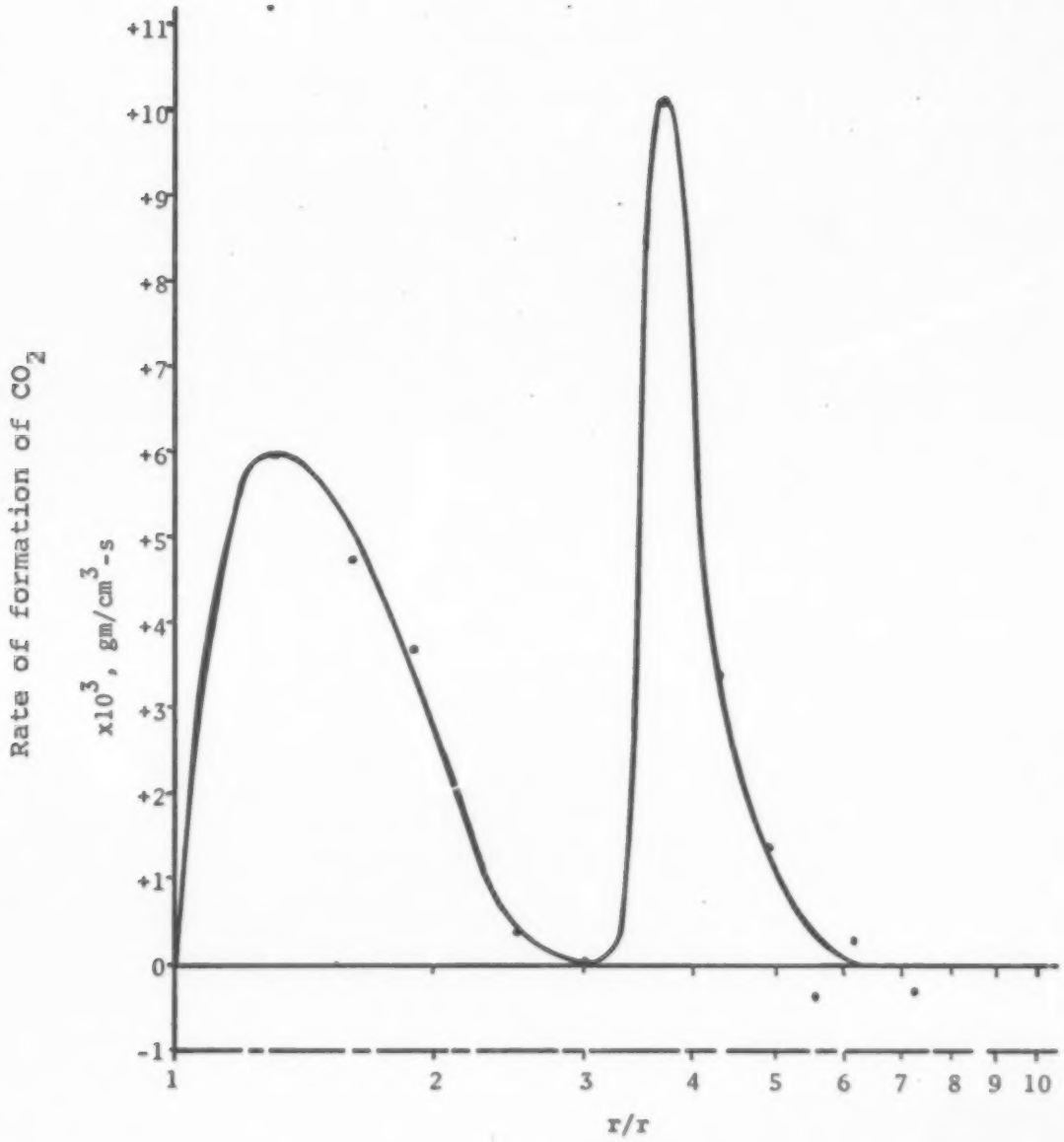

FIGURE 22: RATE OF FORMATION OF CO_2 WITH POSITION IN FLAME, BASED ON RUN NO.3.

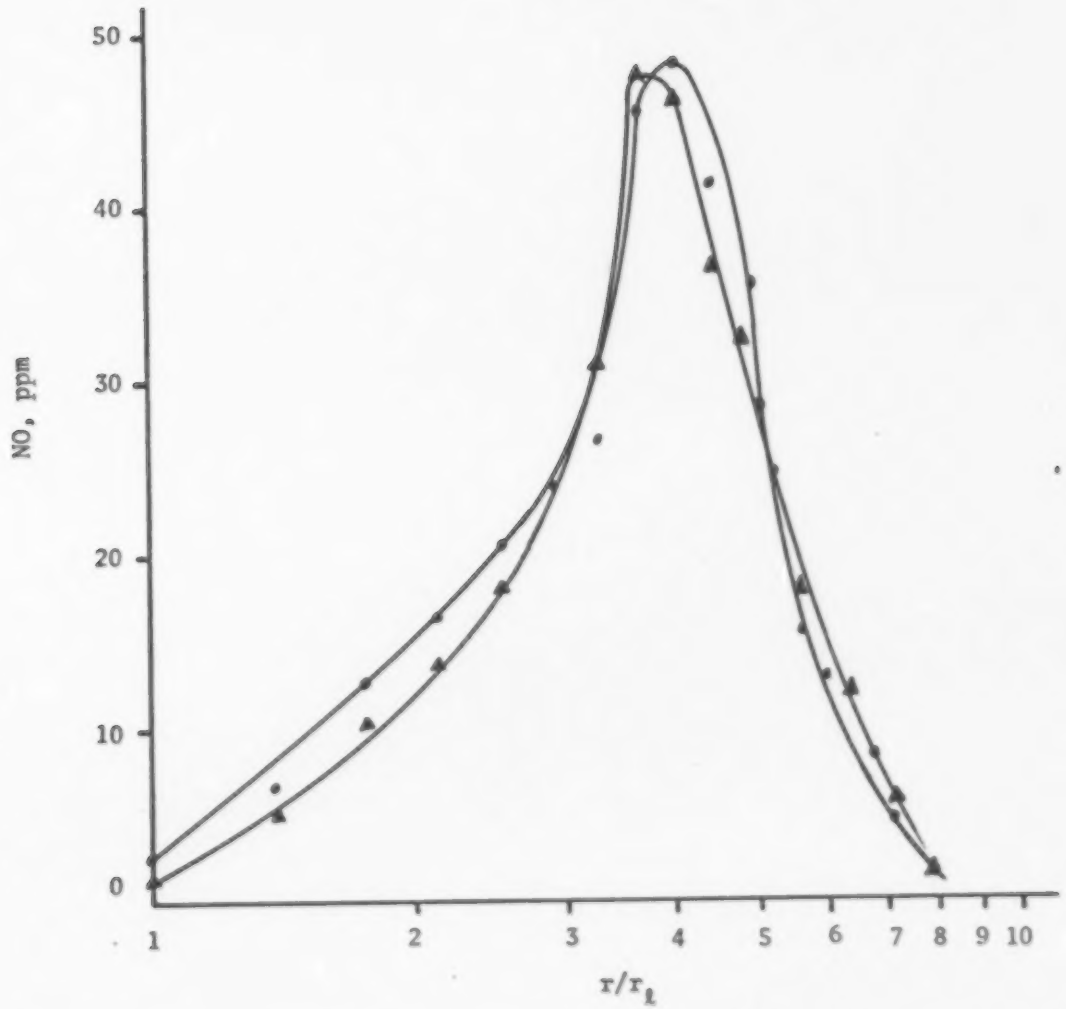

FIGURE 23: NITRIC OXIDE PROFILES, r_ℓ = .66 mm, PURE ETHANOL

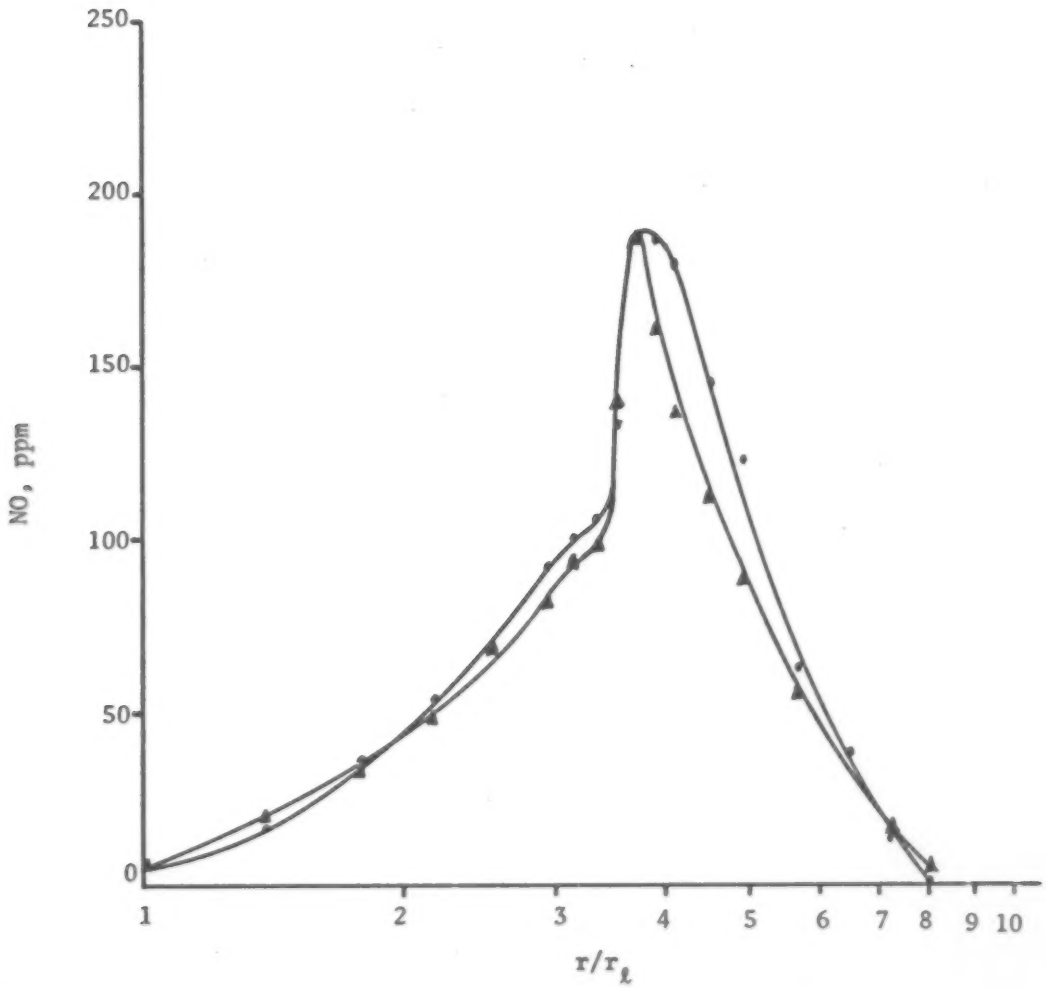

FIGURE 24: NITRIC OXIDE PROFILES, r_ℓ = .648 mm, .096% PYRIDINE

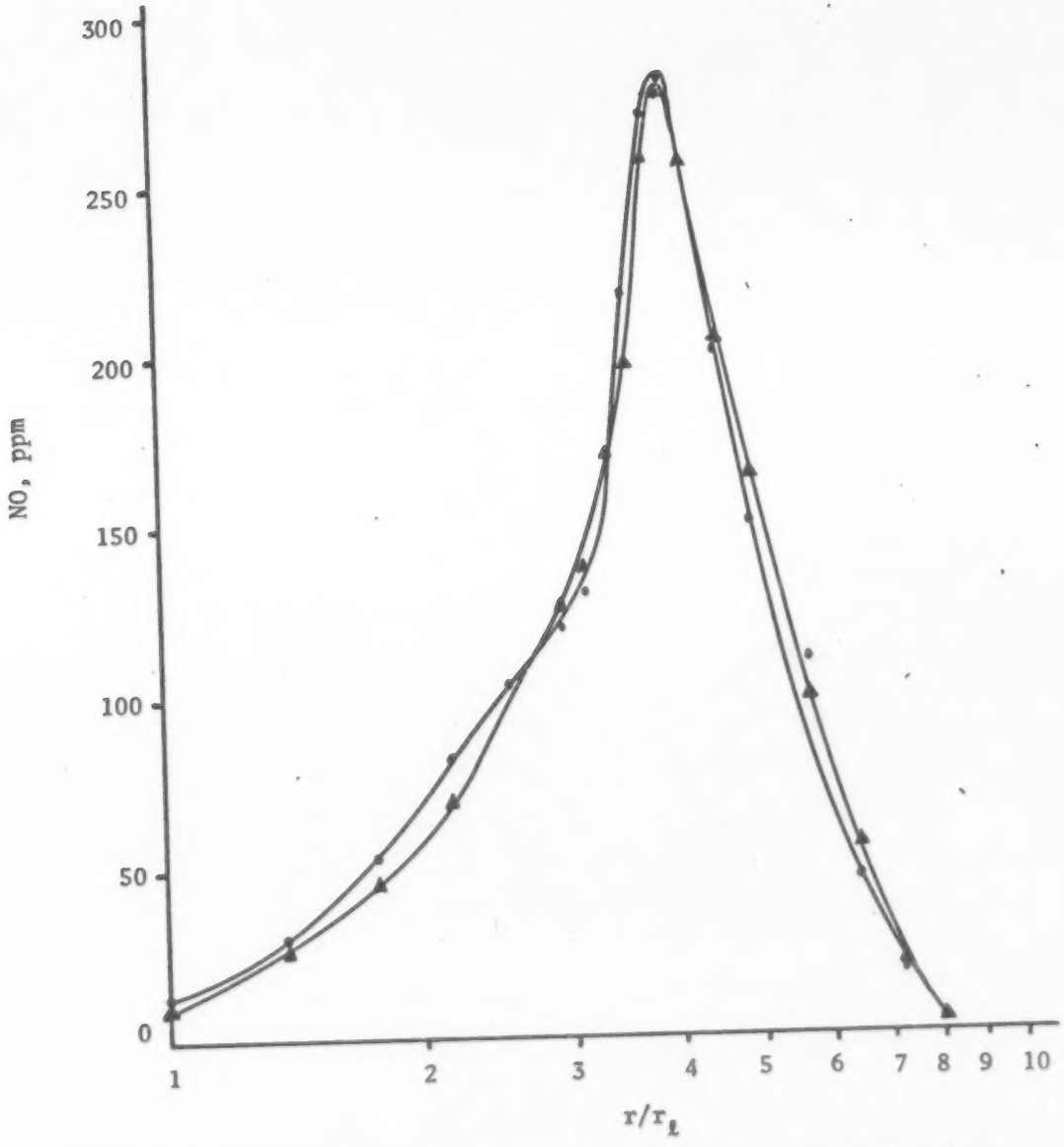

FIGURE 25: NITRIC OXIDE PROFILES, r_ℓ = .648 mm, .1999% PYRIDINE

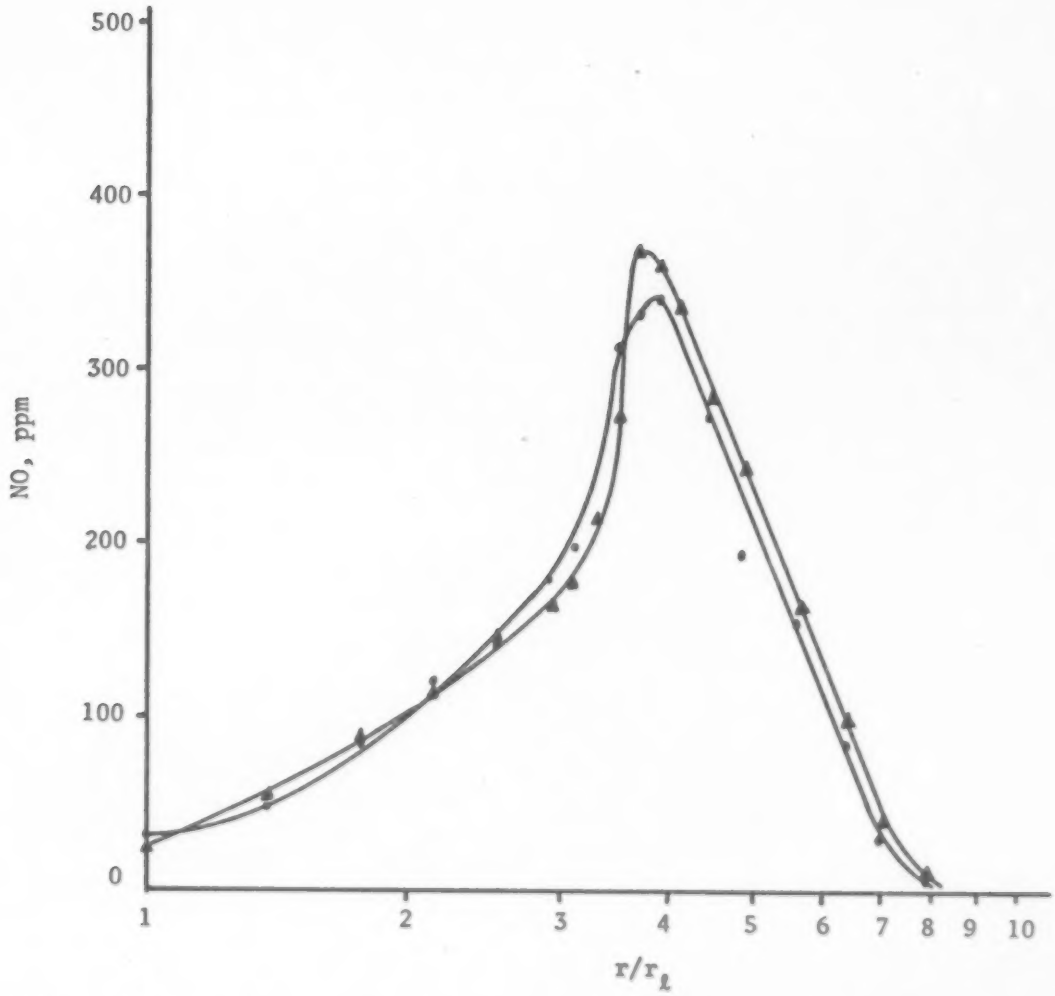

FIGURE 26: NITRIC OXIDE PROFILES, r_ℓ = .66 mm, .3853% PYRIDINE

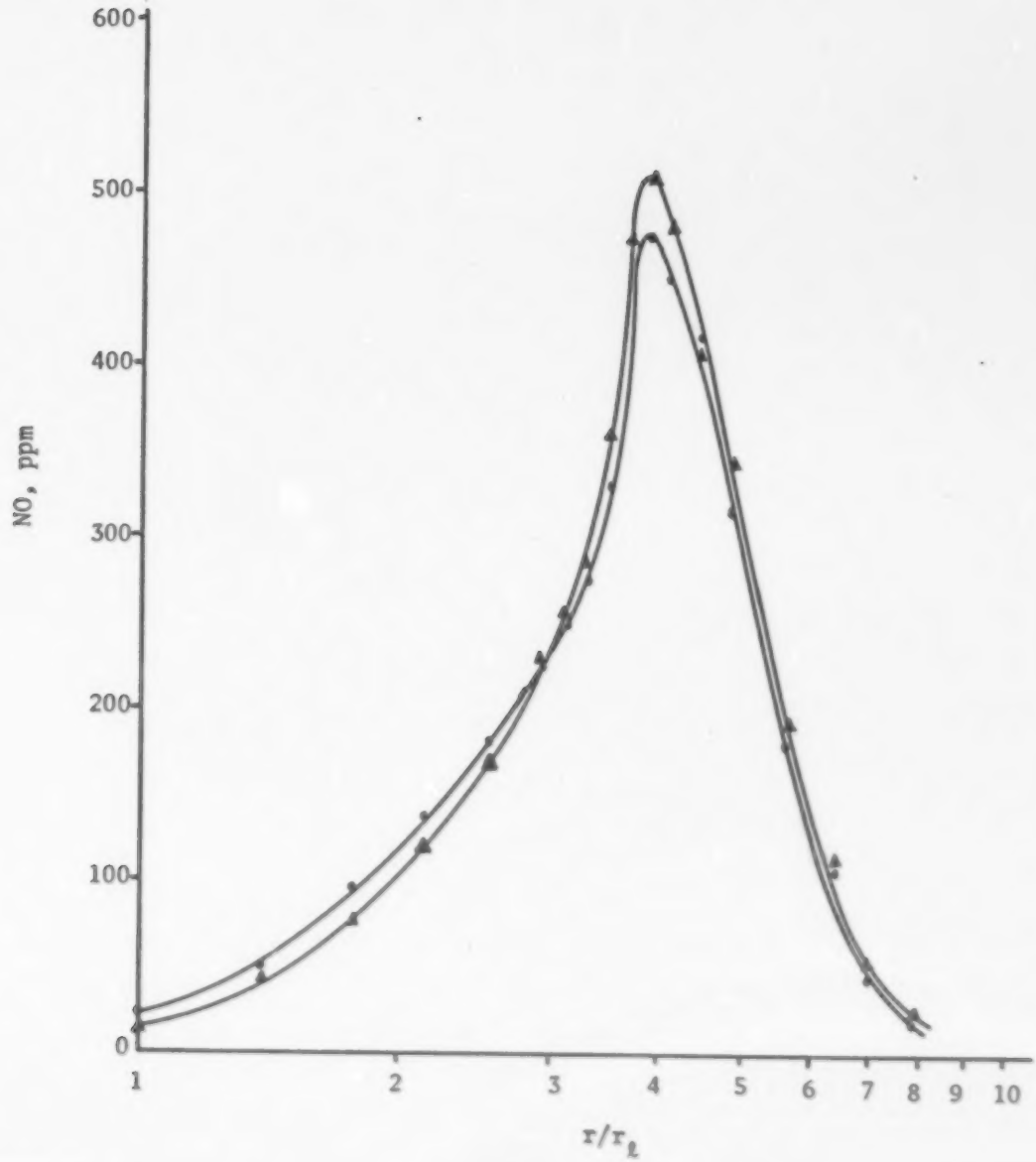

FIGURE 27: NITRIC OXIDE PROFILES, r_ℓ = .66 mm, .591% PYRIDINE

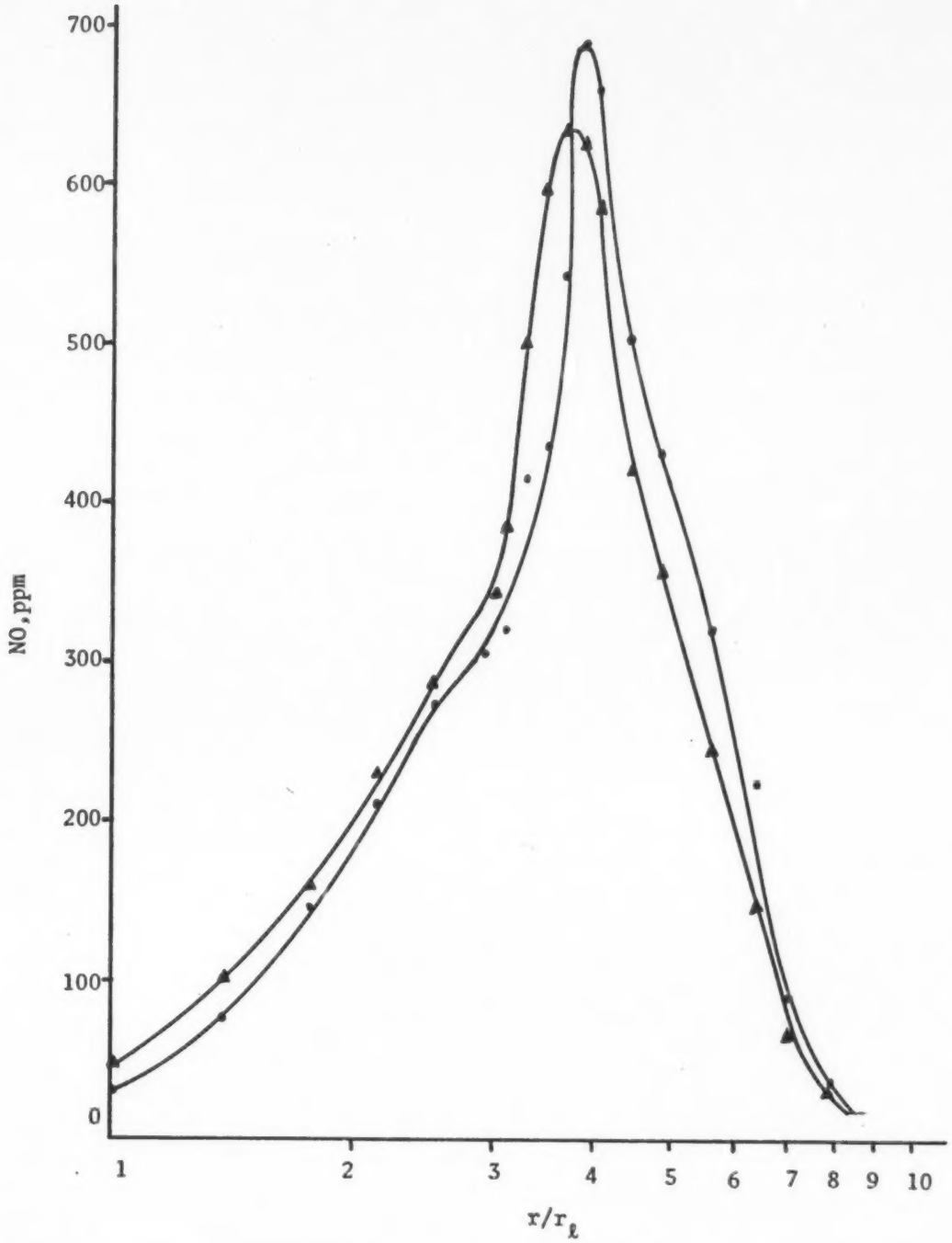

FIGURE 28: NITRIC OXIDE PROFILES, r_ℓ = .66 mm, .78% PYRIDINE

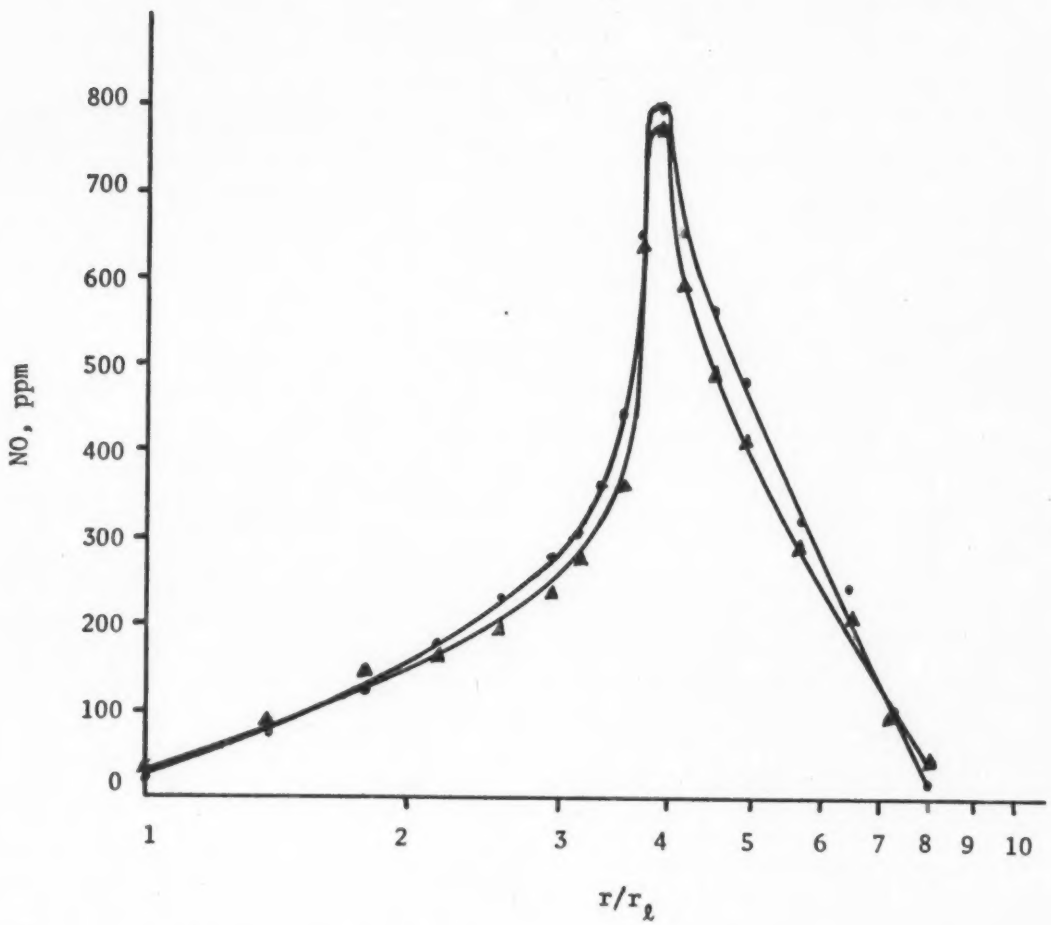

FIGURE 29: NITRIC OXIDE PROFILES, r_ℓ = .66 mm, 0.9878% PYRIDINE

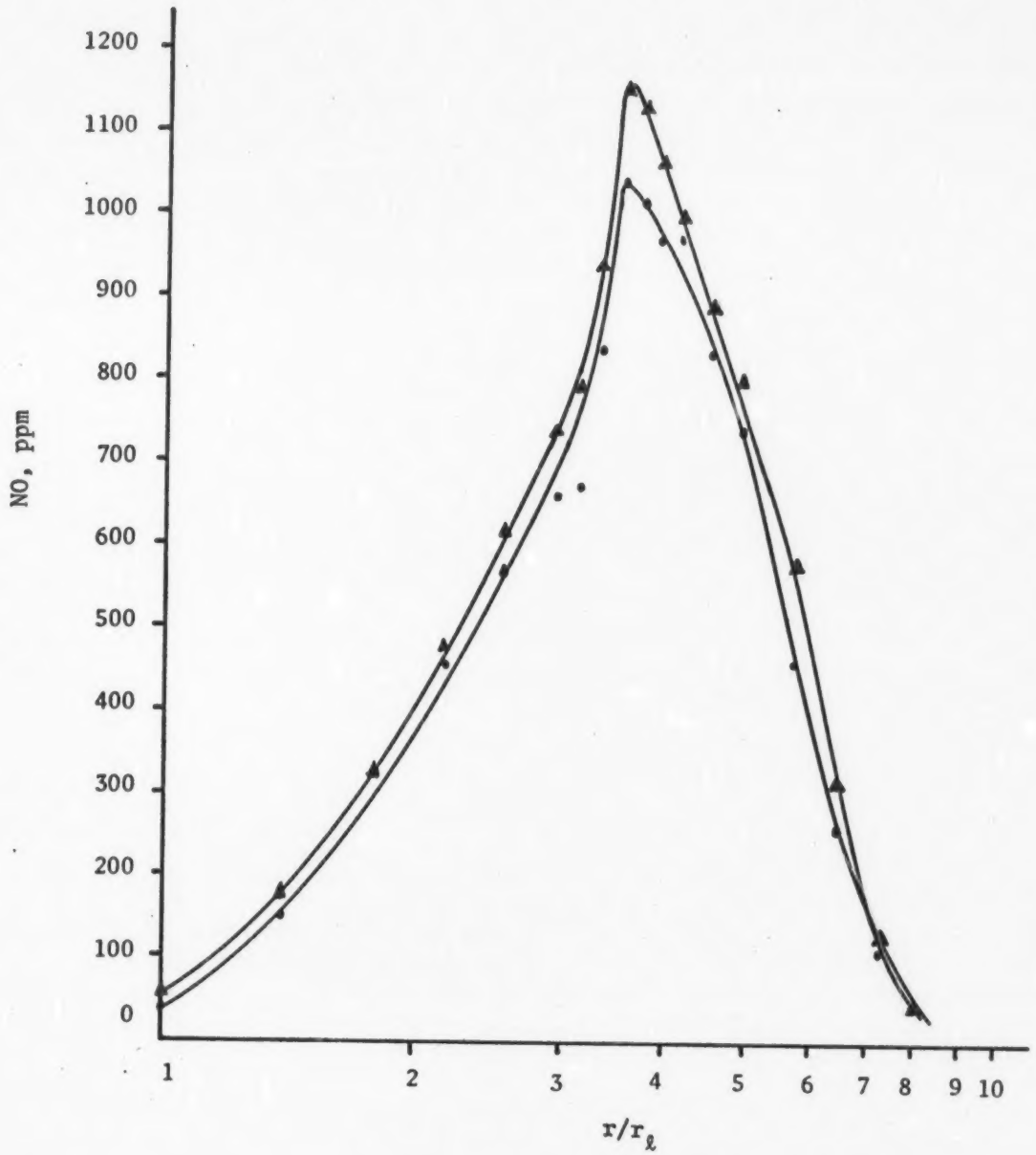

FIGURE 30: NITRIC OXIDE PROFILES, r_ℓ = .648 mm, 1.976% PYRIDINE

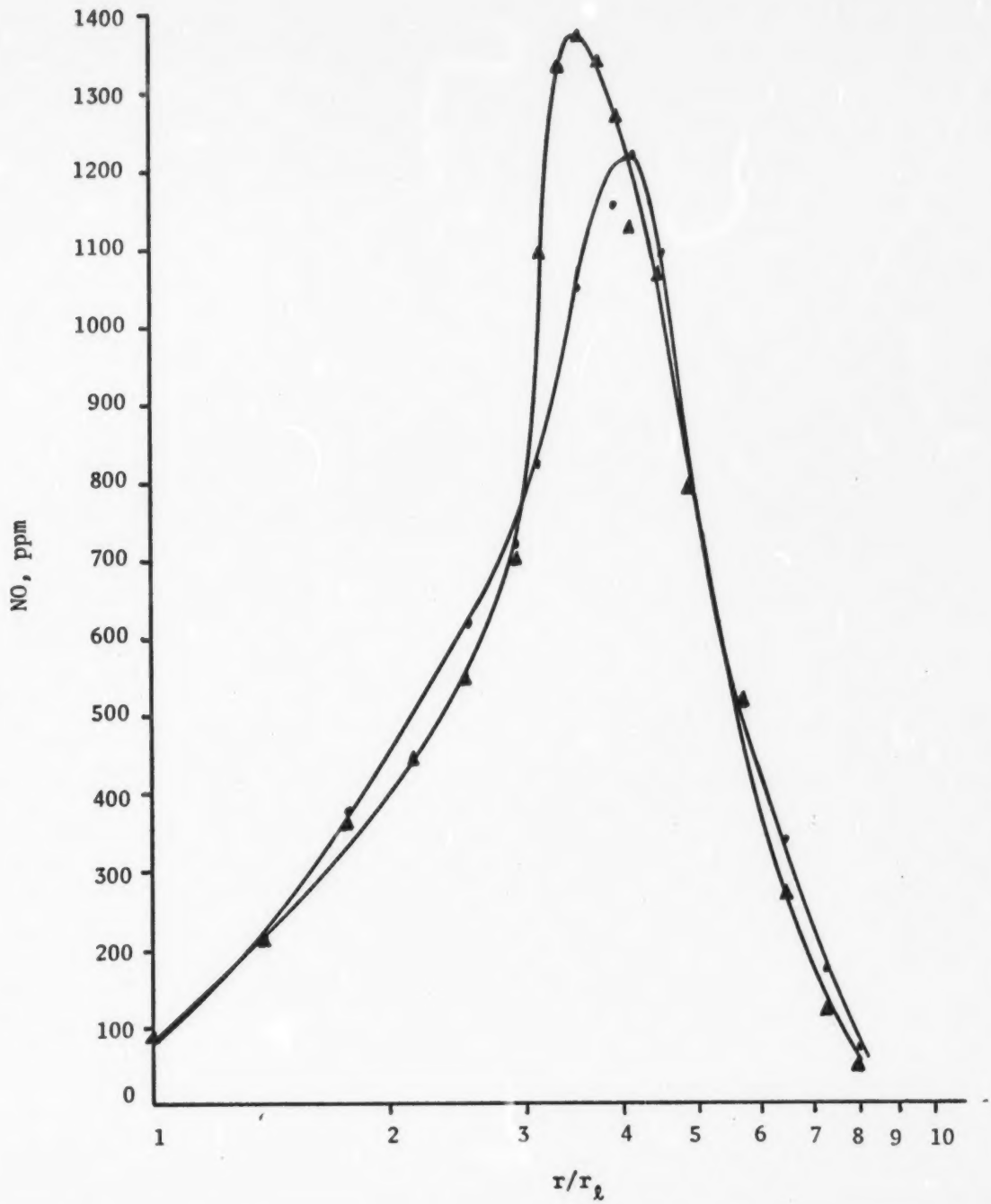

FIGURE 31: NITRIC OXIDE PROFILES, r_ℓ = .648 mm, 3.98% PYRIDINE

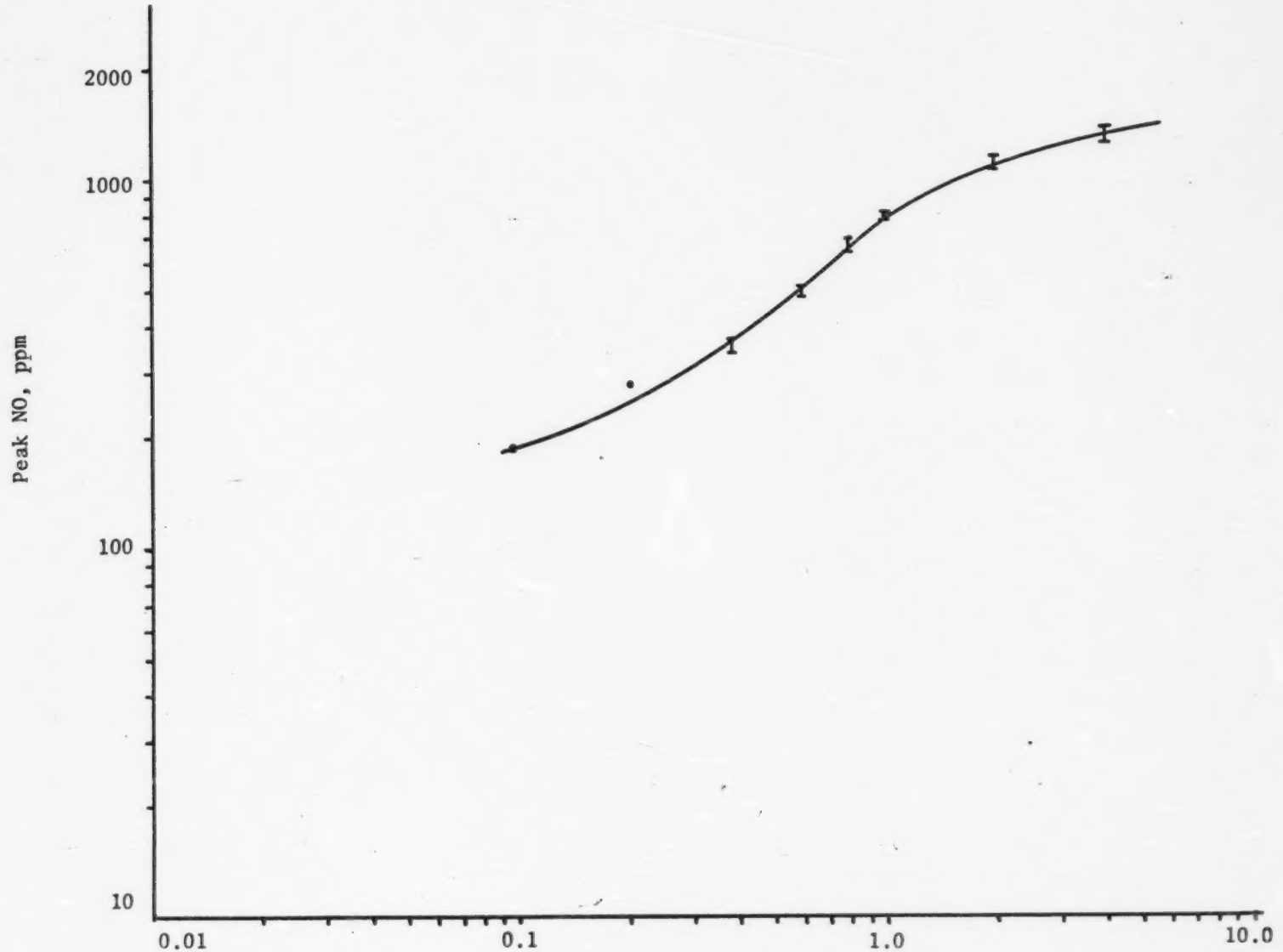

FIGURE 32: CONVERSION OF FUEL N to NO

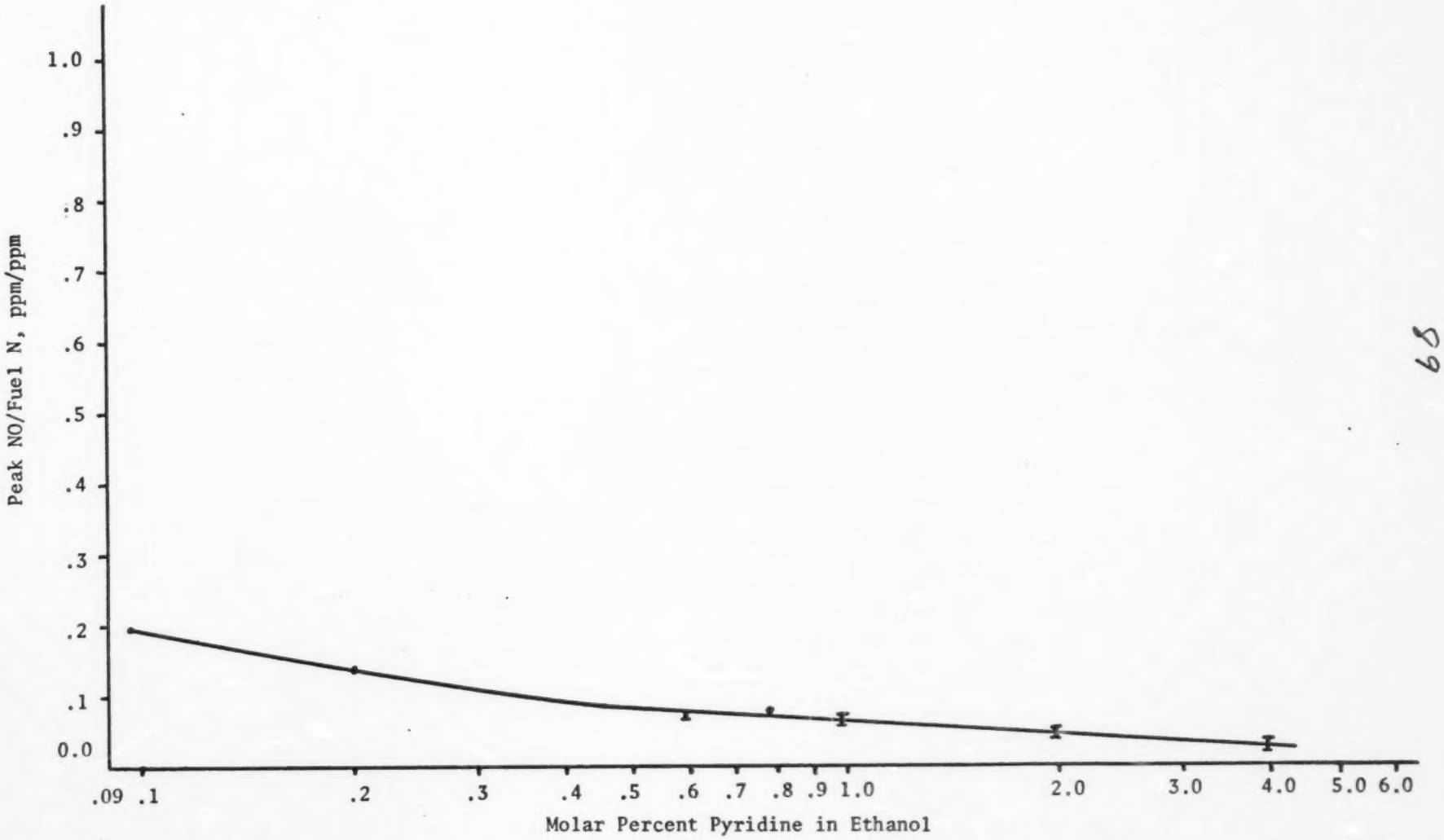

FIGURE 33: CONVERSION OF FUEL N TO NO

APPENDIX A

THEORETICAL ASPECTS OF DROPLET BURNING

Flame Structure

Many theoretical solutions for a fuel droplet burning in a gravity free atmosphere have been reported, however the majority of them have dealt with infinite rate chemical reaction. As consequence of this assumption, the flame zone becomes a surface with zero thickness. It is readily apparent from the data, however, that this is clearly not the case. Meaningful interpretation of the data can be made only if this assumption is not employed.

Bracco's analysis,[13] whose results have been used as a basis for comparison in this work, begins by considering the basic conservation equation for mass and energy for a steady, spherically symmetric flame burning in an oxidizing quiescent gas:

$$\frac{1}{r^2}\frac{d}{dr}\left[r^2 \rho v\right] = 0 \tag{1}$$

$$\frac{1}{r^2}\frac{d}{dr}\left\{r^2\left[\rho \sum_{i=1}^{n} y_i h_i (v + v_i) - \lambda \frac{d}{dr} T\right]\right\} = 0 \tag{2}$$

$$\frac{1}{r^2}\frac{d}{dr}\left\{r^2\left[\rho y_i (v_i + v)\right]\right\} = w_i \,, \qquad \text{for each species} \tag{3}$$

The assumptions employed in the above equations are that the pressure is constant everywhere, and that body forces, viscosity, and thermal and pressure diffusions are negligible.

The diffusion velocities and source terms must also be specified. Assuming binary diffusion of each species into nitrogen, one can employ

* Note Nomenclature on pg. A-11

Fick's Law:

$$y_i v_i = - D_i \frac{d}{dr} (y_i) \tag{4}$$

Because the detailed kinetic mechanisms are not known, the source terms are usually specified in terms of an overall reaction rate. If one also assumes that fuel and oxidizer are consumed in stoichiometric proportions, α , then one obtains the following source equations

$$w_F = - W_F \omega = - W_F B^* e^{-E/RT} C_x^m C_F^n \tag{5}$$

$$w_x = - \alpha W_F \omega \tag{6}$$

$$w_p = (\alpha + 1) W_p \omega \tag{7}$$

To complete the problem, the boundary conditions at the surface and at infinity must be specified. Assuming that the fuel is pure, the jump conditions across the liquid-gas interface become:

$$\rho_+ y_{i+} (v_+ + v_{i+}) = 0 \quad , \quad i = X, P, G \tag{8}$$

$$\rho_+ y_{F+} (v_+ + v_{i+}) = \dot{M} / 4\pi r^2 \tag{9}$$

$$\lambda_+\left(\frac{dT}{dr}\right)_+ - \lambda_-\left(\frac{dT}{dr}\right)_- = \dot{M}L/4\pi r_1^2 \qquad (10)$$

and as $r \to \infty$, Y_i and T must be specified. The above set of equations constitutes an eigenvalue problem with iteration on several parameters. Numerical solutions to problems involving iteration on more than one parameter are very costly and time consuming. One would therefore desire to simplify the problem.

If one assumes that the diffusion coefficients of all the species are given by the same function of T and p, and if the Lewis number is assumed to be unity $\left(\rho D = \frac{\lambda}{c_p}\right)$, then the equations become

$$\frac{d}{dr}\left[\dot{M}\frac{Y_F}{W_F} - 4\pi r^2 \rho D \frac{d}{dr}\frac{Y_F}{W_F}\right] = -4\pi r^2 \omega \qquad (11)$$

$$\frac{d}{dr}\left[\dot{M}\frac{Y_X}{\alpha W_F} - 4\pi r^2 \rho D \frac{d}{dr}\frac{Y_X}{\alpha W_F}\right] = -4\pi r^2 \omega \qquad (12)$$

$$\frac{d}{dr}\left[\dot{M}\frac{Y_P}{(\alpha+1)W_F} - 4\pi r^2 \rho D \frac{d}{dr}\frac{Y_P}{(\alpha+1)W_F}\right] = 4\pi r^2 \omega \qquad (13)$$

$$\frac{d}{dr}\left[\dot{M} Y_G - 4\pi r^2 \rho D \frac{d}{dr} Y_G\right] = 0 \qquad (14)$$

$$\frac{d}{dr}\left[\dot{M}\frac{h}{h^\circ W_F} - 4\pi r^2 \rho D \frac{d}{dr}\frac{h}{h^\circ W_F}\right] = 4\pi r^2 \omega \qquad (15)$$

$$-w_F \omega h^\circ = \sum_{i=1}^{4} h_i^\circ \omega_i \tag{16}$$

$$h = \sum^{4} y_i \int_{T^\circ}^{T} c_{pi}\, dT \tag{17}$$

where $h^\circ = h^\circ_F + h^\circ_x - (\alpha+1)h^\circ_P$ is the stoichiometric heat of reaction at T°. The boundary conditions become

$$\dot{M} y_F - 4\pi r^2 \rho D \frac{d}{dr} y_F = \dot{M} \quad \text{at} \quad r = r_l \tag{18}$$

$$\dot{M} y_i - 4\pi r^2 \rho D \frac{d}{dr} y_i = 0 \quad , i = X, P, G \, , \text{at } r = r_l \tag{19}$$

$$\dot{M} h - 4\pi r^2 \rho D \frac{d}{dr} h = -\dot{M}\left[L^\circ - \bar{C}_{p_{F_l}} (T_l - T^\circ)\right] = -\dot{M} L^* \tag{20}$$

$$\text{as } r \to \infty, \; y_i \to y_{i,\infty} \quad \text{where} \quad i = X, F, P, G \tag{21}$$

The temperature of the drop has also been assumed constant and uniform.

These equations can be mathematically simplified by employing the well known Shvab-Zeldovich variables which are formed from linear combinations of the differential equations with source terms. This technique permits elimination of the source terms in all equations but one. By letting

$$\beta_F = \frac{-Y_F}{W_F} + \frac{Y_X}{\alpha W_F} \tag{22}$$

$$\beta_P = \frac{Y_P}{(\alpha+1) W_F} + \frac{Y_X}{\alpha W_F} \tag{23}$$

$$\beta_T = \frac{h}{h^0 W_F} + \frac{Y_X}{\alpha W_F} \tag{24}$$

and by introducing a new dependent variable

$$\zeta = \dot{M} \int_r^\infty \frac{dr}{4\pi r^2 \rho D} \tag{25}$$

the linearly combined differential equations can all be written as

$$\frac{d\beta_i}{d\zeta} = -\frac{d^2\beta_i}{d\zeta^2} \quad , \quad i = F, P, T \tag{26}$$

whose solution is $$\beta_i = A_i + B_i e^{-\zeta} \tag{27}$$

Substituting this equation into the proper linear combinations of the boundary conditions, one obtains:

$$1 - Y_F + \frac{Y_X}{\alpha} = \left[1 - Y_{F,\infty} + \frac{Y_{X,\infty}}{\alpha}\right] e^{-\zeta} \tag{28}$$

$$\frac{Y_P}{\alpha+1} + \frac{Y_X}{\alpha} = \left[\frac{Y_{P,\infty}}{\alpha+1} + \frac{Y_{X,\infty}}{\alpha} \right] e^{-\xi} \tag{29}$$

$$\frac{h}{h^0} + \frac{L^*}{h^0} + \frac{Y_X}{\alpha} = \left[\frac{h_\infty}{h^0} + \frac{L^*}{h^0} + \frac{Y_{X,\infty}}{\alpha} \right] e^{-\xi} \tag{30}$$

$$Y_G = Y_{G,\infty}\, e^{-\xi} \tag{31}$$

Once one of the differential equations for either Y_F, or Y_x or Y_p or h is solved, all other dependent variables can then be found from the above relations.

The above system is still not readily solved, however, because $\dot{M}$, $Y_{i,\ell}$, and h must still be iterated upon. Therefore another condition is needed. If it is assumed that vaporization occurs under thermodynamic equilibrium, then the Clausius-Clapeyron equation can be employed:

$$Y_{F,\ell} = \frac{W_F}{W}\, e^{-\frac{L}{R}\left(\frac{1}{T_\ell} - \frac{1}{T_b}\right)} \tag{32}$$

This relation considerably simplifies the system, however, iteration must still be made on two parameters, $\dot{M}$ znd ζ.

In order to simplify the system and reduce the problem to iteration on only one parameter, Bracco employed the following additional assumptions:

a) ρD = constant

b) $C_{pi} = C_p$ = constant and equal for all species

c) $W_i = W$ = constant and equal for all species

the procedure for solution then involves the following steps:

a) Assume a value for $\dot{M}$ and compute $\xi_\ell = \frac{\dot{M}}{4\pi r_\ell \rho D}$

b) Algebraically combine Eq. (28) and Eq. (30) to compute T_ℓ:

$$T_\ell = T^\circ - \frac{L^*}{C_p} - \frac{h^\circ}{C_p}(Y_{F,\ell} - 1) + \left[T_\infty - T^\circ + \frac{L^*}{C_p} + \frac{h^\circ}{C_p}(Y_{F,\infty} - 1)\right] e^{-\xi}$$

and compute $Y_{F,\ell}$ from Eq. (32).

c) Using the relations $\xi = \frac{\dot{M}}{4\pi r \rho D}$, $P = \rho RT$

$$\omega = -B^* e^{-E/RT} C_x^m C_F^n \qquad \text{and}$$

$$\frac{d}{dr}\left[\dot{M}\frac{Y_F}{W} - 4\pi r^2 \rho D \frac{d}{dr}\left(\frac{Y_F}{W}\right)\right] = -4\pi r^2 \omega$$

one can derive and solve (assuming m = n = 1)

$$\frac{dY_F}{d\xi} + \frac{d^2 Y_F}{d\xi^2} = \left(\frac{\dot{M}_\infty}{4\pi RT}\right)^2 \frac{B^* W}{(\rho D)^3 \xi^4} Y_F Y_x e^{-E/RT}$$

where Y_x is determined directly from Eq. (28)

and T is determined from Eq. (30)

The boundary conditions imposed on the system are

$$Y_F(\xi_\ell) = Y_{F,\ell}$$

$$\left.\frac{dY_F}{d\xi}\right|_{\xi=\xi_\ell} = 1 - Y_{F,\ell}$$

$$Y_F(0) = Y_{F,\infty}$$

d) If $Y_F(0)$ and specified $Y_{F,\infty}$ do not agree within specified limits, a new guess for $\dot{M}$ is used and the iteration procedure

is continued until $Y_F(0)$ and $Y_{F,\infty}$ agree.

Nitric Oxide Formation

Computation of the nitric oxide produced within the flame is a relatively simple matter once the flame structure is known (note that the formation of nitric oxide was assumed to have a negligible effect on the flame structure calculation). For thermally produced nitric oxide, the Zeldovich mechanism is assumed to apply:

$$O_2 + N_2 \underset{b_3}{\overset{f_3}{\rightleftharpoons}} 2O + N_2$$

$$NO + O \underset{b_1}{\overset{f_1}{\rightleftharpoons}} O_2 + N$$

$$NO + N \underset{b_2}{\overset{f_2}{\rightleftharpoons}} N_2 + O$$

where f_i indicates a forward rate constant, and b_i indicates the rate constant for the reverse reaction. From these equations and their respective rate constants, the source terms (w_o, w_N, w_{NO}) can be calculated. Nitric oxide in the flame is then computed from the mass conservation equation:

$$\frac{d}{dr}\left[\dot{M} Y_i - 4\pi r^2 \rho D_i \frac{d}{dr} Y_i\right] = 4\pi r^2 W_i w_i \quad , \quad i = O, N, NO$$

The boundary condition at the drop surface are

$$\dot{M} Y_{i,l} - 4\pi r^2 \rho D_i \frac{d}{dr} Y_i = 0 \quad , \quad i = O, N, NO, \text{ at } r = r_l$$

Far from the drop, the boundary conditions are

$$Y_i\big|_{r\to\infty} = Y_{i,\infty} \quad , i = O, N, NO \text{ as } r \to \infty$$

In his work, Bracco assumed that the O concentration is in equilibrium with the O_2 concentration and that the N concentration is in steady state. This was done partly to simplify the problem and partly because of lack of sufficient kinetic data. However, a recent study by Bowman[31] strongly suggests that these assumptions are not physically realistic, particularly the assumption of equilibrium between O and O_2. He noted that in the flame zone region of methane-air flames, NO formation rates exceed those predicted under the above assumptions. The same observations were made for shock tube studies of NO formation from hydrogen and methane combustion. In the region where NO is rapidly formed, O and OH radicals were measured and found to be considerably in excess of calculated equilibrium values. If the super-equilibrium O and OH concentrations are used in the following kinetic mechanisms,

$$O + N_2 \rightleftharpoons NO + N$$

$$N + O_2 \rightleftharpoons NO + O$$

$$N + OH \rightleftharpoons NO + H$$

then NO formation rates can be properly predicted. Using previously reported NO formation data and his own calculations, Bowman was able to show a strong, direct relation between NO formation and O-atom concentration. These considerations may explain, in part, the observed higher NO concentrations than predicted under the assumptions employed by Bracco. Based on these assumptions and the assumptions previously discussed for the flame structure,

the differential equation which must be solved is

$$\frac{dY_{NO}}{d\xi} + \frac{d^2Y_{NO}}{d\xi^2} = -\frac{W_{NO}\,4\pi\dot{M}^2}{(4\pi\rho D)^3\,\xi^4}\,w_{NO}$$

where

$$w_{NO} = \frac{dC_{NO}}{d\xi} = \frac{2C_0\left[k_{b_1}k_{b_2}C_{O_2}C_{N_2} - k_{f_2}k_{f_1}C_{NO}^2\right]}{k_{b_1}C_{O_2} + k_{f_2}C_{NO}}$$

$$C_0 = \left[C_{O_2}k_{f_2}/k_{b_3}\right]^{1/2}$$

$$C_N = C_0\left[k_{f_1}C_{NO} + k_{b_2}C_{N_2}\right]/\left[k_{b_1}C_{O_2} + k_{f_2}C_{NO}\right]$$

$$C_{O_2} = \frac{p}{RT}\,Y_{O_2}$$

$$C_{N_2} = \frac{p}{RT}\,Y_{N_2}$$

with the boundary condition

$$\left.\frac{dY_{NO}}{d\xi}\right|_{\xi=\xi_2} = -Y_{NO}$$

$$Y_{NO}(0) = 0.0$$

These equations were solved by assuming a value for Y_{NO} at the droplet surface, integrating the differential equation, and checking to see if $Y_{NO}(0) = 0.0$. If not, a new guess was used for Y_{NO} and the process continued until the calculated $Y_{NO}(0) = 0.0$.

NOMENCLATURE FOR APPENDIX A

B^*	= reaction rate pre-experimental factor	cm^3/moles sec
C_i	= concentration of species i	moles/cm^3
C_p	= specific heat at constant pressure	erg/gm
D	= diffusion coefficient	cm^2/sec
E	= overall reaction activation energy	cal/mole
h	= total enthalpy	erg/gm
k_f	= rate constant in forward direction	cm^3/moles sec
k_b	= rate constant in backward direction	cm^3/moles sec
L	= latent heat of vaporization	erg/gm
$\dot{M}$	= fuel burning rate	gm/sec
p	= pressure	dynes/cm^2
r	= radial distance from droplet center	cm
R	= Gas constant	cal/mole$^\circ$K
T	= Temperature	$^\circ$K
T°	= reference temperature	$^\circ$K
v	= mass averaged gas velocity	cm/sec
v_i	= diffusion velocity of species i	cm/sec
W	= molecular weight	gm/mole
$\overline{W}$	= average molecular weight	gm/mole
Y_i	= mass fraction of species i	
α	= stoichiometric coefficient	(gramsx/$grams_F$)stoich
λ	= thermal conductivity	erg/cm sec$^\circ$K
ρ	= gas density	gm/cm^3
ω	= rate of reaction	moles/cm^3 sec
τ	= dependent variable see eqn. (25) pg. A-5	

Subscripts

i = general reference to a species

P = refers to combustion product

G_t = refers to inert gas (nitrogen)

X = refers to oxidizer

F = refers to fuel

s = refers to drop surface

b = refers to boiling point

∞ = refers to a distance far from the droplet

O = oxygen atom

N = nitrogen atom

NO = nitric oxide

O_2 = refers to oxygen molecule

N_2 = refers to nitrogen molecule

Superscript

$( )^\circ$ = reference value at 298.15 °K

APPENDIX B

EXPERIMENTAL OBSERVATIONS AND SUGGESTIONS FOR IMPROVEMENT

Syringe Feed System

As theory predicts and as intuition would indicate, for a specific droplet diameter, the burning rate is unique. This was born out by control problems experienced using a syringe feed system. Periodic oscillations in droplet burning were encountered. These turned out to coincide with one revolution of the lead screw which was directly linked to the syringe piston. Examination indicated that the lead screw was very slightly bent. Efforts to correct the bend were unsuccessful. It was found, however, that the problem could be completely corrected by introducing into the syringe a bubble about 6 inches long.

Droplet Burning

Using the system of suspending the droplet on top of the feed line presented the problem of maintaining a spherical liquid surface. The tendency was for the ethanol to flow over the high temperature cement and down the feed tube so that the burning surface appeared more like a tear drop than a sphere. The problem was particularly acute when high concentrations of pyridine were added to the ethanol. An unknown dark brown substance would polymerize on the feed line and acted like a sponge by soaking up ethanol. The problem could be essentially overcome by trimming the high temperature cement to form a ridge which (by surface tension effects) prevented flow of alcohol down the feed line (see Figure 2b).

The ideal solution would be to invert the system so that the droplet is fed from above by the feed line. This will require a water cooled

jacket to prevent premature vaporization of the fuel inside the feed line. It will, however, minimize control problems and assure that a nearly spherical alcohol surface is maintained.

The Quartz Microprobe

Extensive experimentation has shown that the probe design illustrated in Figure 2c is the only one we have found which will minimize condensation of carbon on the inside surface and subsequent clogging. Note that the end will usually need to be fire polished to the proper orifice diameter using a microscope and the smallest available ox-acelylene microtorch head. Large slender probes will rapidly clog up from carbon condensation on the inside surface. On the other hand, probes whose taper angle is too large (about 30°) will noticeably disturb the flame front.

The Thermocouple Design

The smallest wire diameter used for thermocouples in this work was .0015 in. This was dictated by practical considerations. It would be preferable to use wires .0005 inches in diameter for two reasons: 1) the spacial resolution would be increased substantially and 2) conductive effects along the wire would be minimized.

The Chromatograph

The modified chromatograph as described in a previous section works very well for analyzing the standard combustion products. However, when attempting to analyze samples containing pyridine, the pyridine peak was never seen (even after waiting one hour for it). The molecule is just too complex to elute at a Porapak Q temperature of 85°C. Hence, if this or similar complex compounds are required in the analysis, further modifications of the gas chromatograph must be considered.

The NO Chemiluminiscent Analyzer

As previously indicated, the primary problem encountered in the operation of this instrument is the non-constant sample flow rate and the tendency of the entire system to continuously drift. These problems must be solved if highly reliable data is to be obtained. Figure 10 indicates a possibility for maintaining a constant sample flow rate into the chemiluminescent reaction chamber. The success of this method, however, requires that the quartz microprobe flow rate always be greater than the sample flow rate into the reaction chamber. Assuming choked flow for both the probe and reaction chamber orifices, a flame temperature and pressure of 2000°K and 76 cm Hg, and constant sample line temperature and pressure of 300°K and 2 cm Hg, we require

$$\left.\frac{\dot{m}_p}{\dot{m}_{\substack{\text{chamber}\\\text{sample}}}}\right|_{\text{choked}} = \frac{A_{probe}\, P_{c_{probe}}}{A_{sample}\, P_{c_{sample}}} \sqrt{\frac{T_{c_{sample}}}{T_{c_{probe}}}} > 1$$

or

$$A_{\text{chamber sample}} < A_{probe} \frac{P_{c_{probe}}}{P_{c_{sample}}} \sqrt{\frac{T_{c_{sample}}}{T_{c_{probe}}}}$$

$$A_{\text{chamber orifice}} < A_{probe}\,(14.7)$$

There will be a slight variation in flow rate due to variation in the molecular weight of the sample line gas. The variation may be significant only very near the droplet surface due to the high concentration of ethanol. The proposed changes in the instrument should, however, improve the accuracy considerably and simplify its operation.

APPENDIX C

ENERGY BALANCE FOR THERMOCOUPLE ELEMENT

The energy equation for a quartz coated thermocouple is derived based on the following assumptions (refer to Figure 6):

1) uniform temperature in the radial direction (on the z plane)
2) negligible axial conduction through the quartz layer
3) steady state.

The heat equation for the thermocouple element is

$$q_1 = q_2 + q_c + q_r$$

Based on Fourier's conduction law

$$q_1 = -\lambda_p A \left.\frac{dT}{dz}\right|_{z_1} = -\pi R_p^2 \lambda_p \left.\frac{dT}{dz}\right|_{z_1}$$

$$q_2 = -\lambda_p A \left.\frac{dT}{dz}\right|_{z_2} = -\pi R_p^2 \lambda_p \left.\frac{dT}{dz}\right|_{z_2}$$

Using a Taylor expansion of the temperature gradient around z_1 , can be written as

$$q_2 = q_1 + \left.\frac{dq_1}{dz}\right|_{z_1} \delta z + \left.\frac{d^2 q_1}{dz^2}\right|_{z_1} \frac{\delta z^2}{2} + \text{higher order terms}$$

The heat flow, q_c , from the surrounding gas to the wire is derived by Chapman:[33]

$$q_c = \frac{2\pi (T - T_g)}{\frac{1}{R_q h} + \frac{\ln (R_q / R_p)}{\lambda_q}} \delta z$$

The heat loss by radiation from a body of area A, with total hemispherical emissivity ϵ, at a surface temperature T and the surroundings at T_a is

$$q_r = \sigma A \epsilon (T^4 - T_a^4) = 2\pi R_g \sigma \epsilon (T^4 - T_a^4) \delta z$$

assuming the surface area of the surroundings is much larger than A.

Combining these terms, we obtain

$$q_1 = q_2 + q_c + q_r$$

$$q_1 = q_1 - \lambda_p (\pi R_p^2) \left[\frac{d^2T}{dz^2} \delta z + \frac{d^3T}{dz^3} \frac{\delta z^2}{2} + \cdots \right] + 2\pi K (T - T_g) \delta z + 2\pi R_g \sigma \epsilon (T^4 - T_a^4) \delta z$$

$$\lambda_p (\pi R_p^2) \left[\frac{d^2T}{dz^2} + \frac{d^3T}{dz^3} \frac{\delta z}{2} + \cdots \right] = K 2\pi (T - T_g) + 2\pi R_g \sigma \epsilon (T^4 - T_a^4)$$

where $$K \equiv \frac{1}{\frac{1}{R_g h} + \frac{\ln (R_g / R_p)}{\lambda_g}}$$

Taking the limit as $\delta z \to 0$ we obtain

$$\lambda_p R_p^2 \frac{d^2T}{dz^2} = K 2 (T - T_g) + 2 R_g \sigma \epsilon (T^4 - T_a^4)$$